MINISTRY OF TECHNOLOGY

AERONAUTICAL RESEARCH COUNCIL

CURRENT PAPERS

An Investigation of the Rolling Moments due to Sideslip on High Tailplanes at Subsonic, Transonic and Supersonic Speeds

by

D. G. Mabey, M.Sc.(Eng.)

AN INVESTIGATION OF THE ROLLING MOMENTS DUE TO SIDESLIP ON HIGH TAILPLANES AT SUBSONIC, TRANSONIC AND SUPERSONIC SPEEDS

by

D. G. Mabey, M.Sc. (Eng.)

SUMMARY

Measurements are presented of the rolling moments due to sideslip on three high tailplanes at subsonic and transonic speeds; the results show large variations with Mach number. At transonic speeds the rolling moments in some cases are affected by shocks and shock induced separations which are sensitive to incidence changes. Measurements at supersonic speeds on one tailplane show that the rolling moment falls rapidly from $M = 1.3$ to $M = 2.0$.

A method of estimating the Mach number variation at subsonic and transonic speeds by extrapolation from the low speed values of tailplane rolling moment, fin lift and tailplane lift is suggested. The method gives reasonable agreement with experiment.

CONTENTS

ILLUSTRATIONS   Fig.

ILLUSTRATIONS (Contd.)   <u>Fig.</u>

4

1   INTRODUCTION

Measurements of the rolling moment due to sideslip on the high tail-plane of Model A (Fig.1), first made by Bristols and then in the Bedford 3ft wind tunnel[1,2] showed a large increase in $|\partial C_{\ell_T}/\partial\beta|$ from a Mach number M = 0.40 to M = 1.00, most of it occurring above M = 0.90 (Fig.2). This effect was thought to be related to the high tailplane position and to confirm this, two other available models with high tailplanes were tested. The first, Model B, was also tested in the 3ft tunnel and it was found that after an increase in $|\partial C_{\ell_T}/\partial\beta|$ from M = 0.40 to M = 0.80 there was a non-uniform variation with Mach number up to M = 1.20 (Fig.4). The second, Model C, was tested in the 8ft × 6ft transonic tunnel at Farnborough. The results shown in Fig.6 indicate that the variation in $|\partial C_{\ell_T}/\partial\beta|$ with Mach number was less regular than for Models A and B but that there was a significant effect due to aircraft incidence.

This paper presents the experimental results together with an analysis which indicates that an increase in $|\partial C_{\ell_T}/\partial\beta|$ may be associated with an increase in both the fin lift and the tailplane lift. A method for estimating the variation is suggested which shows reasonable agreement with the measure-ments. The investigation also shows that shock induced separations on the fin and tailplane, the wing downwash, and the tailplane lift coefficient C_{L_T}, may also affect $\partial C_{\ell_T}/\partial\beta$.

At supersonic speeds, tests on Model A showed a monotonic decrease in $|\partial C_{\ell_T}/\partial\beta|$ from M = 1.3 to M = 2.0.

2   DETAILS OF THE TESTS

2.1   Measurement of tailplane rolling moments

The tailplane of Model A is shown in detail in Fig.7. The tailplane was screwed to a section of the fin which could deflect laterally and carried a strain gauge bridge to measure the rolling moment. This is shown in Fig.7 as the C_{ℓ_T} station. The tailplane itself also carried two independent strain gauged bending moment stations* (C_{B1} and C_{B2} in Fig.7) which were displaced 12% semi span from the centre line. The outputs from

---

* It is advantageous to measure the two bending moments independently because changes in the tailplane rolling moment can then be traced to changes occurring on one side of the tailplane. Due to the finite size of strain gauges the bending moment stations are displaced from the root of the tailplane.

these stations were found by calibration to be independent of the chordwise loading position. The relation between the bending moments and the rolling moments depends, however, on the spanwise load distribution over the tailplane; this aspect is now considered.

The load distribution factor F is defined as the ratio of the centre line moment to the moment at a station distant a from the centre line

i.e.,
$$F = \frac{\int_{0}^{b_T/2} W(x) \cdot (x) \, dx}{\int_{a}^{b_T/2} W(x) \cdot (x-a) \, dx} \quad .$$

The spanwise load distribution due to incidence is symmetric and may be assumed to be approximately elliptic (Fig.8a)

i.e.,
$$W(x) = W_{max} \{1 - (2x/b_T)^2\}^{\frac{1}{2}} \quad .$$

For this loading F is calculated to be 1.33 for Model A $(2a/b_T = 0.12)$.

The spanwise load distribution due to sideslip is asymmetric. The calculated loadings in Ref.3 are antisymmetric, and Fig.8b shows the loading on a high tailplane with a tail/fin span ratio of $b_T/b_F = 2.0$ and a fin aspect ratio $A_F = 1.0$ (Ref.3, Fig.4a). This distribution is nearly triangular: a triangular loading gives

$$F = [b_T/(b_T - 2a)]^3 \quad .$$

The load distribution factor F for a triangular loading on Model A is 1.45.

The tailplane rolling and bending moment coefficients C_{ℓ_T}, C_{B1}, C_{B2} were measured simultaneously while the model sideslip was varied, and C_{ℓ_T} was plotted against $C_{B2} - C_{B1}$ for different Mach numbers. The slope of these lines is the experimental value of the load distribution factor for the loading due to sideslip on Model A.

Fig.9 shows that the load distribution factor is $F = 1.42$ from $M = 0.40$ to $M = 1.00$, which agrees satisfactorily with the factor for a triangular loading.

On Model B two bending moment stations were provided as close as possible to the centre line - at 11% semi span (Fig.10). It is assumed that the load distribution on the tailplane due to sideslip was again approximately triangular. The load distribution factor is then calculated to be F = 1.44. The values of the tailplane rolling moment coefficients quoted for Model B are thus determined by the relation

$$C_{\ell_T} = 1.44 \left(C_{B2} - C_{B1} \right) . \tag{1}$$

On Model C the bending moment stations were at 14% semi span (Fig.11) and the rolling moment coefficients quoted are determined by the relation

$$C_{\ell_T} = 1.59 \left(C_{B2} - C_{B1} \right) .$$

It is possible that the load distribution due to sideslip is not triangular (because, for example, of wing downwash effects) and the load distribution factor is then in error. This error is unlikely to be worse than the difference between the factors for the triangular and elliptic loadings, which for Model A is 1.45 - 1.33 = 0.08. Thus when rolling moments are determined from bending moments (as on Models B and C) they may be in error to 0.08/1.45 × 100% ≑ 6%.

Apart from this error the accuracy of the C_{ℓ_T} measurements is estimated to be better than ±0.001.

2.2 Description of the models

All the models described are sting supported and the rear fuselages of Models A and B differ considerably from those of the full scale aircraft.

It has been reported in another investigation[4] that small changes in the rear fuselage affected the flow over the fin at transonic speeds and produced a significant effect on the directional stability. There is thus a possibility that the fuselage distortion on Models A and B did affect the magnitude of the tailplane rolling moments: this would not affect the general conclusions of this paper (see 3.1 below).

The general arrangement of Model A is shown in Fig.1: the dotted lines show the fairings used to make the rear fuselage cylindrical. The fuselage cross-section is shown in Fig.12.

The general arrangement of Model B is shown in Fig.3: the dashed lines indicate the fuselage shape of the full scale aircraft. The model body is distorted to compensate for the absence of the jets as well as to cover the support sting. Fig.10 shows that inserts could be fitted into the fin to provide tail settings of $\eta_T = -4^\circ$ and $\eta_T = 0^\circ$. Force measurements could not be made with the slot between the fin and the tailplane sealed without affecting the calibration of the bending moment gauges. Due to a manufacturing error on the -4° tailplane the slots were not symmetric. However, the bullet covered most of the slots, as Figs.28b and d show.

The general arrangement of Model C is shown in Fig.5. There is little fuselage distortion as the sting enters the model at a position corresponding roughly with the jet exit on the full scale aircraft.

2.3 Scope of the tests

The configurations used and the test conditions are given in the following tables. The sign convention is shown in Fig.12.

Model A

| Mach numbers | Configuration | | | | Range of α_B deg. | Range of β deg. |
	Wings	Rudder angle deg.	Aileron angle deg.	Fairings		
Subsonic and	On	0	0	Off	0	-4, +10
transonic	On	9.4	0	Off	0	-4, +10
0.40, 0.70,	On	0	10.3	Off	0	-4, +10
0.80, 0.85,	On	0	10.3	Off	-4, +10	$\beta = -3$
0.90, 0.95,	Off	0	-	Off	0	-4, +10
1.00	Off	0	-	On	0	-4, +10
Supersonic	Off	0	-	Off	0	-4, +10
1.31, 1.61, 1.82	Off	0	-	On	0	
2.00						

Model B

Mach numbers	Configuration		Range of α_B deg.	Range of β deg.
	Tail setting deg.	Bullet		
Subsonic and transonic 0.40, 0.70, 0.80, 0.85, 0.90, 0.93, 0.96, 0.99, 1.02, 1.15, 1.20	-4	Fitted	0	-4, + 8
	-4	Fitted	3	-4, +10
	-4	Fitted	-4, +10	$\beta = -3$
	-4	Not fitted	3	-4, +10
	0	Fitted	3	-4, +10
	0	Fitted	-4, +10	$\beta = -3$

Model C

Mach numbers	Values of α_B deg.	Range of β deg.
0.50, 0.75, 0.85, 0.90, 0.95, 1.00, 1.19	0	
	3	-2, +10
	9	

Test conditions

Model	A	B	C
Boundary layer condition	Transition fixed by roughness band extending from 0-10°C on wings, fin and tailplane. 0.50" band on fuselage nose		Transition free
Reynolds number based on c_T	Subsonic and transonic		
	0.45×10^6	0.62×10^6	0.58×10^6
	Supersonic		
	0.30×10^6	-	-

3   DISCUSSION OF RESULTS

3.1   Model A

3.1.1   Subsonic and transonic speeds

In Fig.13 the tailplane rolling moment coefficient C_{ℓ_T} is plotted against the sideslip angle β for tests at zero body incidence α_B both with the wings off and with the wings on $(\alpha_W = 2^\circ)$. It will be seen that C_{ℓ_T} increases linearly with β up to $\beta = 6^\circ$, that there is a large increase in $\partial C_{\ell_T}/\partial\beta$ with Mach number, and that the wings have little effect on C_{ℓ_T}.

The slopes of the $C_{\ell_T} - \beta$ curves of Fig.13 are reduced beyond $\beta = 6^\circ$ because no further increase occurs on the leeward side of the tailplane, as Fig.14 shows. There is probably a small separation on the leeward side of the tailplane for $\beta > 6^\circ$ and Fig.14 also shows that this effect is apparently suppressed at M = 1.00.

Fig.15 shows the variation of tailplane rolling moment with sideslip when the rudder is deflected 9.4°. There is little change in $\partial C_{\ell_T}/\partial\beta$ but the curves are displaced compared with Fig.13 by an amount corresponding to $\beta = -2^\circ$ at M = 0.70 and 0.80, and to $\beta = -1.7^\circ$ at M = 0.90. This displacement disappears at M = 1.00 because of a marked change in the loading on the windward side of the tailplane (Fig.16), probably due to a shock movement. Fig.16 also suggests that the separation on the leeward tailplane still persists beyond $\beta = 6^\circ$, but is now apparently suppressed at M = 0.90 as well as at M = 1.00.

Fig.17 shows the variation of the tailplane rolling moment with sideslip when the starboard aileron is deflected 10.3°. There is a small increase in $|\partial C_{\ell_T}/\partial\beta|$ and a displacement of the curves by an amount corresponding to $\beta = -1^\circ$. The curves now show a kink beyond $\beta = 6^\circ$ from M = 0.70 to M = 0.90. This kink is probably caused by the change in wing downwash influencing the separation on the leeward side, as a comparison of Figs.14 and 18 indicates. The variation of tailplane rolling moment with incidence when $\beta = -3^\circ$ and the aileron is deflected is shown in Fig.19: the slope at $\alpha = 0^\circ$ is $\partial C_{\ell_T}/\partial\alpha = 0.03$ and is roughly independent of Mach number. Fig.19 shows that the effect of incidence on the tailplane rolling moments on this model is small.

Finally it should be remarked that this tailplane is mounted on a large body with a 53% reduction in area between the cylindrical section forward of the fin (shown in Fig.12) and the circular section at the trailing edge of the fin. A removable fairing added to the rear fuselage to make the body cylindrical to 1" downstream of the fin trailing edge (Fig.1) had little effect on the tailplane rolling moments (Fig.20). These measurements were necessary as the fin and tailplane lifts, needed for the analysis which is given in 4.1, were measured on another model having a cylindrical rear fuselage. The present measurements suggest that body distortion cannot affect the general conclusions of this paper.

3.1.2 Supersonic speeds

In Fig.21 the tailplane rolling moment coefficient C_{ℓ_T} has been plotted against β for tests with the wings off. The curves are linear up to $\beta = 6^\circ$ from $M = 1.32$ to $M = 1.82$. It will be seen that $\left| \partial C_{\ell_T} / \partial \beta \right|$ decreases rapidly from $M = 1.32$ to $M = 2.00$. The fairings have little effect on the tailplane rolling moments, except at $M = 2.00$ when the graphs of C_{ℓ_T} against β are slightly non linear.

In Fig.22 the corresponding bending moments C_{B1} and C_{B2} have been plotted against β. It will be seen that the non linearity at $M = 2.00$ appears on the tailplane on the windward side of the fin at about $|\beta| = 3^\circ$.

These results are discussed later in section 4.4.

3.2 Model B - subsonic and transonic speeds

In Fig.23 C_{ℓ_T} is plotted against β for the tail setting $\eta_T = 0^\circ$ and a body incidence $\alpha_B = 3^\circ$. The slope at the origin, $\partial C_{\ell_T} / \partial \beta$, has been plotted against Mach number in Fig.5, which shows an increase from $M = 0.40$ up to $M = 0.70$ but a sharp decrease from $M = 0.80$ to $M = 0.96$. This decrease is associated with separations, which are described later.

In Figs.24 ($\alpha_B = 3^\circ$) and 25 ($\alpha_B = 0^\circ$) the corresponding results are given for $\eta_T = -4^\circ$. The curves of Fig.24 show decided non linearities from $M = 0.90$ to $M = 1.02$ and hence the slope at the origin has not been plotted for this configuration. Fig.25 shows that when $\alpha_B = 0^\circ$ and $\eta_T = -4^\circ$ the curves are non linear from $M = 0.85$ to $M = 1.02$ so that the separations are more extensive for $\alpha_B = 0^\circ$ than for $\alpha_B = 3^\circ$.

The effect of incidence on the rolling moments is shown more forcefully in Figs.26 and 27. Here the tailplane rolling moments measured at $\beta = -3^\circ$ have been plotted against Mach number for several incidences*. Fig.26 $(\eta_T = -4^\circ)$ shows that as the incidence increases the tailplane rolling moments increase. The same trend is shown by Fig.27 for $\eta_T = 0^\circ$ but here the losses in rolling moment due to separations are much smaller. In fact Fig.27 suggests that with $\eta_T = 0^\circ$, $\alpha_B = 10^\circ$ the separations are largely suppressed.

Some oil flow photographs were taken when the separations were severe, i.e., with $\eta_T = -4^\circ$. Fig.28a shows a shock induced separation on the leeward side of the fin at the junction of the fin and tailplane when M = 0.90, $\beta = 3^\circ$ and $\alpha_B = 0^\circ$. This separation covers about 10% of the fin. However, Fig.28b shows that the separation covers about 50% of the tailplane. The bending moment on the leeward side remained almost constant as β varied from $+3^\circ$ so that this separation clearly produced a large reduction in the tailplane rolling moments. The formation of the shock induced separation can be explained qualitatively by the superposition of the tailplane load distributions due to incidence (Fig.29a) and sideslip (Fig.29b). When the critical Mach number is exceeded an increase in loading increases the shock strength on the suction surface. Thus on the leeward side of the tailplane where the loads due to incidence and sideslip are additive, there is a loading concentration towards the root (Fig.29c), and a shock is formed which is strong enough to separate the boundary layer to about 20% semi span, (Figs.28b and 29d). On the windward side of the fin the loads due to incidence and sideslip are subtracted. Fig.28c shows that the flow is attached over the windward side of the fin, except for a small region just forward of the bullet which may be influenced by the flow through the slot. Fig.28d shows that the shock on the tailplane has not produced a marked separation and in fact the bending moment still varied with β from $\beta = +3^\circ$.

The flow on the tailplane depends on the combination of incidence and sideslip: the incidence may be deduced from force measurements on the model[5]. For $\alpha_B = 0^\circ$, the example just considered, it is found that $\alpha_T (= \eta_T + \alpha_B - \varepsilon) = -7^\circ$ but that for $\alpha_B = 10^\circ$, $\alpha_T = -1^\circ$. Thus for $\alpha_B = 10^\circ$ the shocks should be weaker and the separations smaller than for $\alpha_B = 0^\circ$. Fig.30 (compared with Fig.28a) confirms this and shows why the tailplane rolling moment increases with incidence.

---

* C_{ℓ_T} has been plotted positive downwards to facilitate comparison with Fig.4.

Fig.28d shows a small trace of flow through the slot at the fin/tailplane junction. An oil flow photograph with the gap sealed (Fig.31) shows little difference from Fig.28a so that sealing this gap has little influence on the flow in the junction. However, some tests without the bullet with $\eta_T = -4^\circ$ revealed asymmetries (Fig.32 compared with Fig.24) which were attributed to the flow through the slots.

It has been noted in these tests on Model B that separations can reduce the tailplane rolling moment. It is possible that the separations on the full scale aircraft may be less severe due to the higher Reynolds number and the virtual elimination of gaps. It might therefore be unwise to stress an aircraft tailplane for the rolling moments measured when there are extensive separations on the model. A safer procedure would be to assume the values of rolling moment obtained from model tests in which the separations are eliminated. In these present tests Figs.26 and 27 show that this condition is approximated at the highest incidence ($\alpha_B = 10^\circ$) and the most positive tail setting ($\eta_T = 0^\circ$). Tests of another model of the tailplane in the A.R.A. 9' x 8' tunnel (transition fixed) at a Reynolds number about 3 times that of the present tests[6], suggested that the separations were still present.

3.3 Model C – subsonic and transonic speeds

In Fig.33 the tailplane rolling moments are plotted against β for $\alpha_B = 0^\circ$, 3° and 9°. The curves are rather non linear and since the scope of these tests was limited little analysis is possible. The values of $\partial C_{\ell_T}/\partial \beta$ given in Fig.6 are measured at the origin for consistency with Figs.2 and 4. It is interesting to note that the curves of Fig.33 for $\alpha_B = 9^\circ$ appear to be more linear than for $\alpha_B = 0^\circ$ or 3°: this result may be comparable with those for Model B.

4 THE ESTIMATION OF MACH NUMBER EFFECTS ON TAILPLANE ROLLING MOMENTS

4.1 Subsonic and transonic speeds

The subsonic and transonic results from Model A illustrate a Mach number effect on the rolling moments on high tailplanes which has been apparently overlooked previously. Fig.34a shows that the increase in tailplane rolling moments is much larger than the increase in the fin lift in Fig.34b. This extra increase in rolling moment is associated with the increase in the tailplane lift, Fig.34c. In fact the rolling moment on this high tailplane varies roughly as the product of the fin and the tailplane lift, as Fig.34d shows. A qualitative explanation follows.

Consider the idealised high tailplane shown in Fig.35. When this is yawed at zero geometric incidence the fin lift will induce positive and negative incidence distributions on the starboard and port sides of the tail-plane. These incidence distributions may be related to equivalent mean incidences

$$
\left.\begin{array}{l}
\alpha_1 = k_1\,\beta \\[2mm]
\alpha_2 = -k_2\,\beta
\end{array}\right\} \tag{2}
$$

where k_1 and k_2 are some functions of a_{1F}. For slender fins $k_1 = k_2$ and Fig.14 shows that for Model A, $k_1 \simeq k_2 = k$. The tailplane rolling moment is then

$$
L_T \simeq \tfrac{1}{2}\,S_T\,q\,a_{1T}\,2k\,\beta\,\ell\,b_T{}^* \tag{3}
$$

where ℓ represents the spanwise centre of the lift distribution, ($\ell = 1/6$ for the triangular loading of Fig.8b) and a_{1T} is the lift curve slope of the tailplane.

Hence

$$
\frac{\partial C_{\ell_T}}{\partial \beta} = \frac{1}{q\,S_T\,b_T}\,\frac{\partial L_T}{\partial \beta} = a_{1T}\,k\,\ell \quad . \tag{4}
$$

Now k is a function of the fin lift and the simplest acceptable relationship is

$$
k = m\,a_{1F} \tag{5}
$$

where m is a constant. On this assumption then

$$
\boxed{\frac{\partial C_{\ell_T}}{\partial \beta}\Big/ a_{1F}\,a_{1T} = m\,\ell = \text{constant}} \quad . \tag{6}
$$

Despite the crudeness of the above analysis, it may be seen that equation (6) applies quite well to the results for Model A, which are plotted

---

* Since the fin provides an end plate on one side of the tailplane it is probably better to use a_{1T} for the complete tailplane, rather than that for the isolated half tailplane. The former can be measured directly on the model.

in Fig.34. The variation of $(\partial C_{\ell_T}/\partial\beta)/a_{1F}\, a_{1T}$ with Mach number is seen from Fig.34d to be reasonably small: certainly the large variation apparent in the $C_{\ell_T} - \beta$ curve of Fig.34a has been considerably reduced. The residual variations may be caused by the small separations which were noticed during oil flow runs.

If equation (6) is valid for other high tailplanes $\partial C_{\ell_T}/\partial\beta$ can be estimated by extrapolation of the low speed values of $\partial C_{\ell_T}/\partial\beta$, a_{1T} and a_{1F}. The low speed value of a_{1F} can be used to determine the effective aspect ratio of the fin and the variation of a_{1F} and a_{1T} can then be estimated using the graphs of Ref.7. The tailplane rolling moment (in the absence of separations) at a Mach number M is then

$$\left(\frac{\partial C_{\ell_T}}{\partial\beta}\right)_M = \left(\frac{\partial C_{\ell_T}}{\partial\beta}\right)_0 \frac{(a_{1T}\, a_{1F})_M}{(a_{1T}\, a_{1F})_0} \quad . \tag{7}$$

Further experimental evidence for the general validity of equation (6) is awaited* but it will now be shown that it is compatible with theoretical calculations made for high aspect ratio configurations which give a large Mach number effect on both the fin and the tailplane.

4.2   Examination of other calculations

The low speed value of $\partial C_{\ell_T}/\partial\beta$ can be calculated reasonably accurately by replacing the fin and tailplane by a number of vortices, although these calculations are tedious, even for simple configurations. An example of these calculations and a comparison with experiment is given in Ref.8 from which Fig.36 has been drawn.

The configuration considered has unswept, untapered fin and tailplane surfaces with a fin aspect ratio $A_F = 2.0$. The fin and tailplane chords were equal. Fig.36 shows that the calculations seem to be reasonably accurate.

Ref.3 gives the rolling moments calculated by this method for a systematic series of unswept and 45° swept fin tailplane combinations. The fin and tailplane root chords were equal so that for a given fin aspect ratio the tailplane aspect ratio varies as the tail span. The quarter chord lines of the fin and tailplane intersected. These results may be used to find the Mach number effects on the unswept configuration with $A_F = 3.0$. The

---

* Model B also shows a considerable increase in ∂C_{ℓ_T} with little change in a_{1F}[5]. Unfortunately the large separations complicate further analysis.

Göthert transformation can be used[9] to transform a configuration of aspect ratio A at a subsonic compressible Mach number M into affinely related configurations of aspect ratio

$$A' = A(1 - M^2)^{\frac{1}{2}}$$

in an incompressible flow. For brevity, these configurations are referred to subsequently as "analogous" configurations. The relations used are given in the following table.

Fin aspect ratio	Aspect ratios of analogous fins	$\beta = (1 - M^2)^{\frac{1}{2}}$	Equivalent Mach number M
3.0	3.0	1	0
	2.0	2/3	0.74
	1.0	1/3	0.94

Fig.37 gives $\partial C_{\ell_T}/\partial \beta$, a_{1F}, a_{1T} calculated from Refs.3 and 7. It is seen that $(\partial C_{\ell_T}/\partial \beta)/a_{1F}\, a_{1T}$ is roughly independent of Mach number. This is an interesting result as it confirms that equation (6) is valid when there is a large Mach number effect on both the fin and the tailplane.

Finally it should be remarked that the theory of Ref.10 quotes rolling moments on fin tailplane combinations in addition to the fin lifts. As the author stated, equation (59), the Joukowski condition on a real tailplane is not satisfied; each side of the tailplane in this theory twists differentially as the sideslip increases. This may not seriously affect the fin lift. The Mach number effects on the rolling moments are given simply by

$$\frac{\partial C_{\ell_T}}{\partial \beta}\bigg/ a_{1F} = \text{constant} \quad ,$$

the Mach number effect on the tailplane having been omitted.

4.3   Analogous model tests

Instead of calculating the loads on the analogous configuration, as in the examples given above in 4.2, the loads on the analogous configuration may be measured in a low speed wind tunnel. Analogous tailplanes for Model A at $M = 0$ and at $M = 0.70$ (fin and tail chords increased 40%) were tested in the 13ft × 9ft tunnel at Bedford to test the validity of

equation (6) at M = 0 and M = 0.70. The model wings were removed and the body was attached by wires to the six component tunnel balance*. The rolling moment on the tailplane was measured by an auxiliary balance. The results of these experiments are now described.

Fig.38 shows the increase in the tailplane rolling moment between M = 0 and M = 0.70**. Fig.39 shows that there is only a very small increase in the fin lift. Fig.40 shows the increase in the tailplane lift. This data has been replotted in Fig.34. The rolling moment and the fin lift measured on the analogous models are lower than for the high speed model (Figs.34a and b) but the tailplane lifts agree well (Fig.34c). Fig.34d confirms that the Mach number effect on this configuration comes primarily from the tail lift, as $(\partial C_{\ell_T}/\partial\beta)/a_{1F}\, a_{1T}$ is constant for the analogous models and agrees reasonably well with that for the high speed model.

4.4 Supersonic speeds

The area of the tailplane influenced by the fin decreases as the Mach number increases and so the rolling moment decreases and the centre of lift due to sideslip moves inboard (F increases). These two effects are illustrated by the simple supersonic case sketched in Fig.41, for which

$$\frac{\partial C_{\ell_T}}{\partial\beta} = -\frac{2}{3}\left(\frac{c}{b_T}\right)^2 \frac{1}{(M^2-1)^{3/2}} \quad .$$

Also

$$F = \frac{1}{\left[1 - \dfrac{a(M^2-1)^{\frac{1}{2}}}{c}\right]^3}$$

which shows that F increases with Mach number.

Similar trends are shown for Model A, although the leading edge of the fin is subsonic in the range of these tests. However F remains about 1.4 from M = 1.3 to 1.6 (Fig.42) and by M = 2.0 has increased to 1.55 which indicates an inboard movement of the centre of lift. Fig.34d has not been extended to supersonic speeds as the simple concepts embodied in equations (2) and (3) are then invalid.

---

* Both tailplanes were tested on the same body, which was correct for M = 0. The body was slender and pointed at the rear so that the results for M = 0.7 should not be greatly in error.

** There is a small contribution of C_{L_T} to the tailplane rolling moments. The data given in Fig.38 has been adjusted to $C_{L_T} = 0$: a linear variation with C_{L_T} was assumed (cf. 4.5 below).

4.5   Tailplane lift effect

It is remarked above that the effects of incidence on the tailplane roll-ing moments are generally small in the absence of separations. The effects are due to both the displacement with sideslip of the wing downwash field (wing lift effect) and the displacement of the tailplane trailing vortices (tailplane lift effect). The contribution to $\partial C_{\ell_T}/\partial\beta$ from the tailplane lift C_{L_T} in the absence of the fin can be estimated by the methods given in Refs.11 and 12 for subsonic and supersonic speeds.

5   CONCLUSIONS

Measurements of the rolling moments due to sideslip on three high tail-planes show considerable variations with Mach number and incidence in the subsonic and transonic speed range.

The increase in $|\partial C_{\ell_T}/\partial\beta|$ with Mach number is associated with increases in both a_{1F} and a_{1T}. A method of estimating this Mach number variation by extrapolation from the low speed values of $|\partial C_{\ell_T}/\partial\beta|$, a_{1F} and a_{1T} has been suggested which gives reasonable agreement with the measurements.

The tailplane rolling moments are generally reduced by separations at transonic speeds. These separations may be reduced at the higher Reynolds numbers in flight thus giving higher rolling moments. The separations are affected by changes in incidence and tail setting.

Measurements on one model show that $|\partial C_{\ell_T}/\partial\beta|$ decreases rapidly from M = 1.30 to 2.00.

SYMBOLS

A	aspect ratio
a	distance of bending moment station from centre line
a_1	lift curve slope
b	span
$\bar{\bar{c}}$	aerodynamic mean chord
c	chord
C_B	bending moment coefficient $=$ moment$/q\,S_T\,b_T$
C_{ℓ_T}	tailplane rolling moment coefficient $=$ $L_T/q\,S_T\,b_T$
$\dfrac{\partial C_{\ell_T}}{\partial \beta}$	slope/radian of $C_{\ell_T} - \beta$ curve at $\beta = 0^{\circ}$
C_{L_T}	tailplane lift coefficient
F	load distribution factor
L	rolling moment
$k,\ \ell,\ m$	experimental constants
M	Mach number
q	kinetic pressure $=$ $\frac{1}{2}\rho\,U^2$
S	area
U	free stream velocity
α	incidence
β	sideslip
ζ	rudder deflection
η	tailplane angle
λ	taper ratio
ξ	aileron angle
ϕ	sweepback angle

Subscripts

B	body
F	fin
T	tailplane
W	wing

REFERENCES

No.	Author(s)	Title, etc.
1	E.P. Sutton A. Stanbrook M.J. Caiger	Performance of the 36 x 35 inch slotted transonic working section of the R.A.E. Bedford 3ft wind tunnel. (A.R.C. R & M 3228) January 1960
2	D.E. Morris	Calibration of the flow in the working section of the 3' x 3' tunnel at N.A.E. (A.R.C. CP.261) September 1954
3	M.J. Queijo D.R. Riley	Calculated subsonic span loads and resulting stability derivatives of unswept and 45° swept tail surfaces in sideslip and steady roll. NACA T.N. 3245 October 1954
4	E.P. Sutton A. Stanbrook	A wind tunnel investigation of the longitudinal stability of the Javelin aircraft at transonic speeds, including a comparison with flight test results. (A.R.C. R & M 3403) December 1959
5	D.G. Mabey	Unpublished Mintech Report
6		A.R.A. wind tunnel test note F2/1. Unpublished
7	A.S. Stanbrook	The lift curve slope and aerodynamic centre position of wings at subsonic and supersonic speeds. R.A.E. T.N. Aero 2328 (A.R.C. 17615) November 1954
8	D.R. Riley	Effect of horizontal tail-span and vertical location on the aerodynamic characteristics of an unswept tail assembly in sideslip. NACA Report 1171 (Formerly NACA T.N. 2907) (1954)
9	S. Goldstein A.D. Young	The linear perturbation theory of compressible flow with applications to wind-tunnel interference. (A.R.C. R & M 1909) July 1943

REFERENCES (Contd.)

No.	Author	Title, etc.
10	J. Weber A.C. Hawk	Theoretical load distributions on fin-body-tailplane arrangements in a side wind. (A.R.C. R & M 2992) August 1954
11	M.J. Queijo	Theoretical span load distributions and rolling moments for sideslipping wings of arbitrary planform in incompressible flow. NACA Report 1269 (Supersedes NACA T.N. 3605) (1956)
12	W.L. Sherman K. Margolis	Theoretical calculations of the effects of finite sideslip at supersonic speeds on the span loading and rolling moment for families of thin swept back tapered wings at an angle of attack. NACA T.N. 3046 November 1953

AILERON DEFLECTED
10 3° FOR ONE TEST

RUDDER DEFLECTED 9·3°
FOR ONE TEST

CYLINDRICAL FAIRING

WING-BODY ANGLE 2°

SCALE   1   2   3   4   5 INCHES
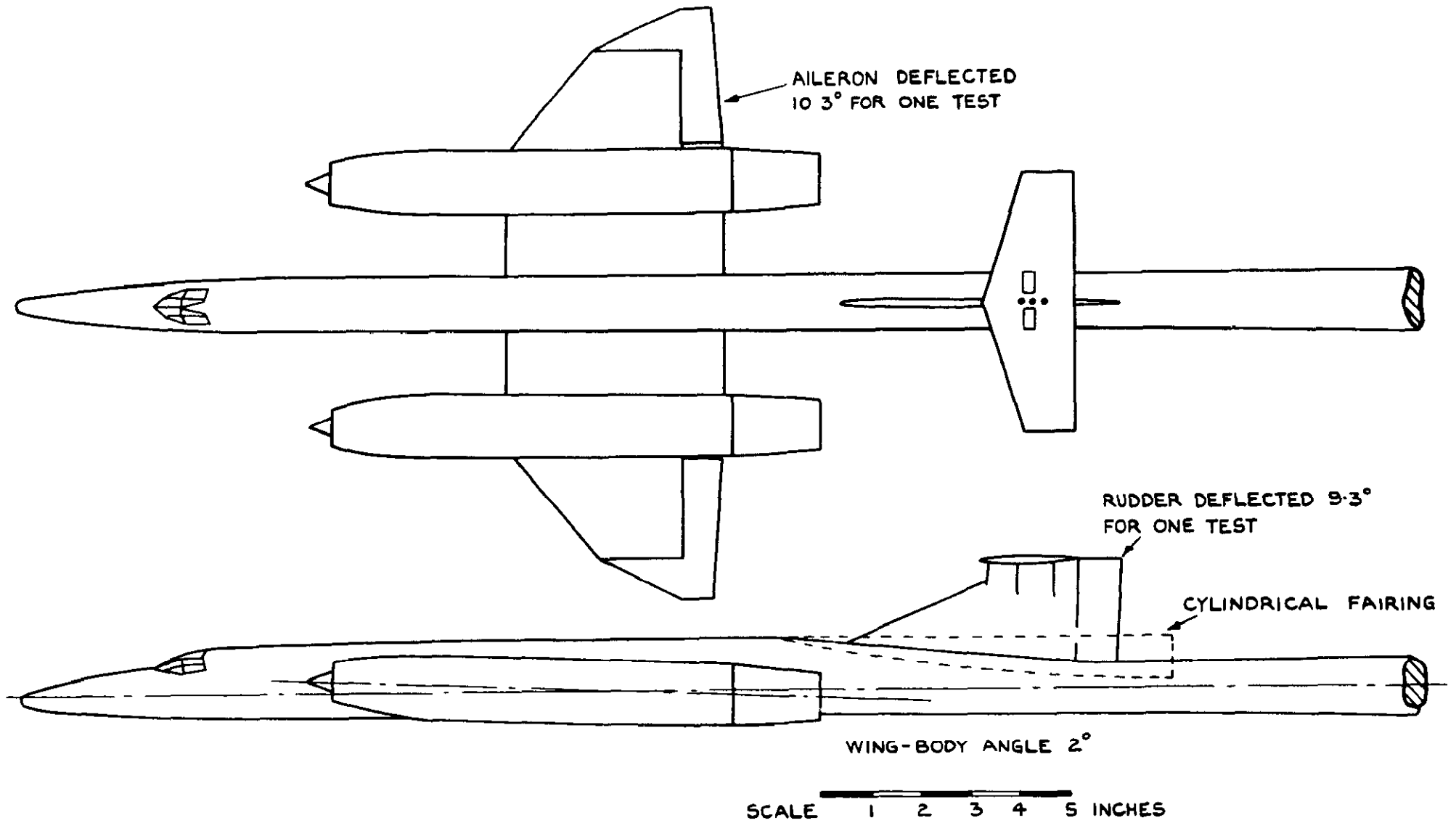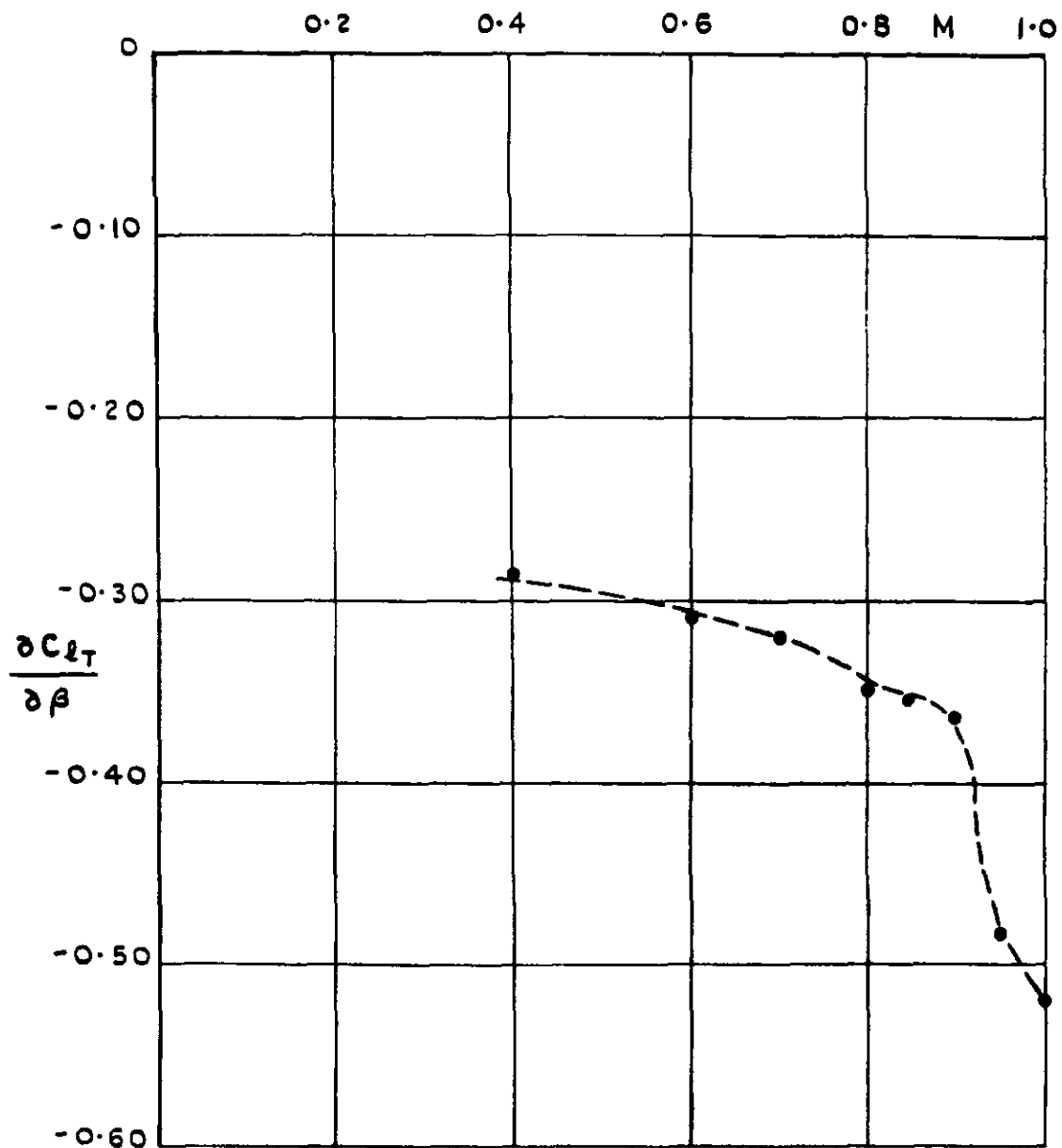
FIG.I. G.A. OF MODEL A.

FIG. 2. MODEL A. VARIATION OF TAILPLANE
ROLLING MOMENT CURVE SLOPE WITH
MACH NUMBER. WINGS OFF $\alpha_B = 0°$.

WING-BODY ANGLE 2·5°

SCALE   1   2   3   INCHES
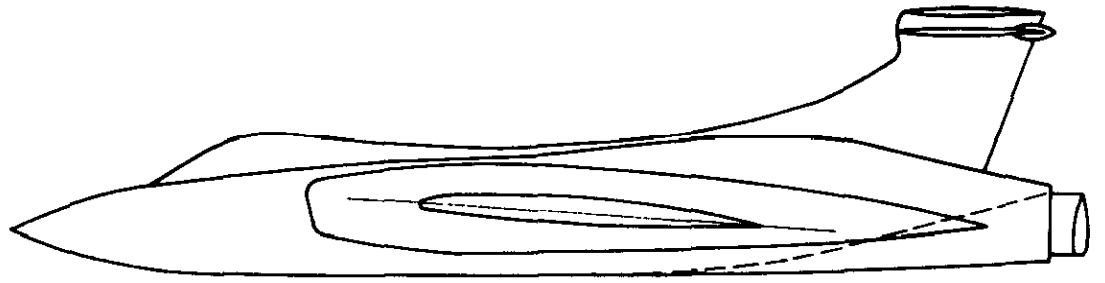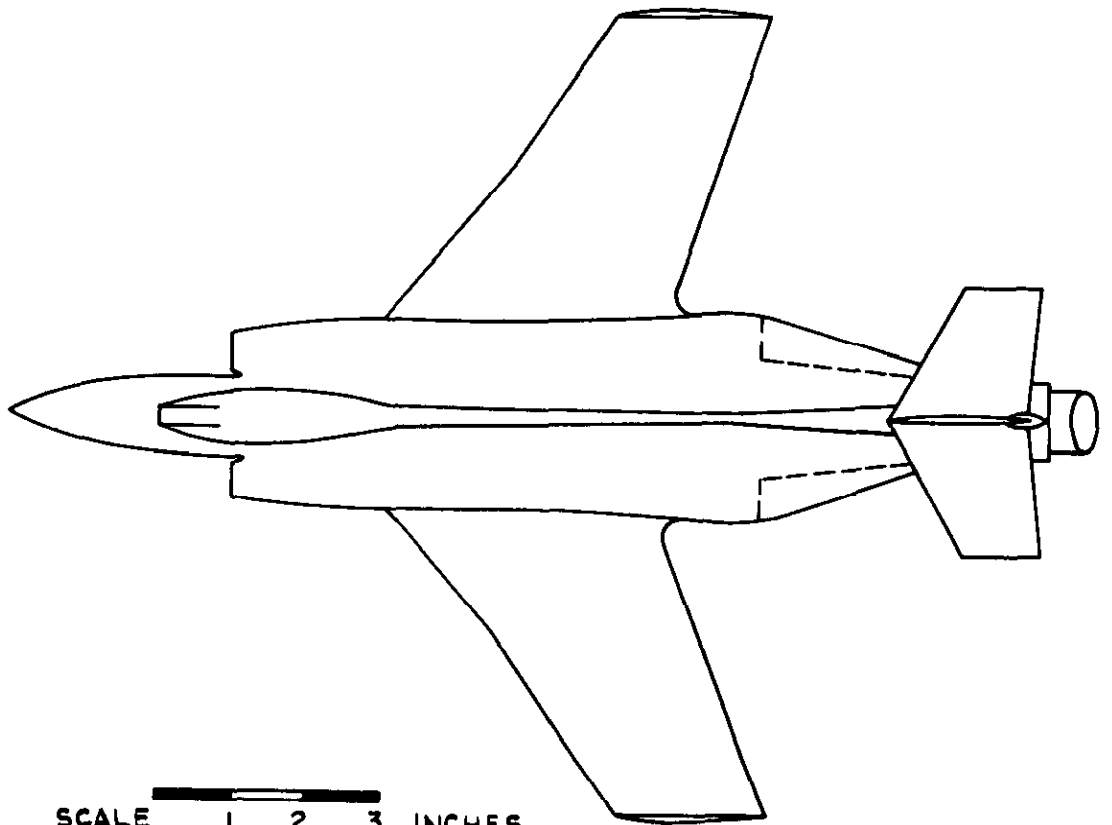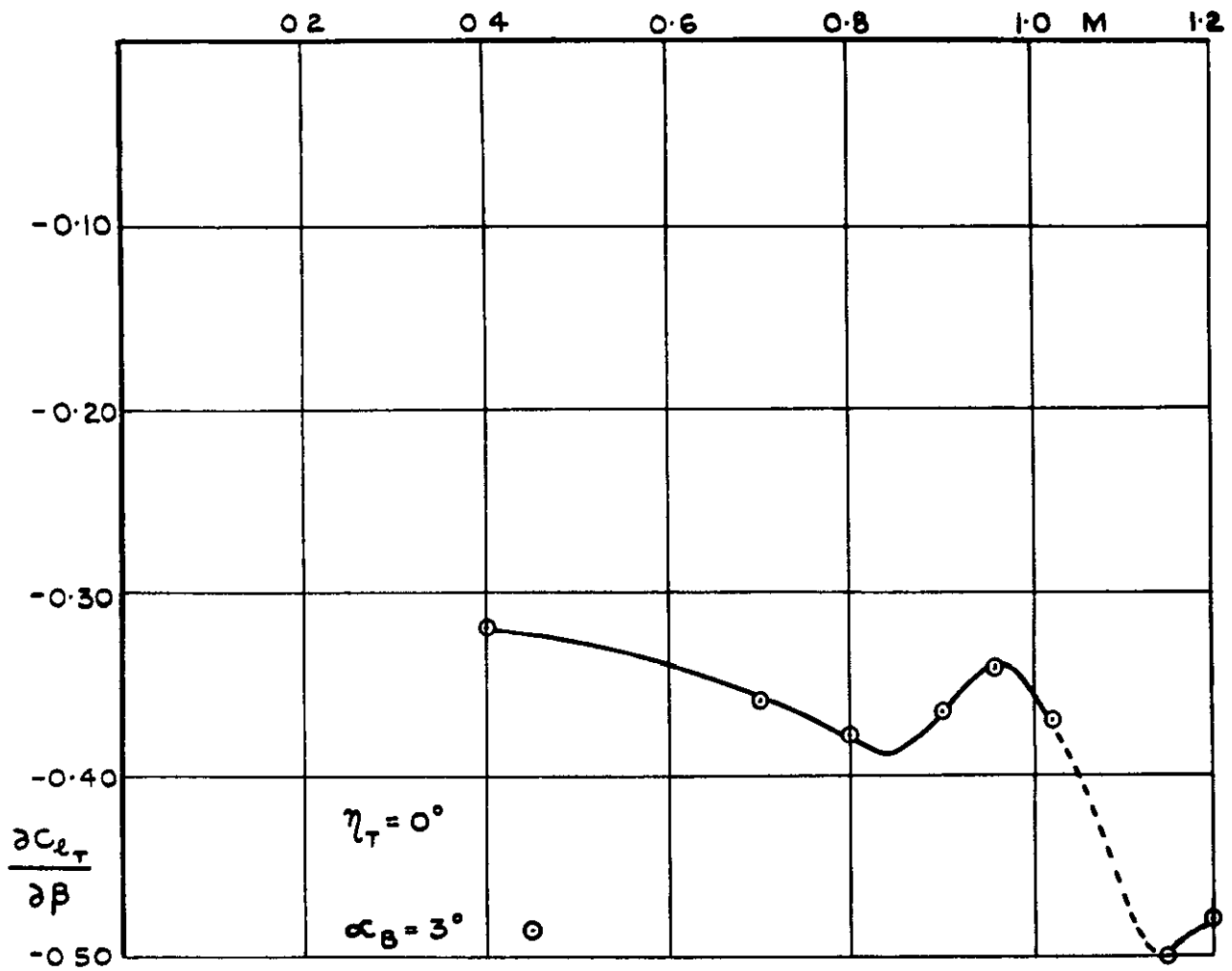
FIG.3. G.A. OF MODEL B.

FIG.4. MODEL B. VARIATION OF TAILPLANE
ROLLING MOMENT CURVE SLOPE WITH
MACH NUMBER $\alpha_B = 3°$ $\eta_T = 0$.

SCALE ▮▯▮▯▮ INCHES
1 2 3 4 5

WING BODY ANGLE 2°
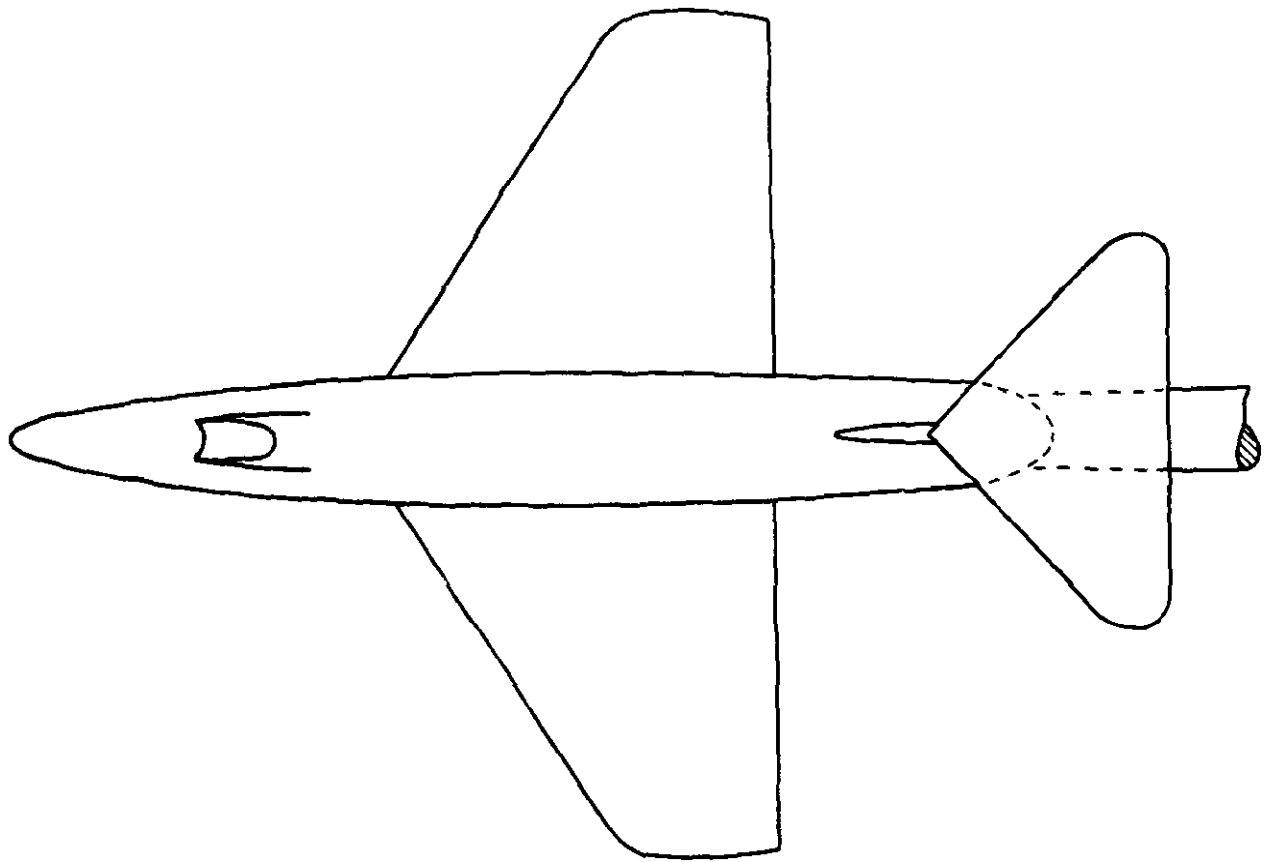
FIG.5. G.A. OF MODEL C.
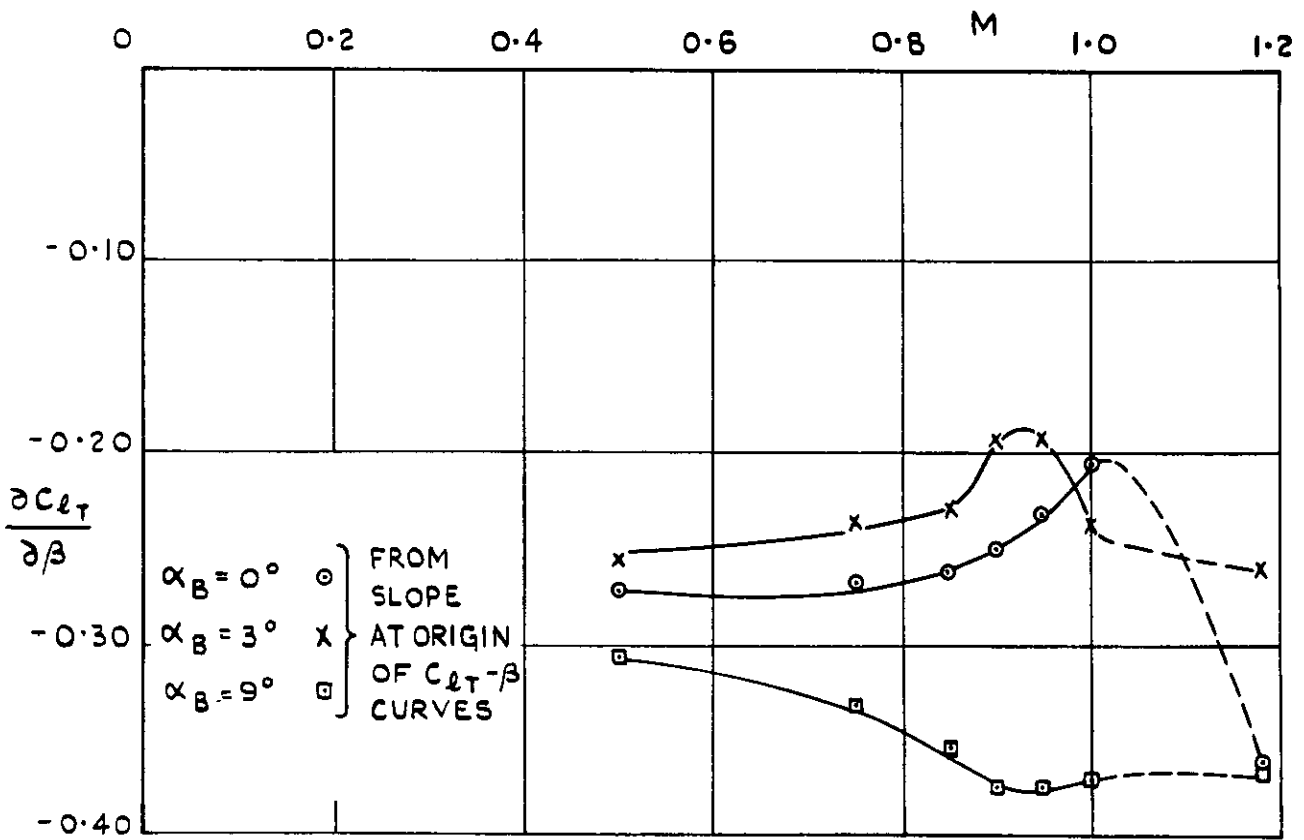
FIG.6. MODEL C. VARIATION OF TAILPLANE
ROLLING MOMENT CURVE SLOPE WITH
MACH NUMBER.

TYPICAL FIN SECTION

0.015"R

0.167" CONSTANT

0.5"

1.2"

$A_F = 0.48$ $\phi_{LE} = 63°$

$S_F = 8.84 \text{ IN}^2$

$b_F = 2.05 \text{ INS.}$

SLOT WIDTHS 0.020"

$t/c = 0.08$

$C_{\ell T}$ GAUGES

$t/c = 0.03$
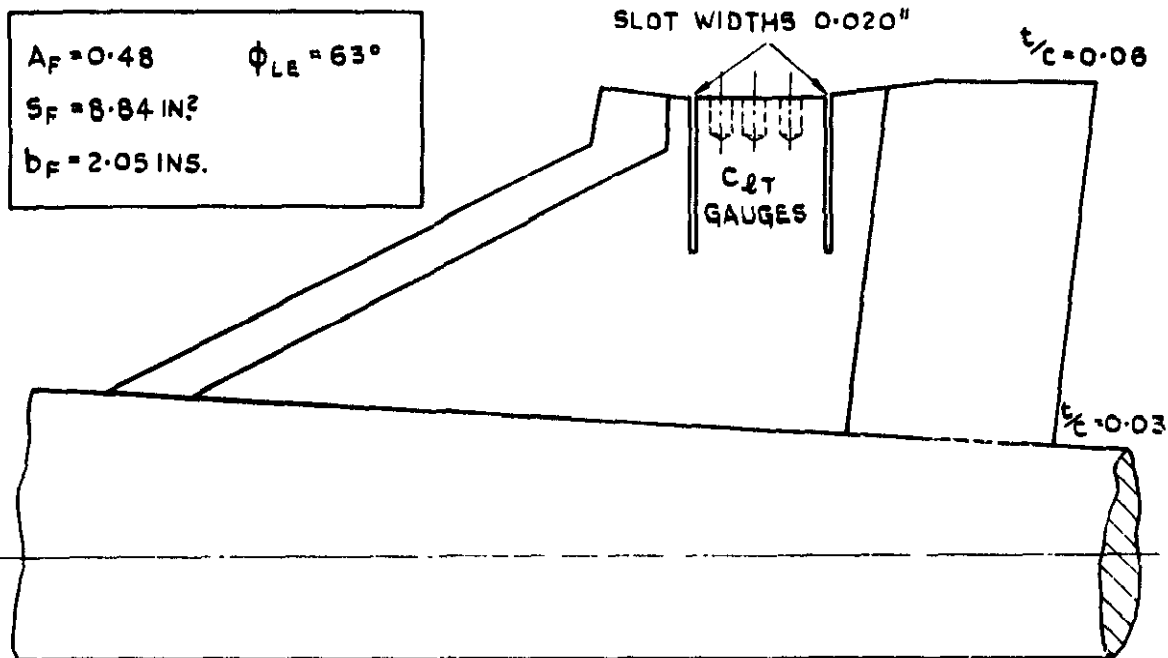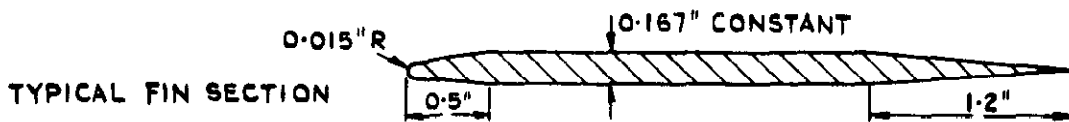
FIN-BUILT INTO BODY

TAILPLANE SECTION - BICONVEX $t/c = 0.04$

$A_T = 3.44$ $\lambda = 0.50$

$S_T = 7.74 \text{ IN}^2$ $\bar{\bar{c}} = 1.55 \text{ INS}$

$b_T = 5.17 \text{ INS.}$

C_{B2} GAUGES

0.30"

0.30"

C_{B1} GAUGES
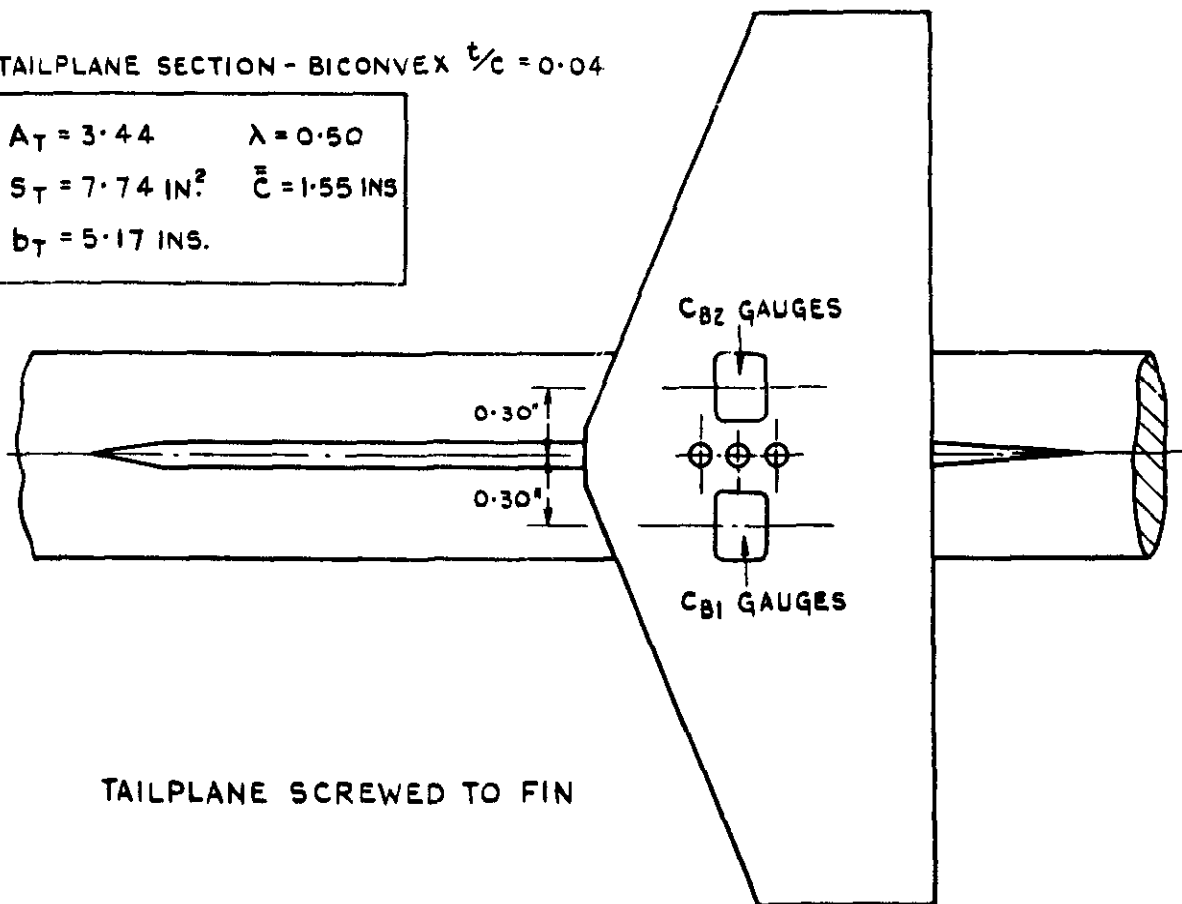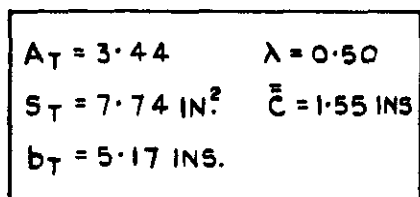
TAILPLANE SCREWED TO FIN

FIG.7. GEOMETRY OF FIN AND TAILPLANE
OF MODEL A.
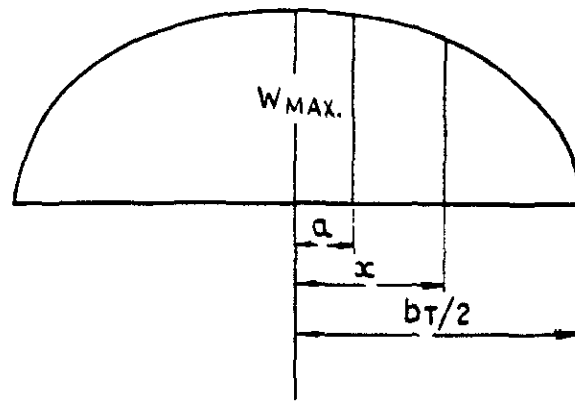
(a). SPANWISE LOAD DISTRIBUTION DUE TO INCIDENCE

$$W(x) = W_{MAX.} \left[1 - \left(2x/b_T \right)^2 \right]^{\frac{1}{2}}.$$
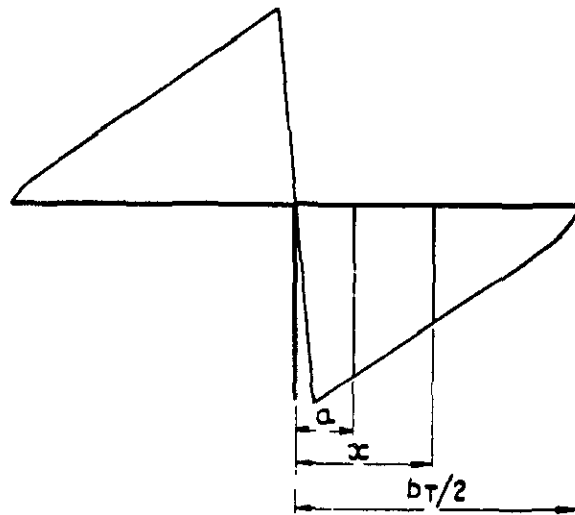
(b). SPANWISE LOAD DISTRIBUTION DUE TO SIDESLIP

$$W(x) \doteqdot W_{MAX} \left(1 - 2x/b_T \right).$$

FIG. 8 (a & b). POSSIBLE TYPES OF LOAD
DISTRIBUTION.
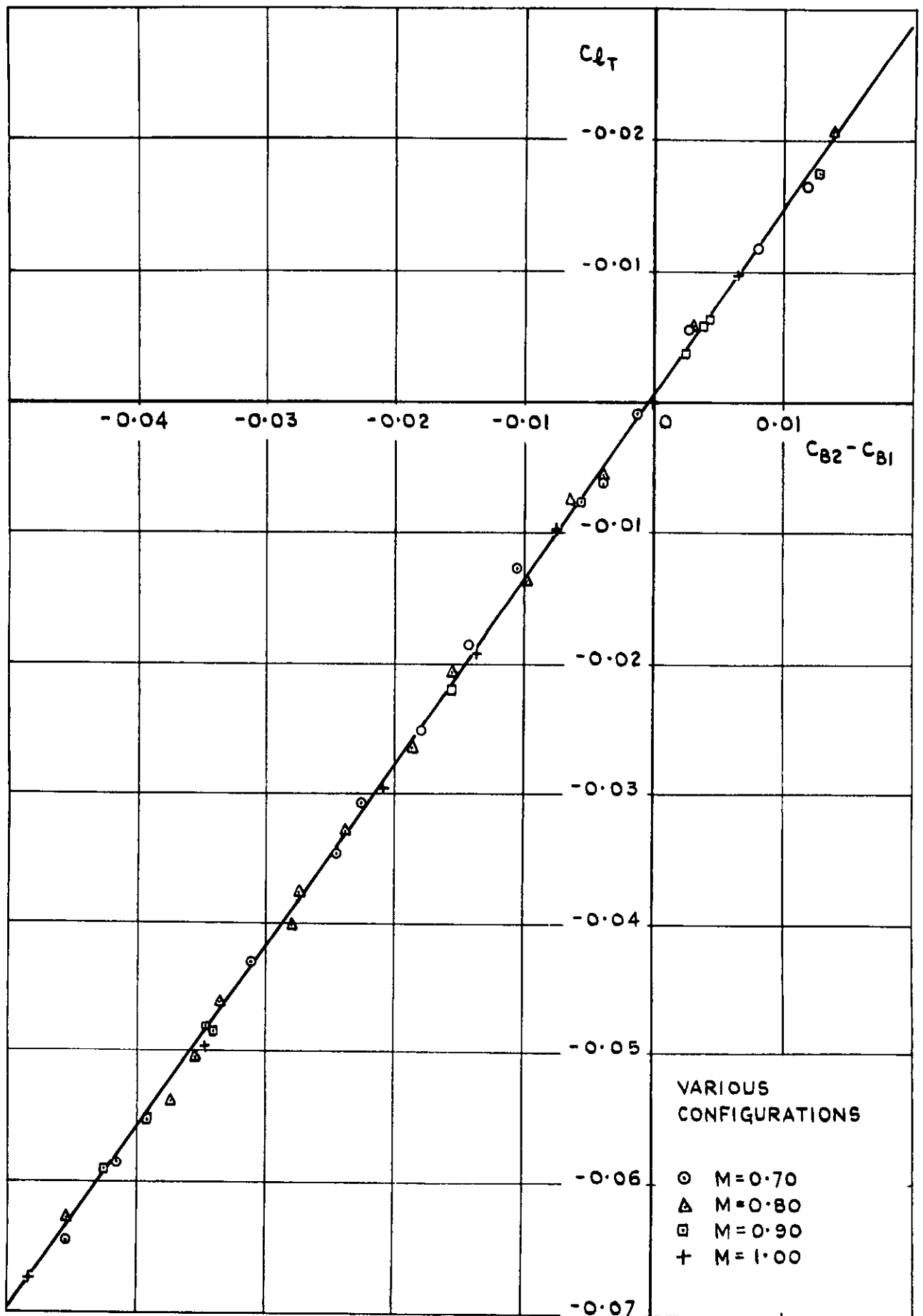
FIG.9. MODEL A. SUBSONIC AND TRANSONIC.
CORRELATION BETWEEN C_{ℓ_T} AND $(C_{B2} - C_{B1})$.

$A_F = 0.76$

$S_F = 3.80$ IN.²

$b_F = 1.70$ INS.

$t/c = 0.07$

$\eta_T = 0°$ AND $\eta_T = -4°$
TAILPLANES
CARRIED ON
INSERTS

N.B.
0.010" CLEARANCE
BETWEEN
BULLET AND
TAILPLANE

$A_T = 2.61$ $\lambda = 0.58$

$S_T = 4.62$ IN.² $\phi_{LE} = 29.5°$

$b_T = 3.49$ INS. $\bar{\bar{C}} = 1.36$ INS

$t/c = 0.05$

C_{B2} GAUGES

C_{B1} GAUGES

SLOT

0.2

0.2

ELLIPSE

t_{MAX}

TANGENTS

0.35 C

0.54 C

C

SECTION OF FIN AND TAILPLANE
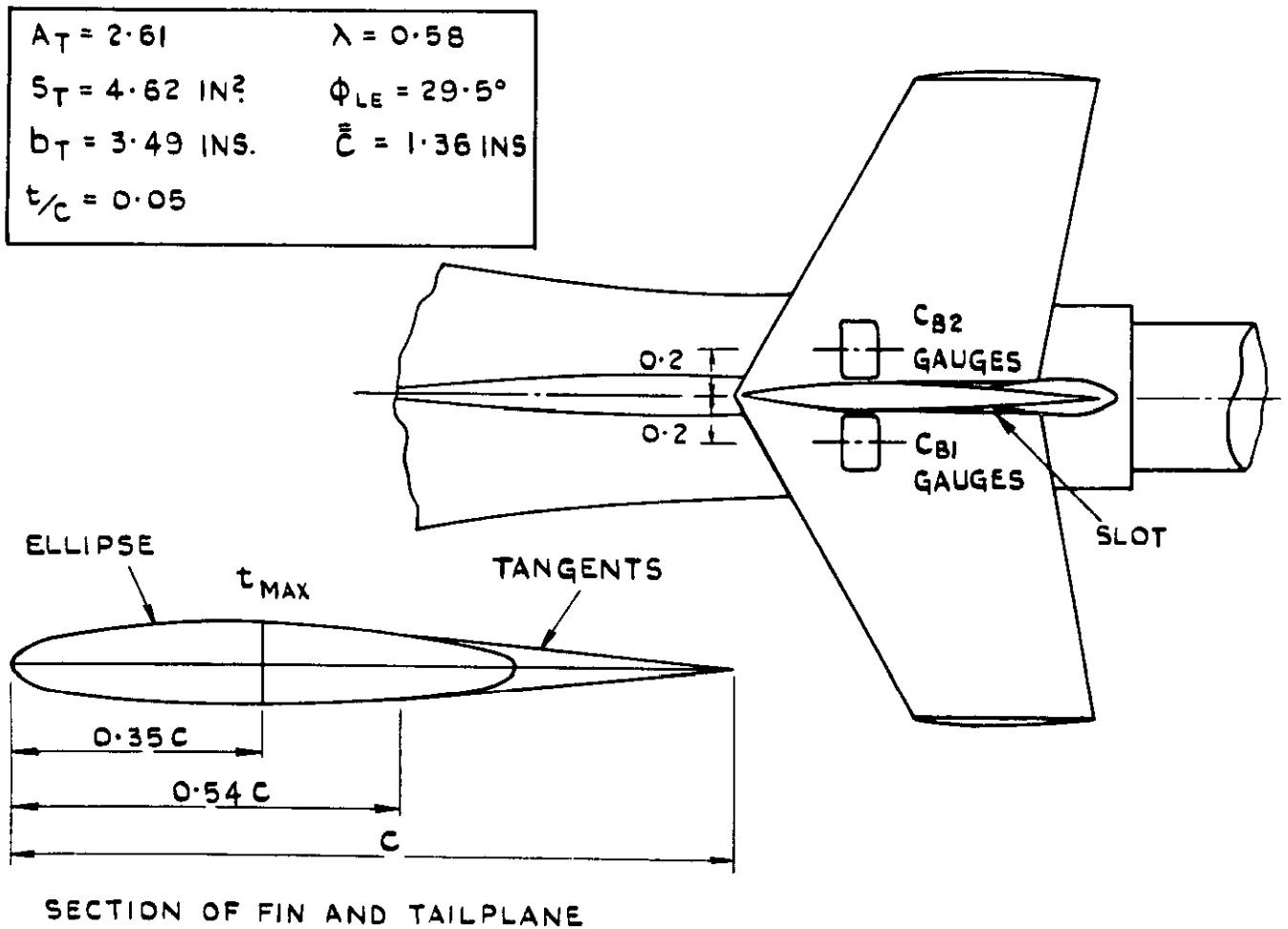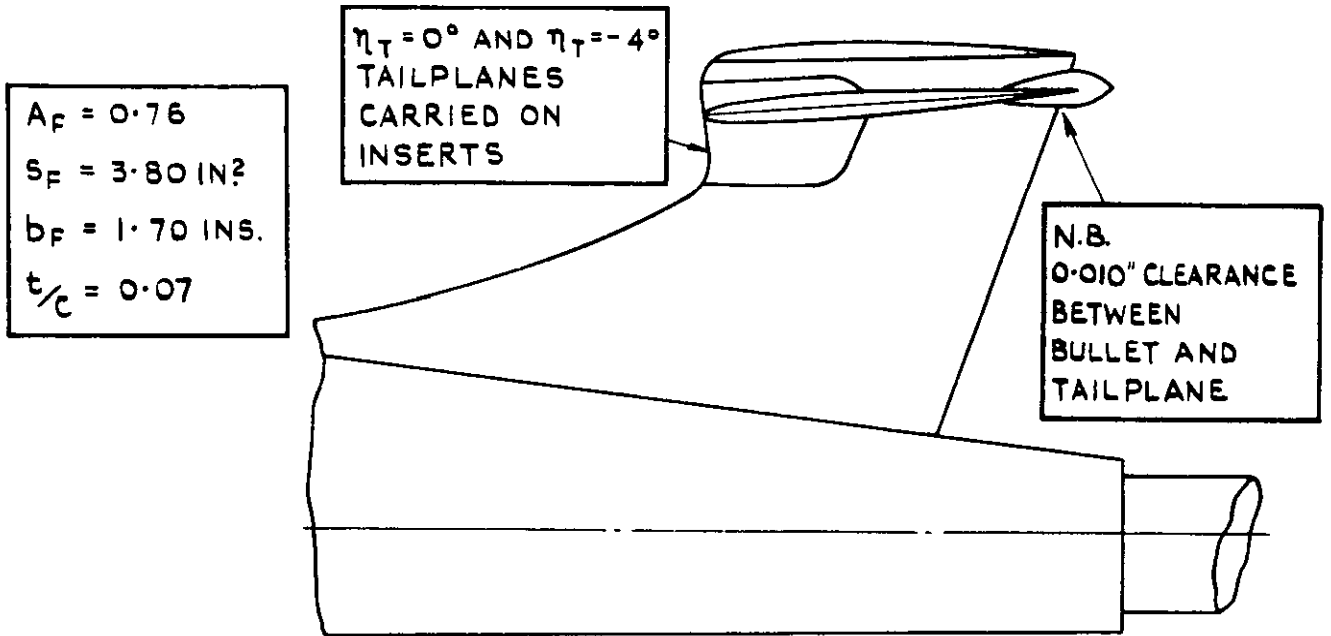
FIG.10. GEOMETRY OF FIN AND TAILPLANE OF MODEL B.

$A_F = 0.50$

$S_F = 28.0 \text{ IN}^2$

$b_F = 3.72 \text{ INS.}$

RAE 102 $t/c = 0.07$
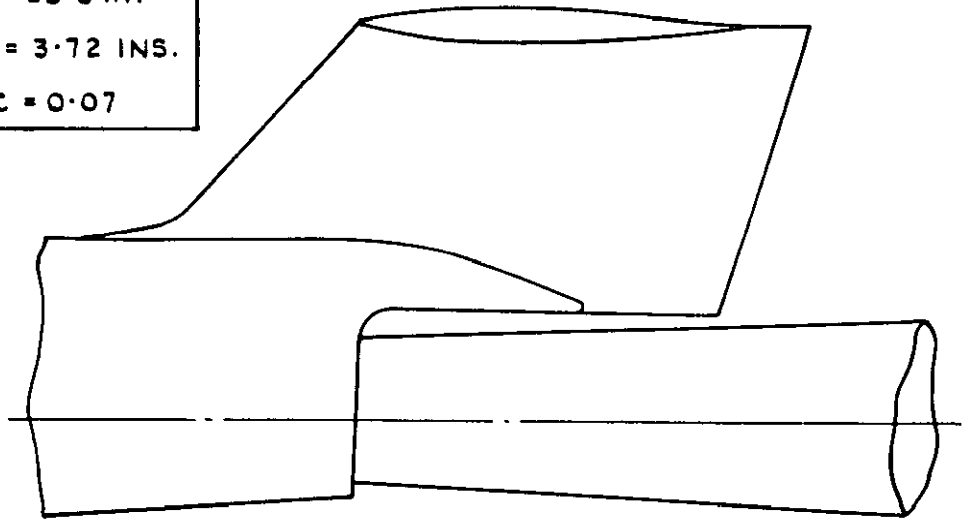
$A_T = 2.57$

$S_T = 41.3 \text{ IN}^2$

$b_T = 10.3 \text{ INS}$

$\bar{\bar{c}} = 5.36 \text{ INS}$

RAE 102 $t/c = 0.06$
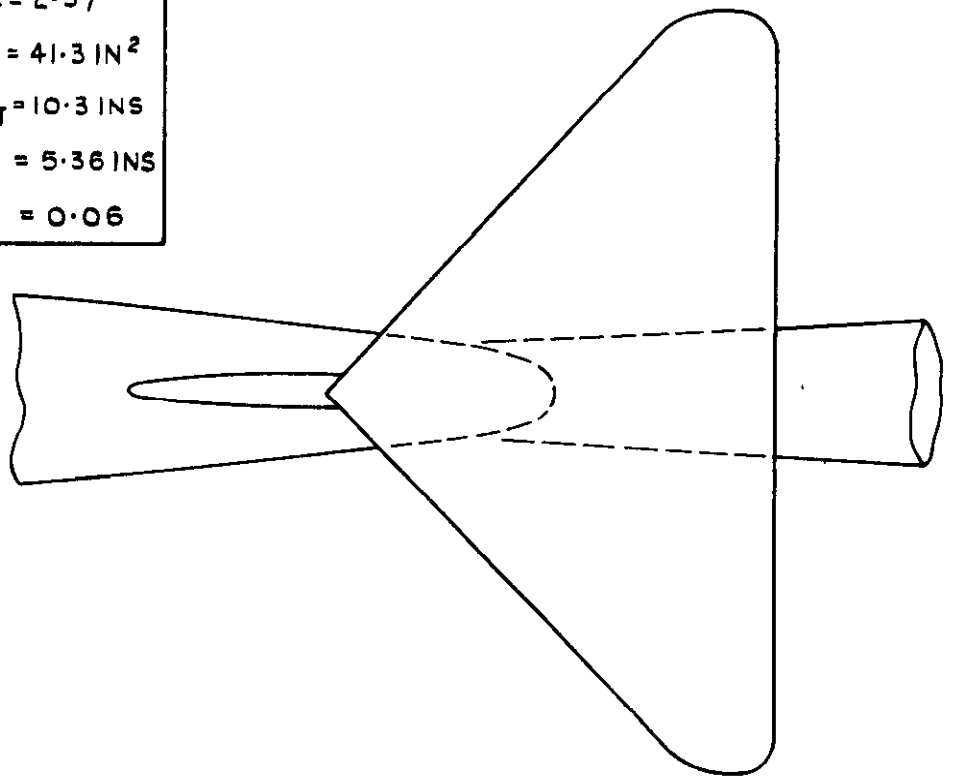
FIG.11. GEOMETRY OF FIN AND TAILPLANE
OF MODEL C.
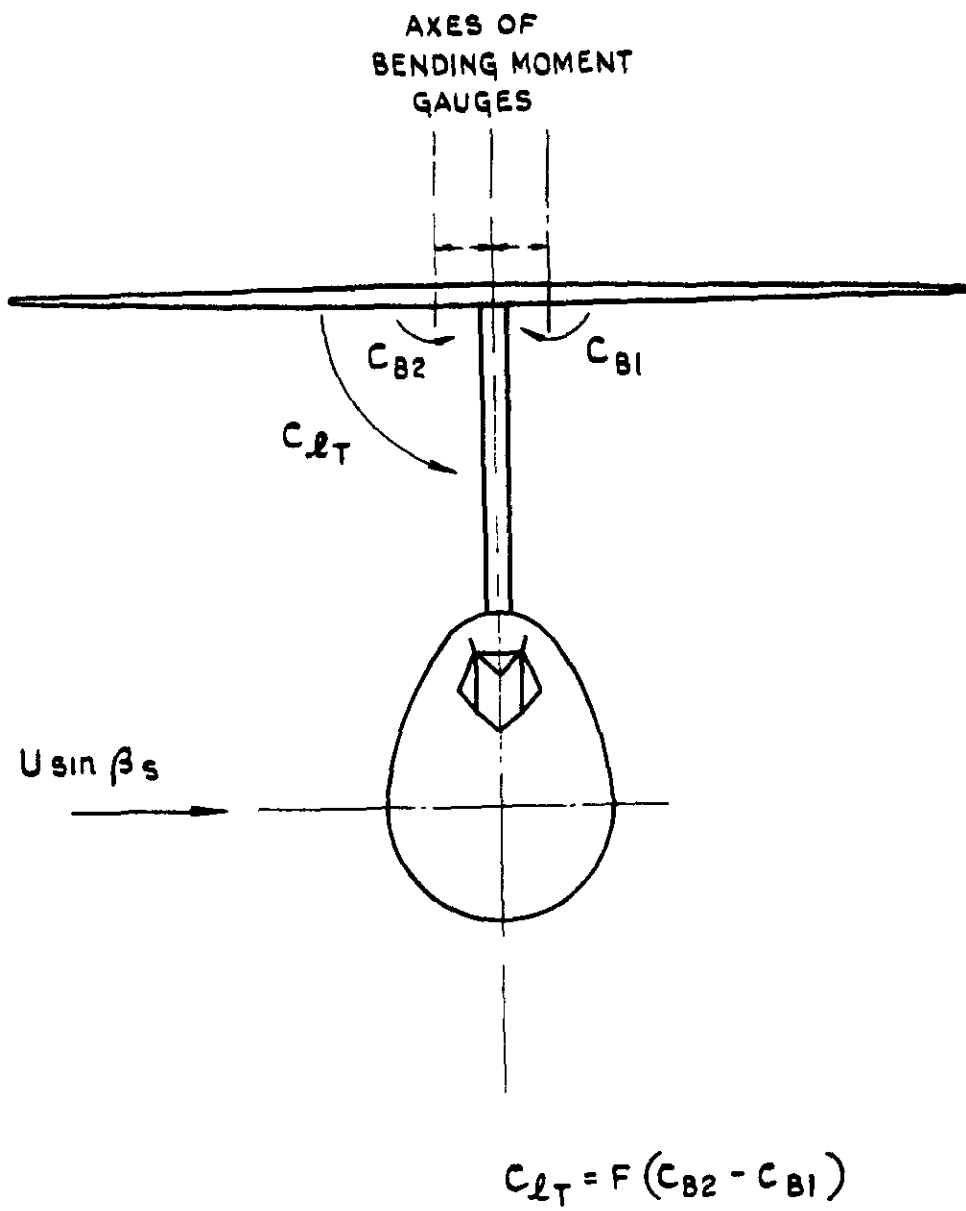
FIG.12. SIGN CONVENTION.
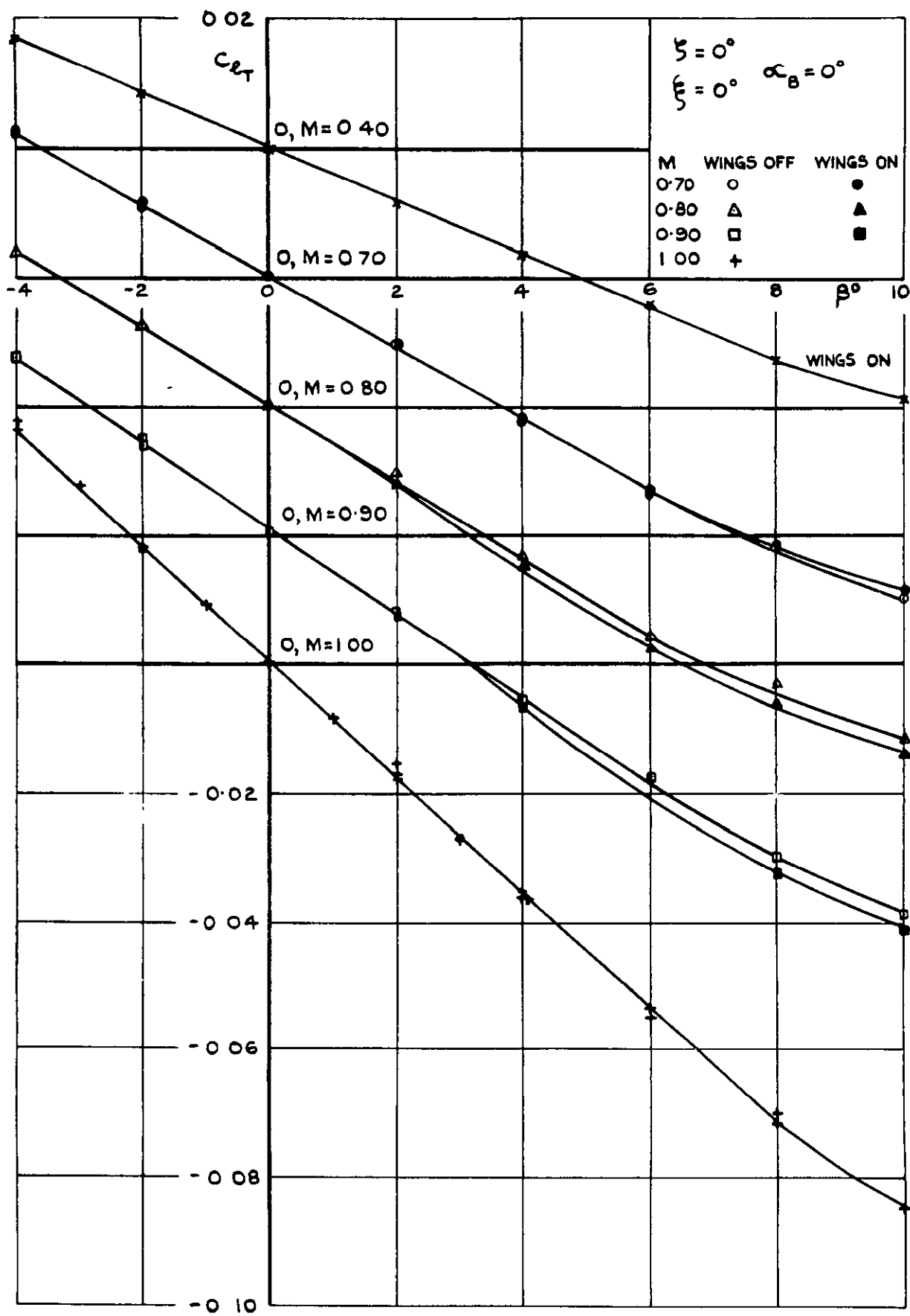
FIG.13. MODEL A - SUBSONIC AND TRANSONIC.
VARIATION OF TAILPLANE ROLLING
MOMENT WITH SIDESLIP. WINGS OFF AND
WINGS ON. $\alpha_B = \zeta = \xi = 0°$.
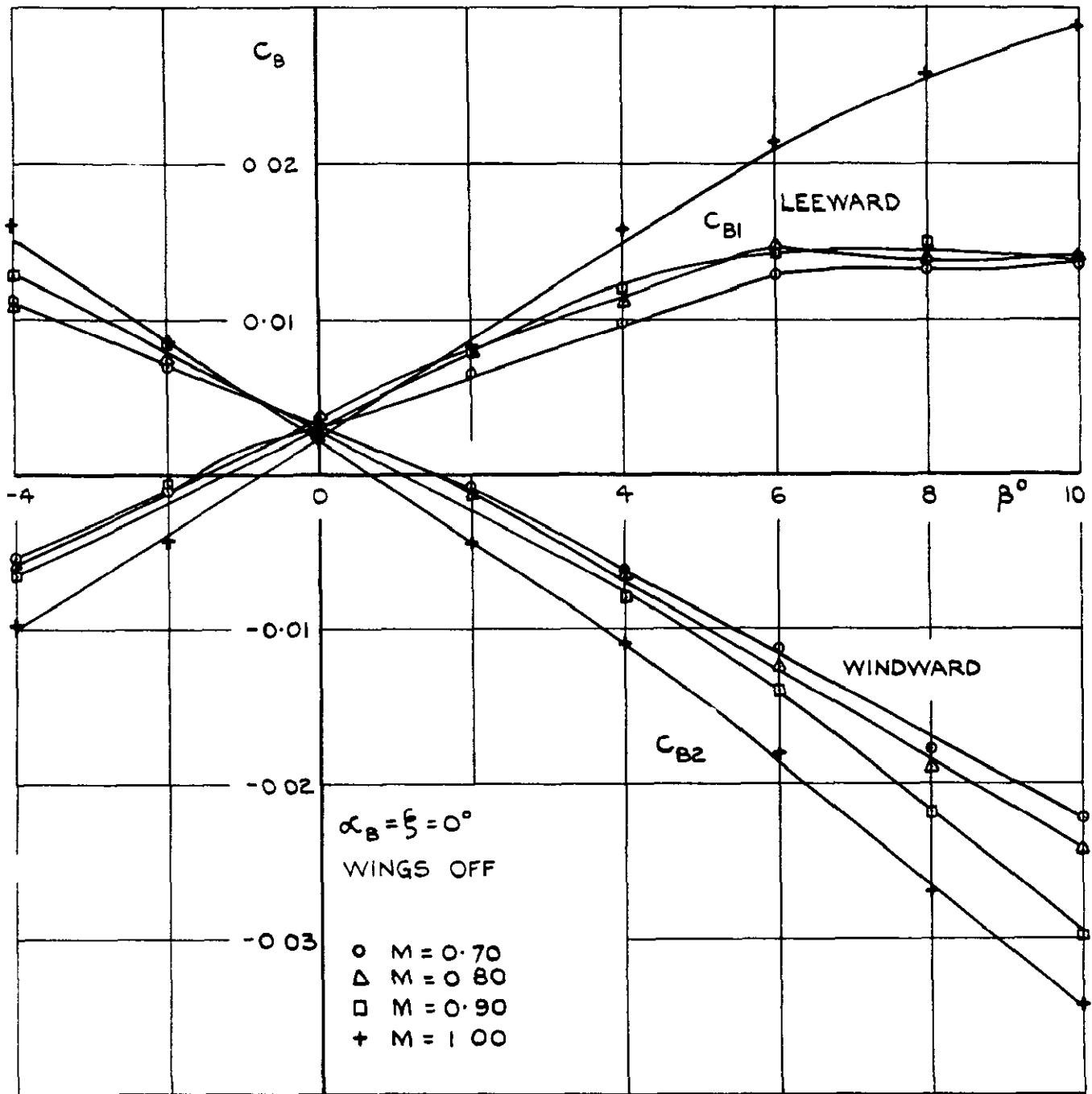
FIG.14. MODEL A - SUBSONIC AND TRANSONIC.
VARIATION OF TAILPLANE BENDING MOMENTS
WITH SIDESLIP. WINGS OFF $\alpha_B = \xi = 0°$.
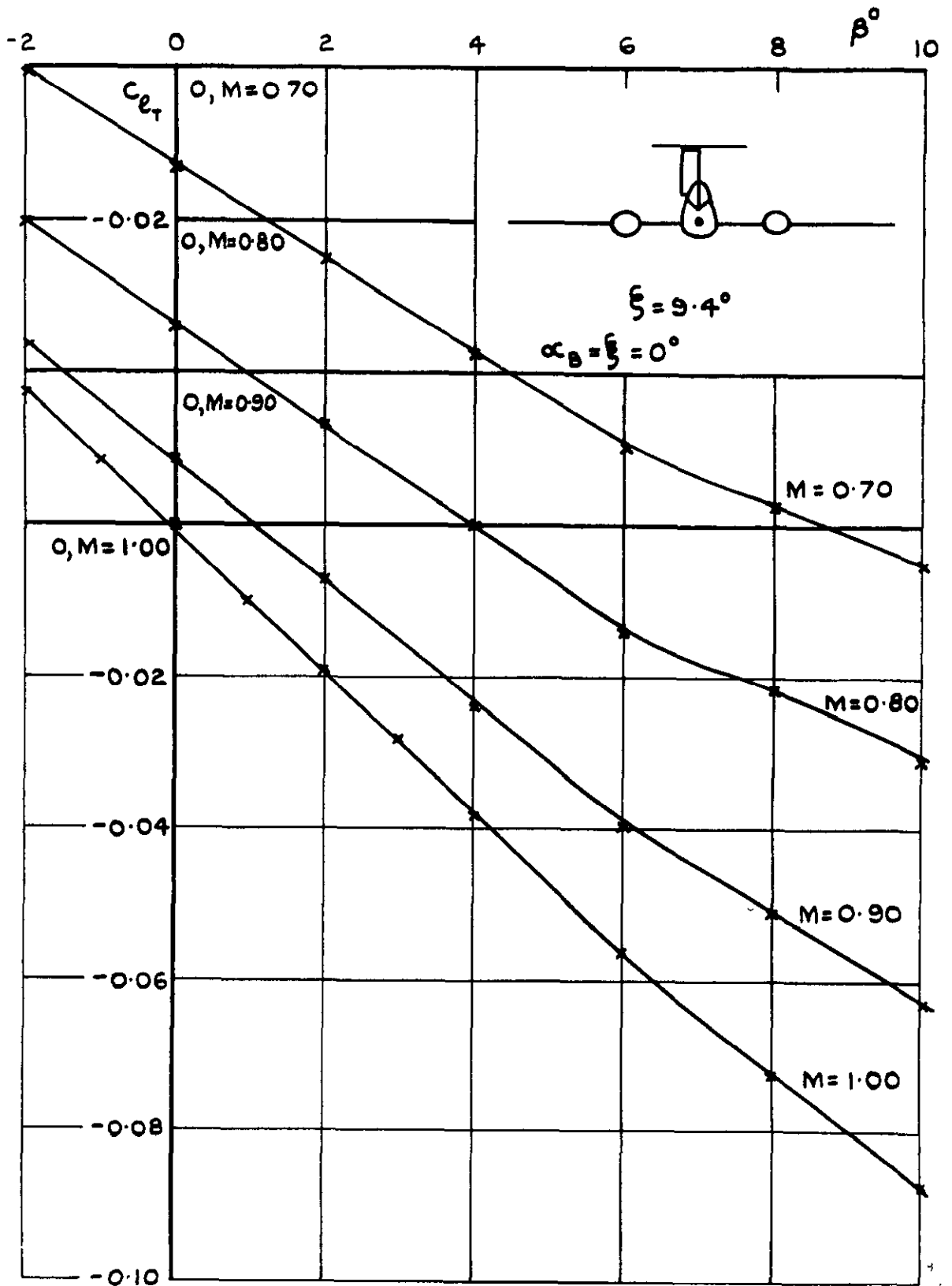
FIG. 15. MODEL A – SUBSONIC AND TRANSONIC.
VARIATION OF TAILPLANE BENDING MOMENTS
WITH SIDESLIP. $\alpha_B = \xi = 0°$. $\xi = 9 \cdot 4$.
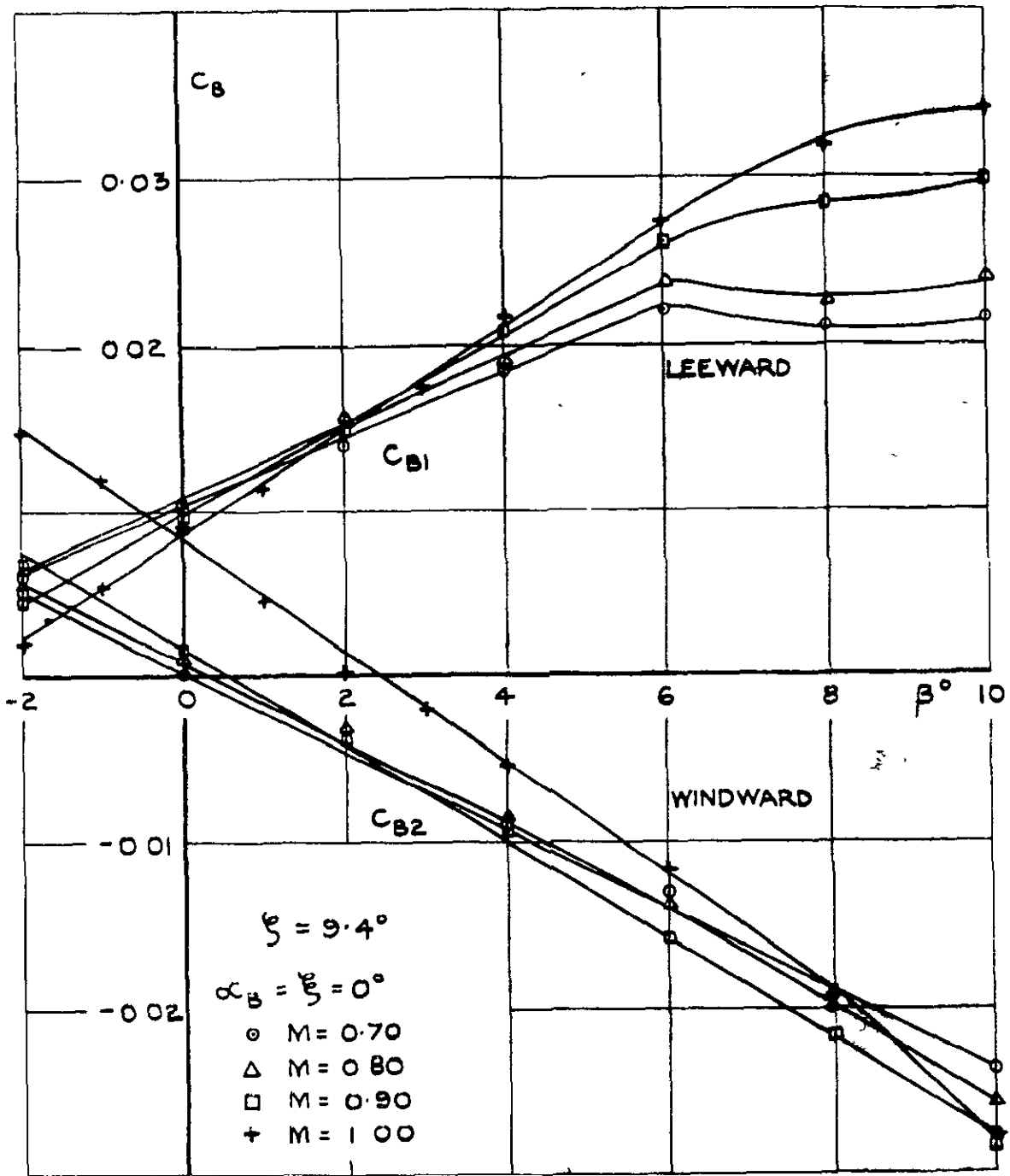
FIG. 16. MODEL A — SUBSONIC AND TRANSONIC. VARIATION OF TAILPLANE BENDING MOMENTS WITH SIDESLIP. $\alpha_B = \xi = 0°$ $\zeta = 9.4°$.
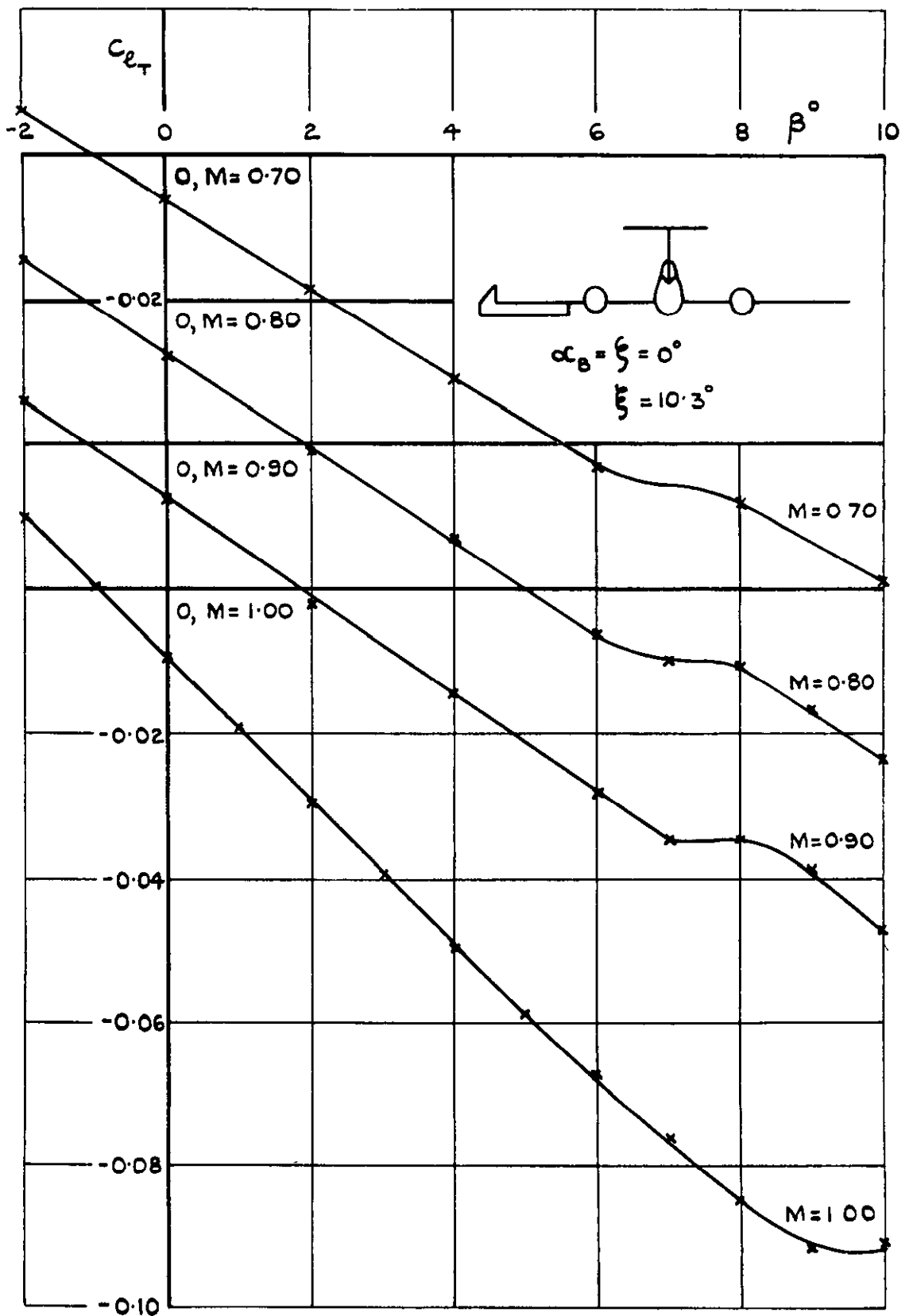
FIG.17. MODEL A – SUBSONIC AND TRANSONIC. VARIATION OF TAILPLANE ROLLING MOMENT WITH SIDESLIP. $\alpha_B = \xi = 0°$ $\xi = 10\cdot3°$.
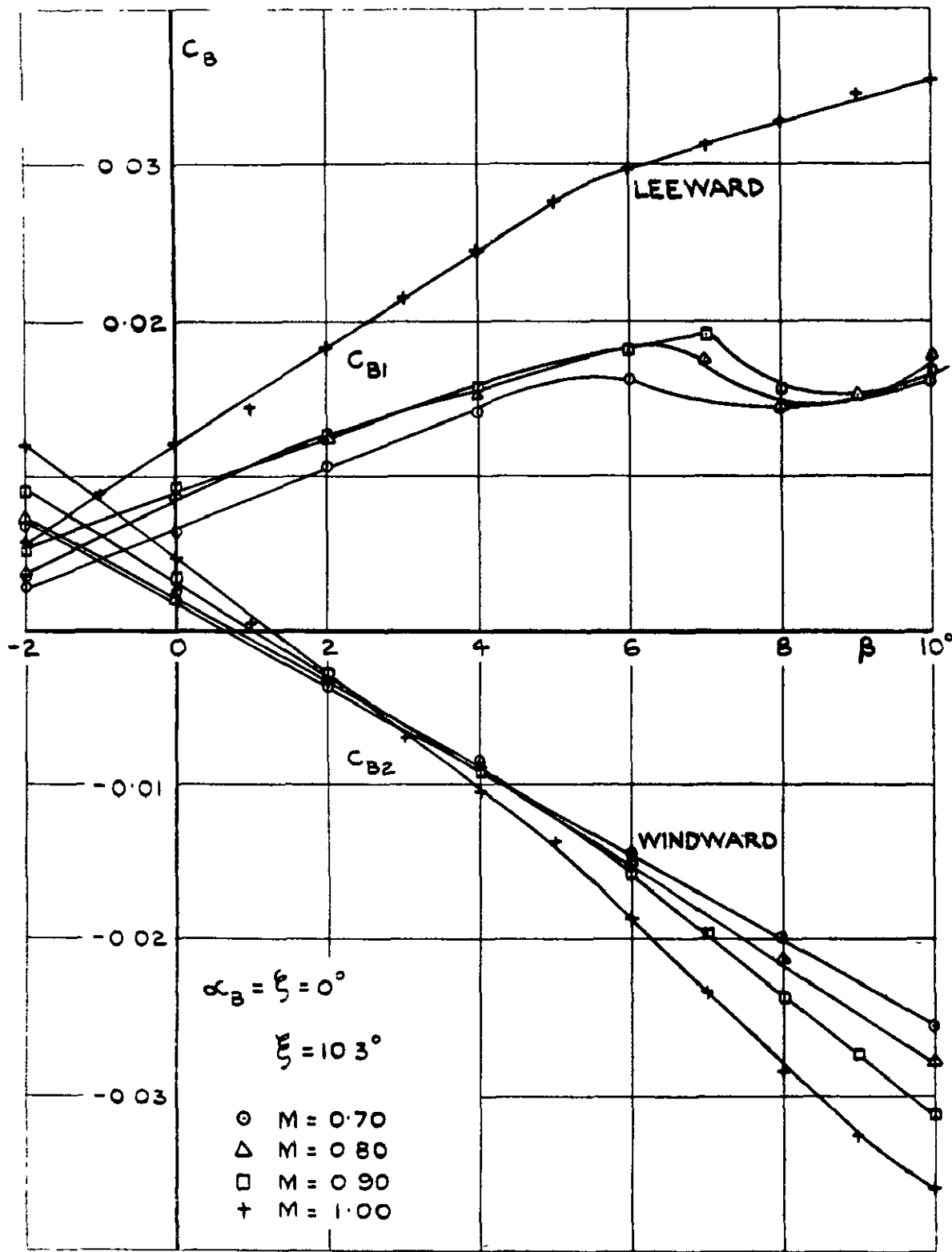
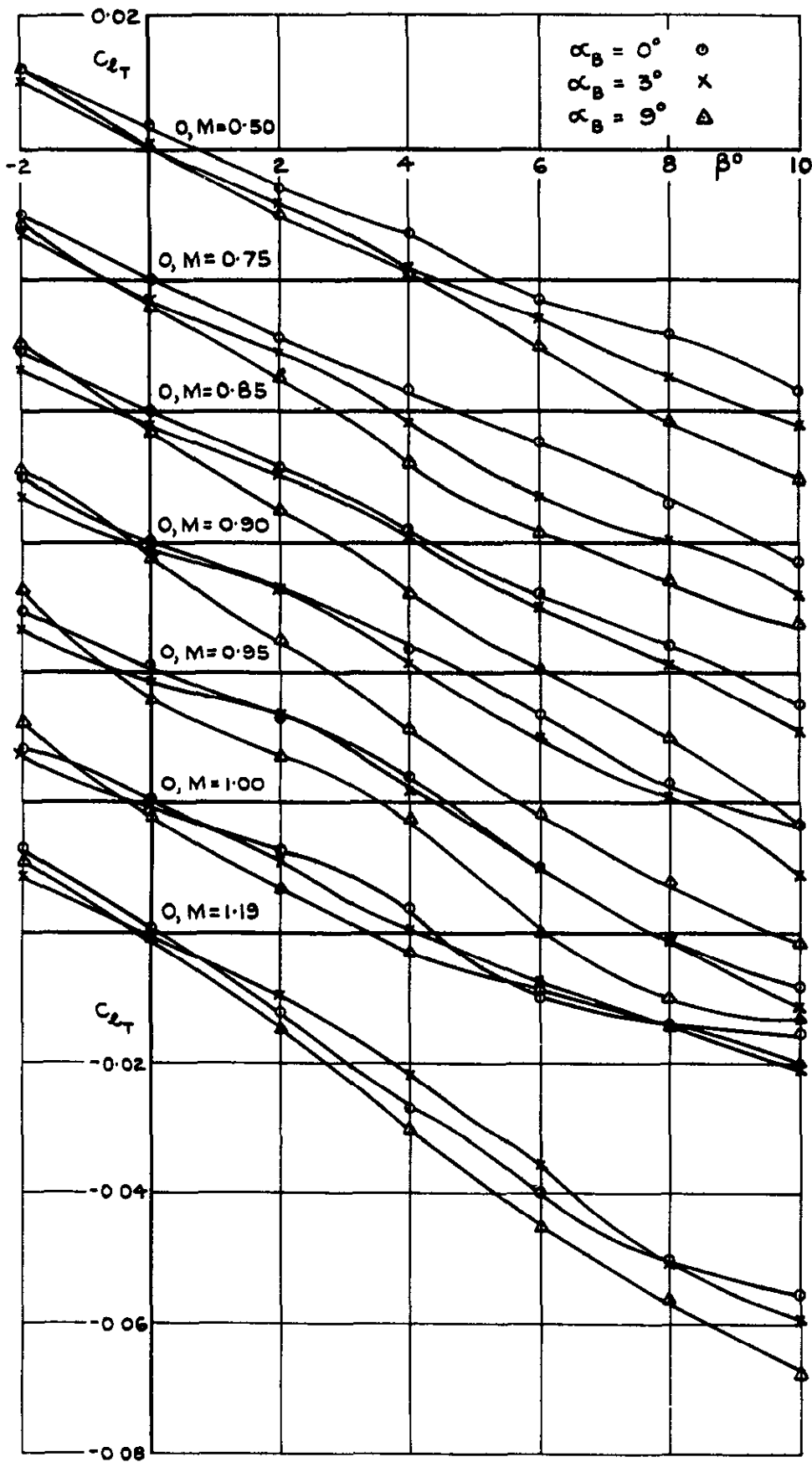FIG.18 MODEL A SUBSONIC AND TRANSONIC. VARIATION OF TAILPLANE BENDING MOMENTS WITH SIDESLIP $\alpha_B = \zeta = 0° \quad \xi = 10\cdot3°$
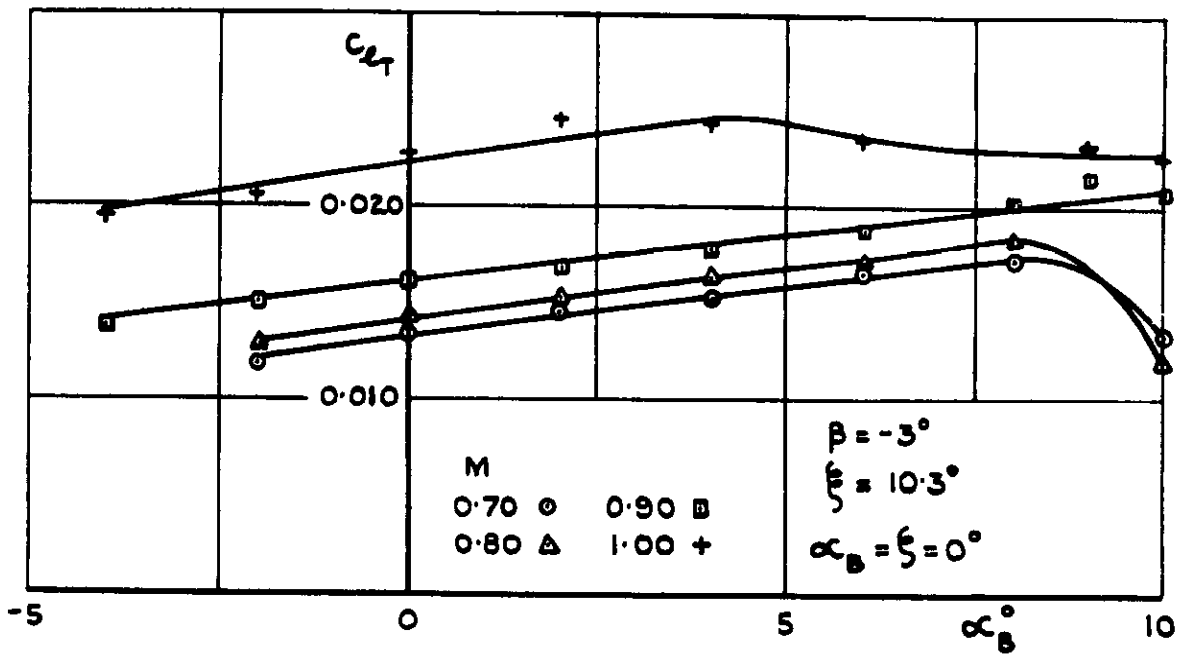
FIG.19. MODEL A SUBSONIC AND TRANSONIC. VARIATION OF TAILPLANE ROLLING MOMENT WITH INCIDENCE $\alpha_B = \xi = 0°$ $\beta = -3°$ $\xi = 10.3°$.
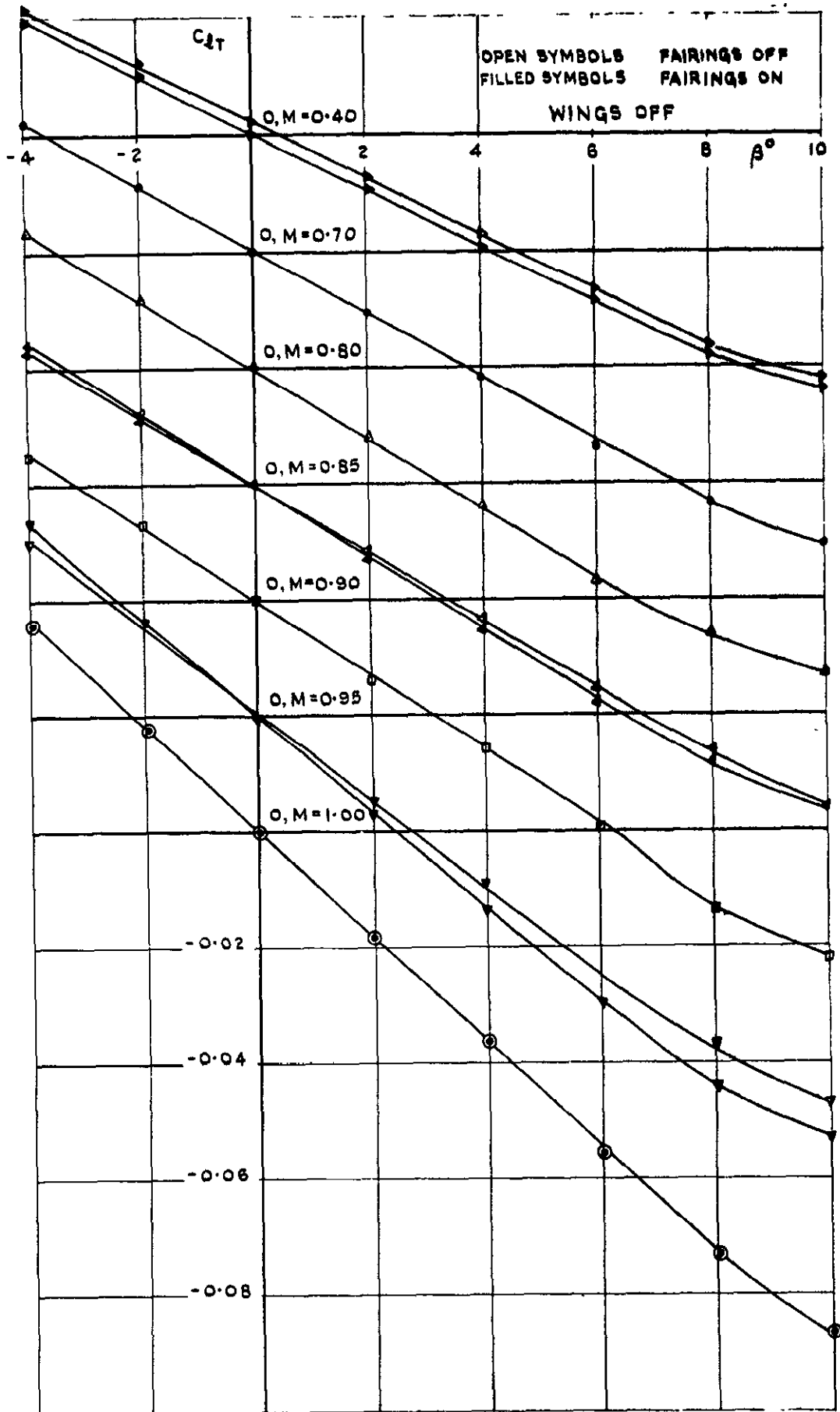
FIG.20. MODEL A. SUBSONIC AND TRANSONIC.
EFFECT OF BODY FAIRINGS ON $C_{l_T} - \beta$ CURVES.
WINGS OFF.
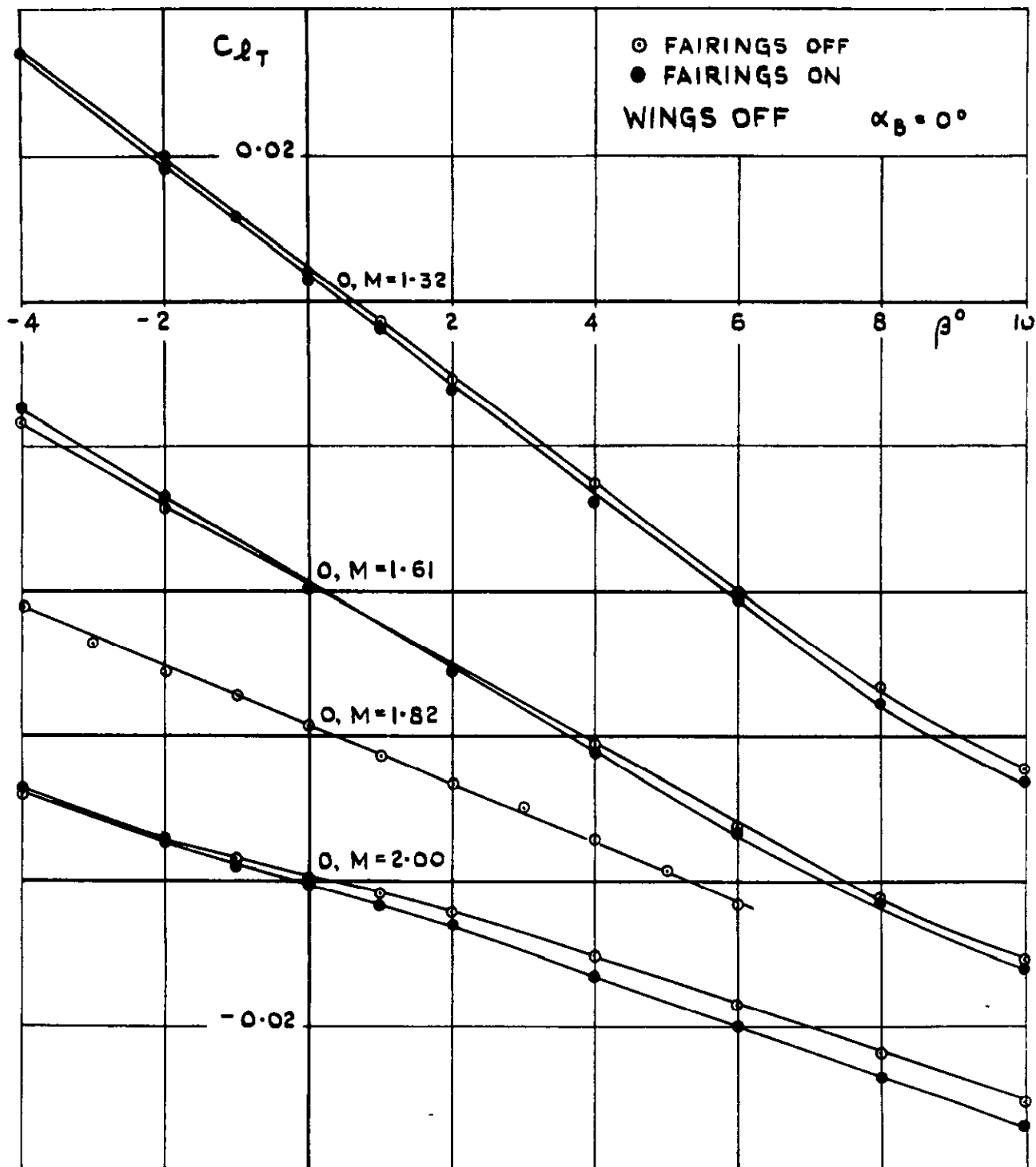
FIG. 21. MODEL A. SUPERSONIC. VARIATION OF
TAILPLANE ROLLING MOMENT WITH SIDESLIP.
WINGS OFF – FAIRINGS ON AND OFF. $\alpha_B = 0^{\circ}$
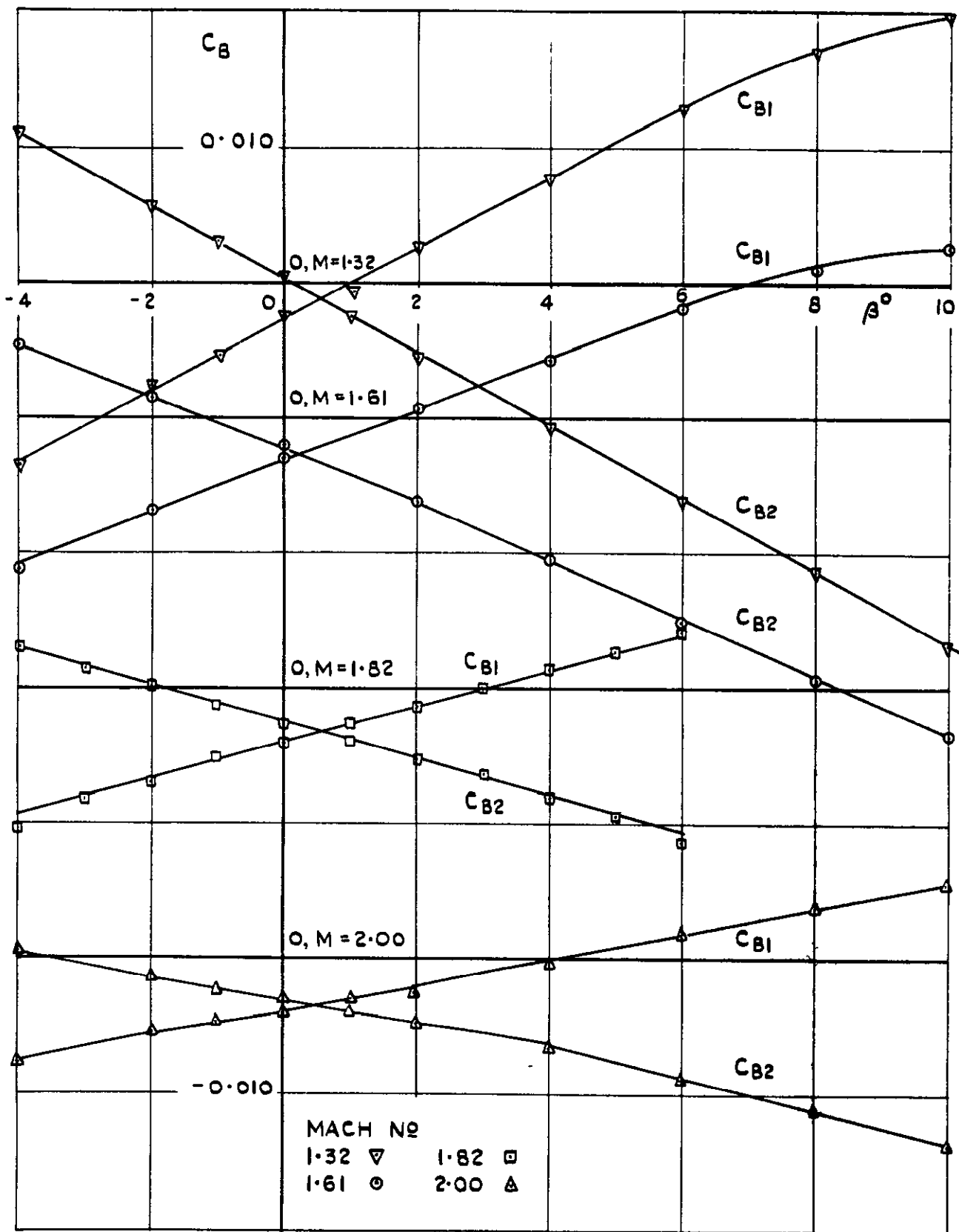
FIG.22. MODEL A. SUPERSONIC. VARIATION OF TAILPLANE BENDING MOMENTS WITH SIDESLIP. WINGS AND FAIRINGS OFF. $\alpha_B = 0°$.
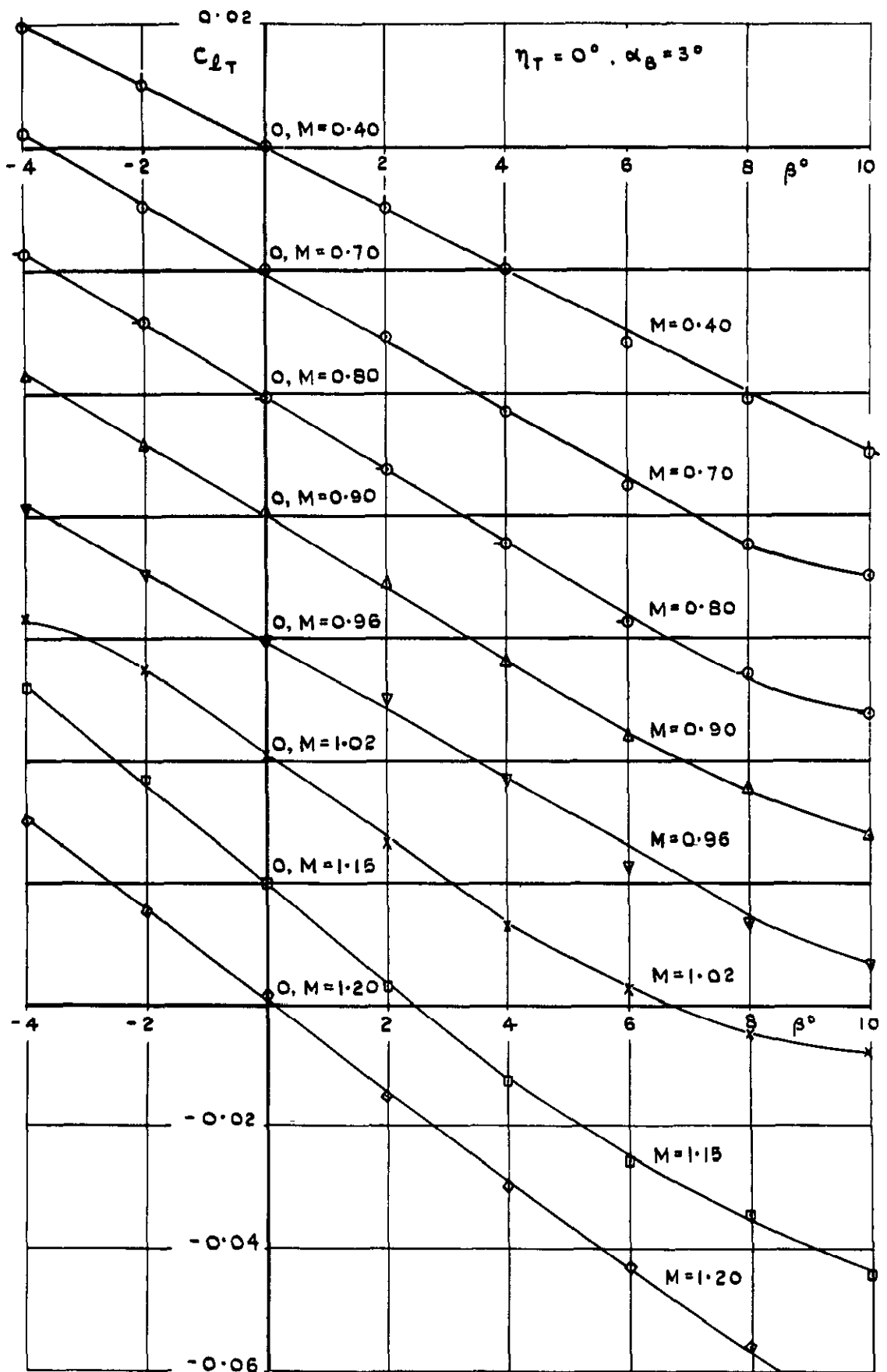
FIG.23. MODEL B. SUBSONIC AND TRANSONIC.
VARIATION OF TAILPLANE ROLLING MOMENT
WITH SIDESLIP. $\eta_T = 0°$, $\alpha_B = 3°$.
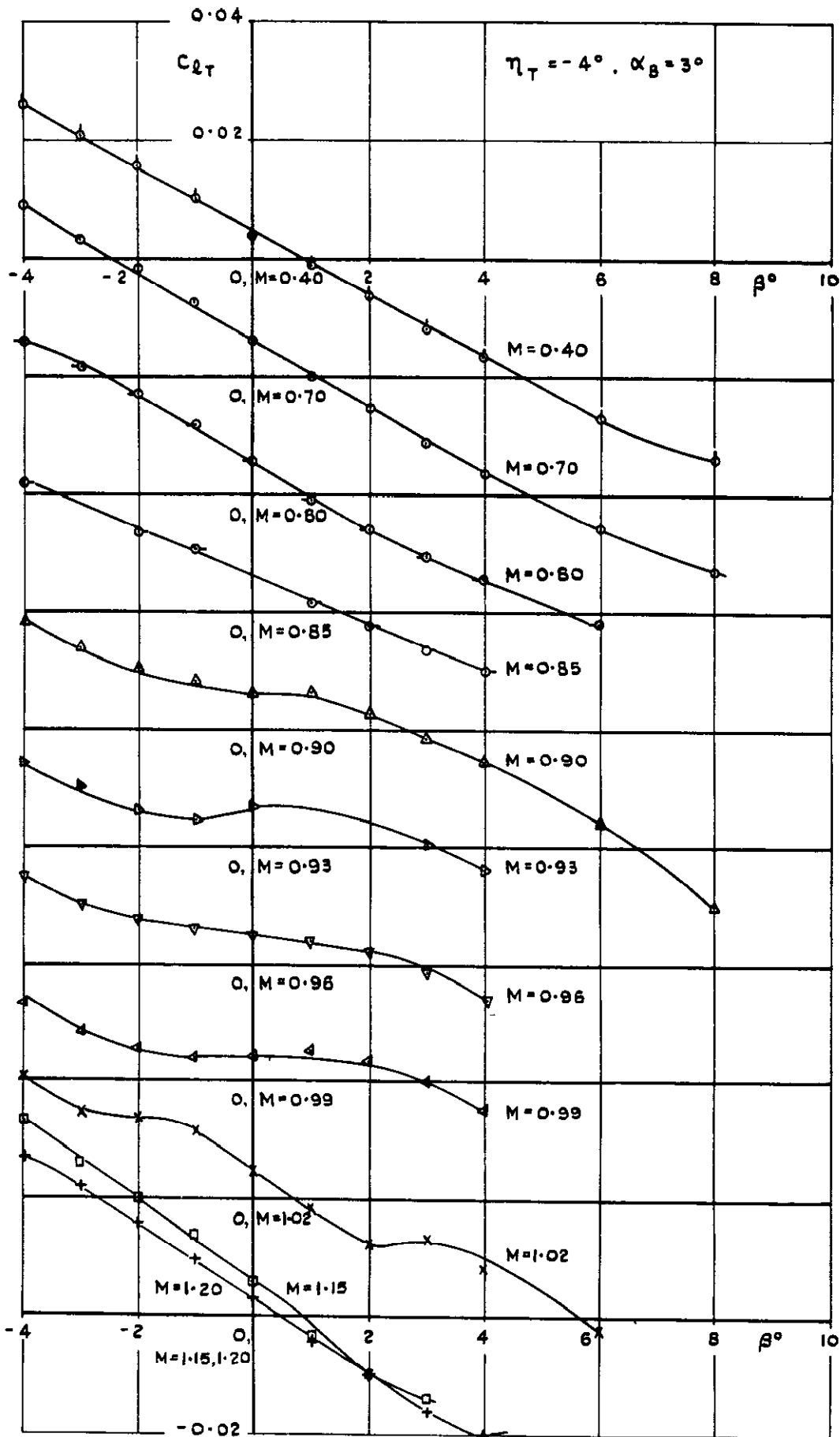
FIG.24. MODEL B. SUBSONIC AND TRANSONIC. VARIATION OF TAILPLANE ROLLING MOMENT WITH SIDESLIP. $\eta_T = -4°$, $\alpha_B = 3°$.
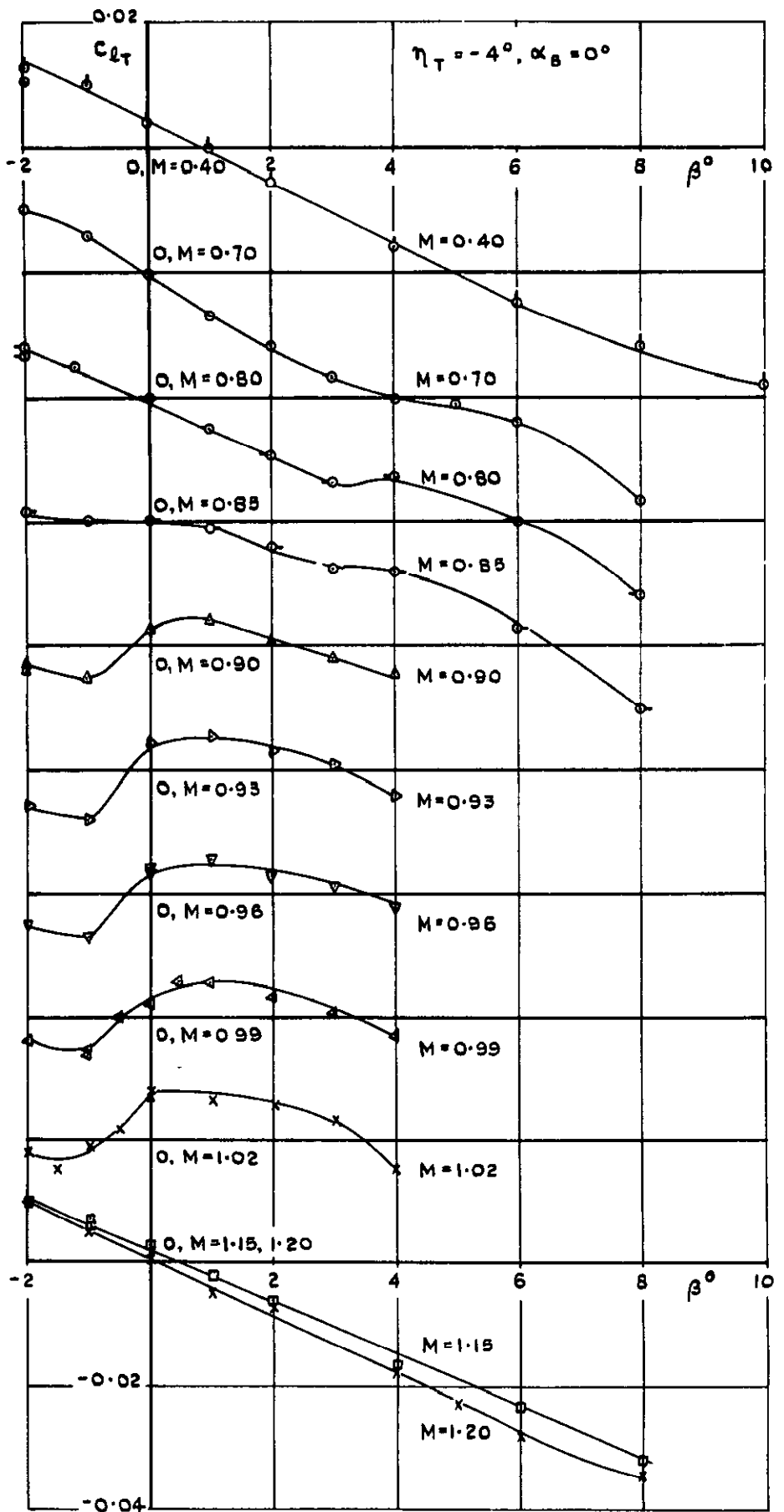
FIG.25. MODEL B. SUBSONIC AND TRANSONIC.
VARIATION OF TAILPLANE ROLLING MOMENT
WITH SIDESLIP. $\eta_T = -4°$, $\alpha_B = 0°$.
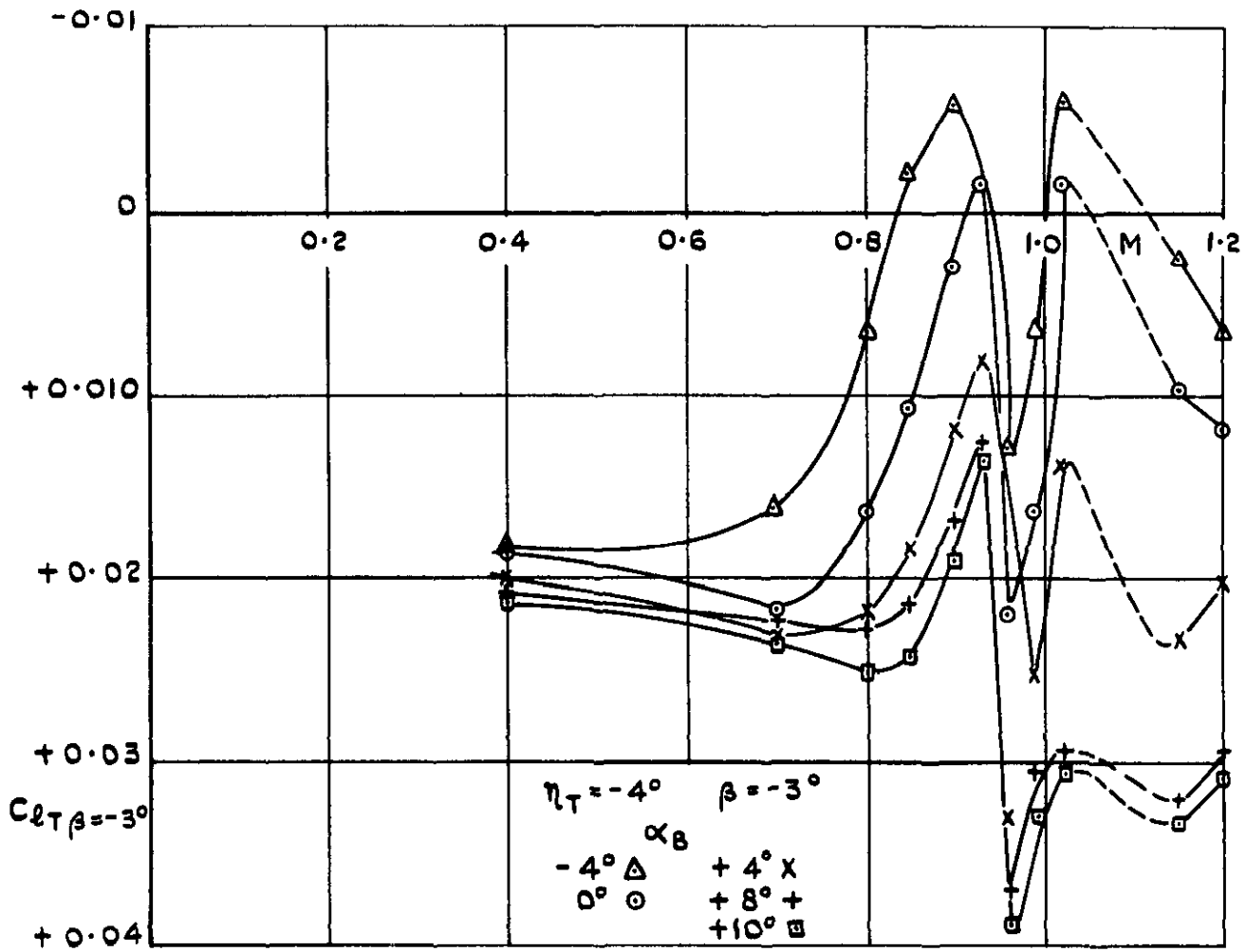
FIG.26. MODEL B. VARIATION OF TAILPLANE ROLLING MOMENT WITH MACH NUMBER AND INCIDENCE. $\eta_T = -4°$, $\beta = -3°$.
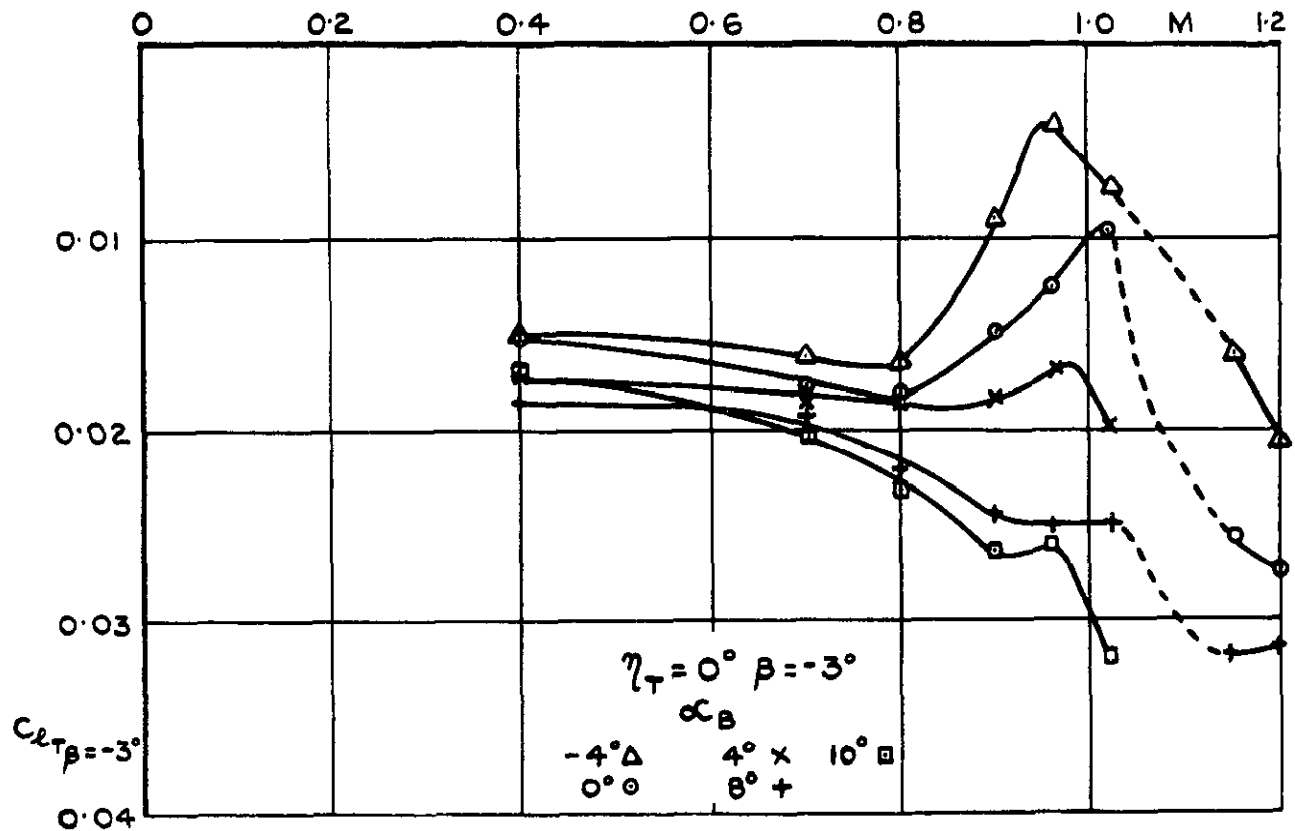
FIG. 27. MODEL B VARIATION OF TAILPLANE
ROLLING MOMENT WITH MACH NUMBER
AND INCIDENCE. $\eta_T = 0°$ $\beta = -3°$.
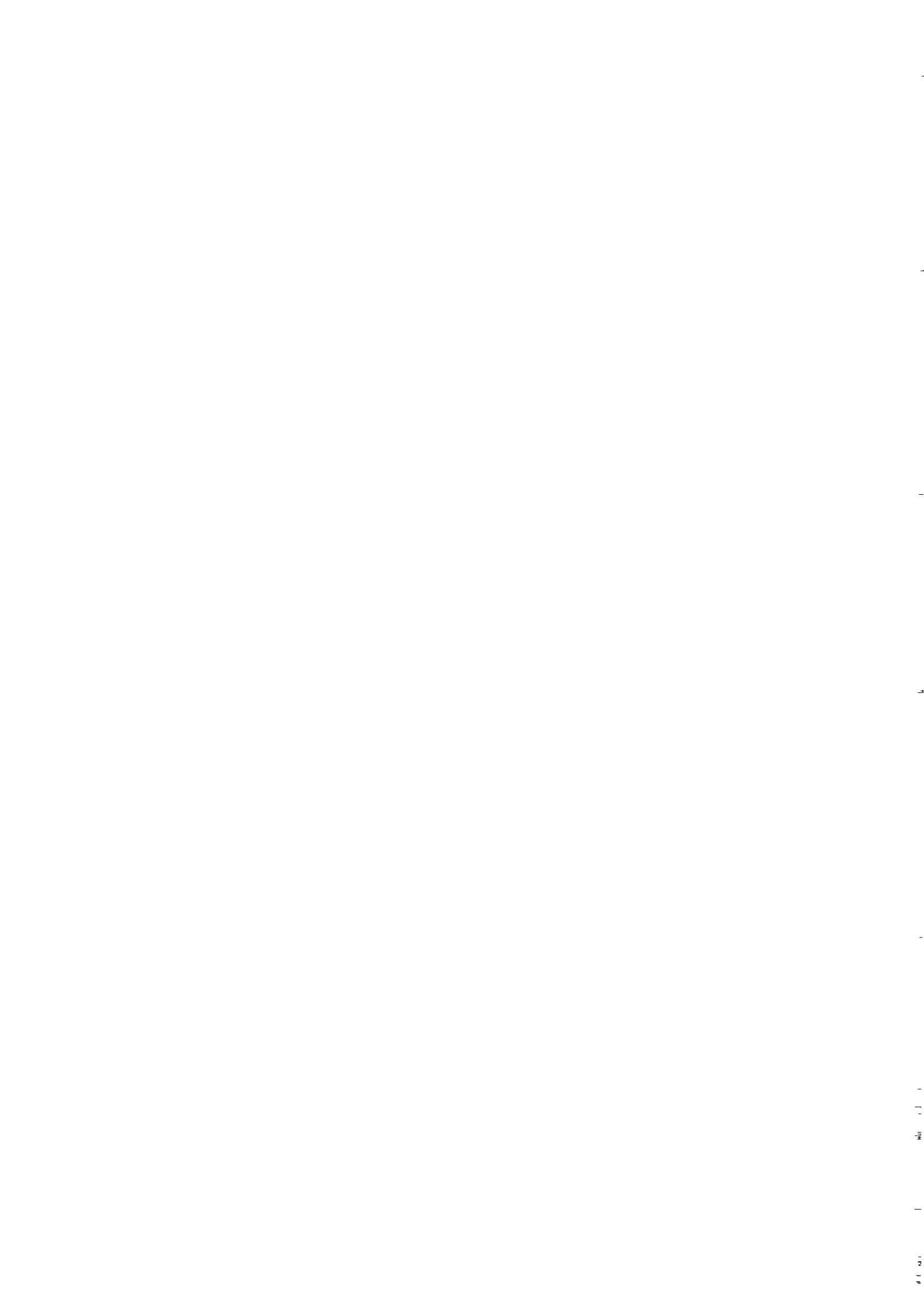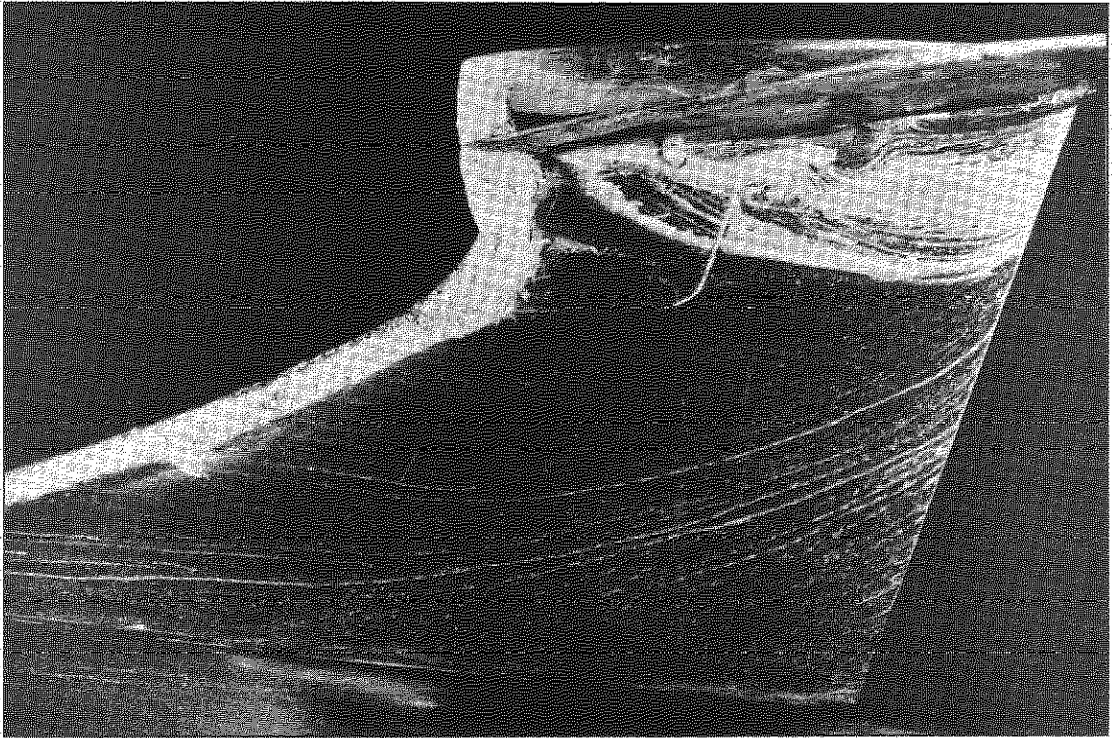
Fig.28a. Separation on leeward side of fin
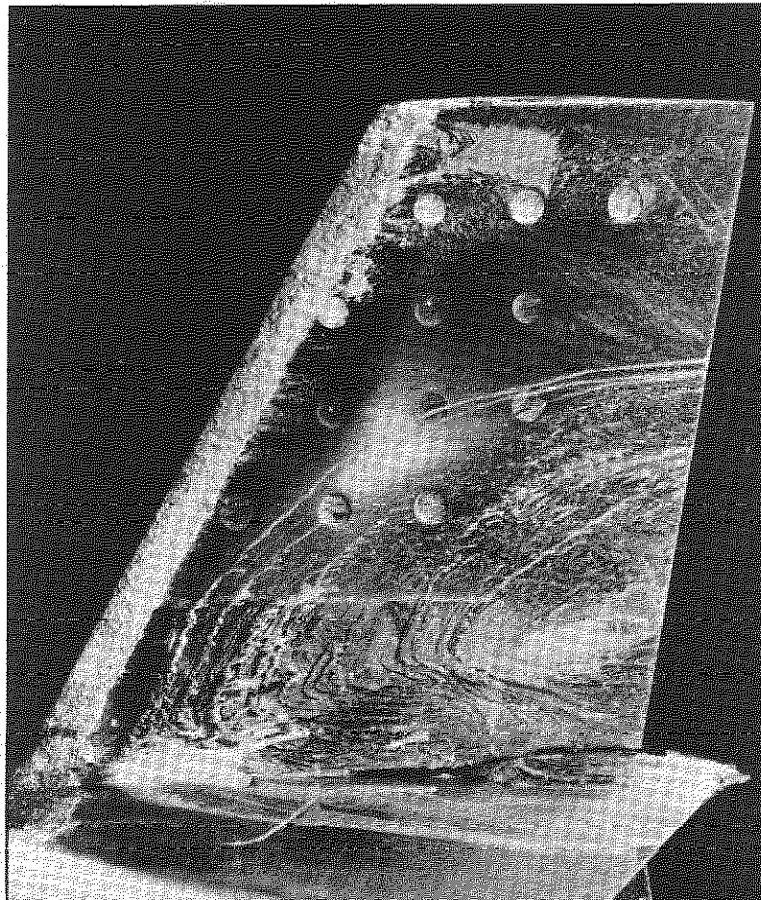
Fig.28b. Separation on under surface of leeward tailplane

Fig.28a&b. Model B. Flow on tailplane. Note- download on tailplane
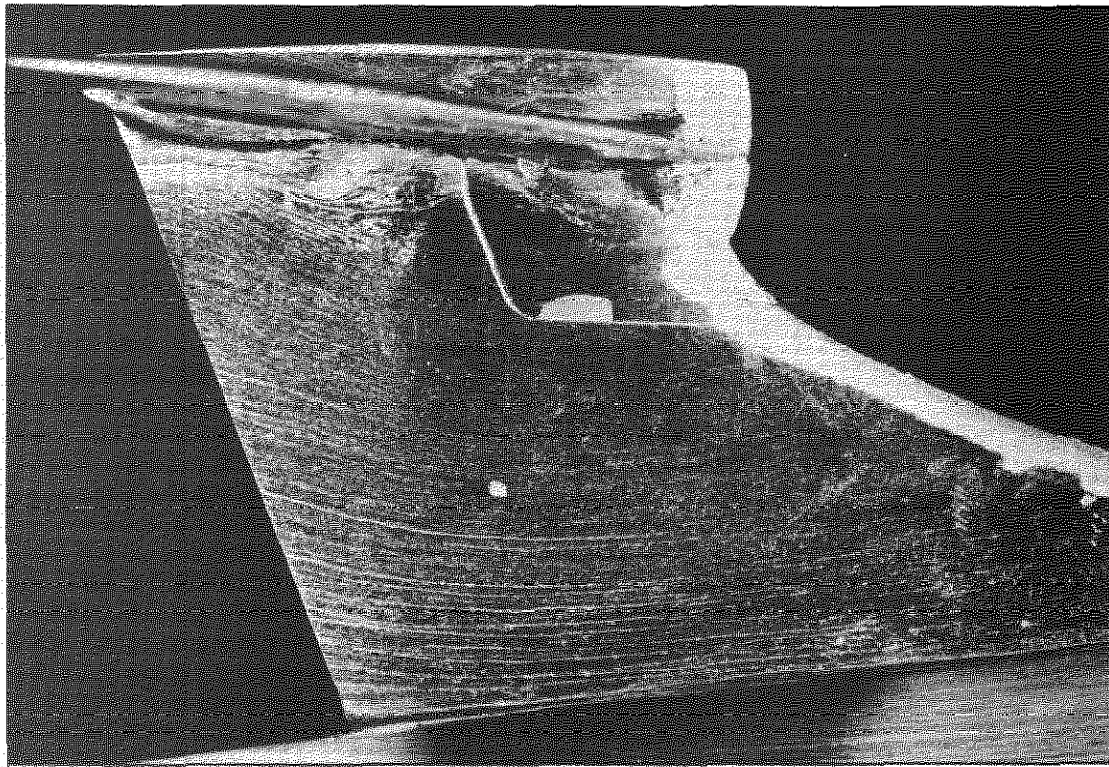
$$M = 0.90 \quad \beta = 3^\circ \quad \alpha_T = -7^\circ$$

Fig.28c. Flow on windward side of fin
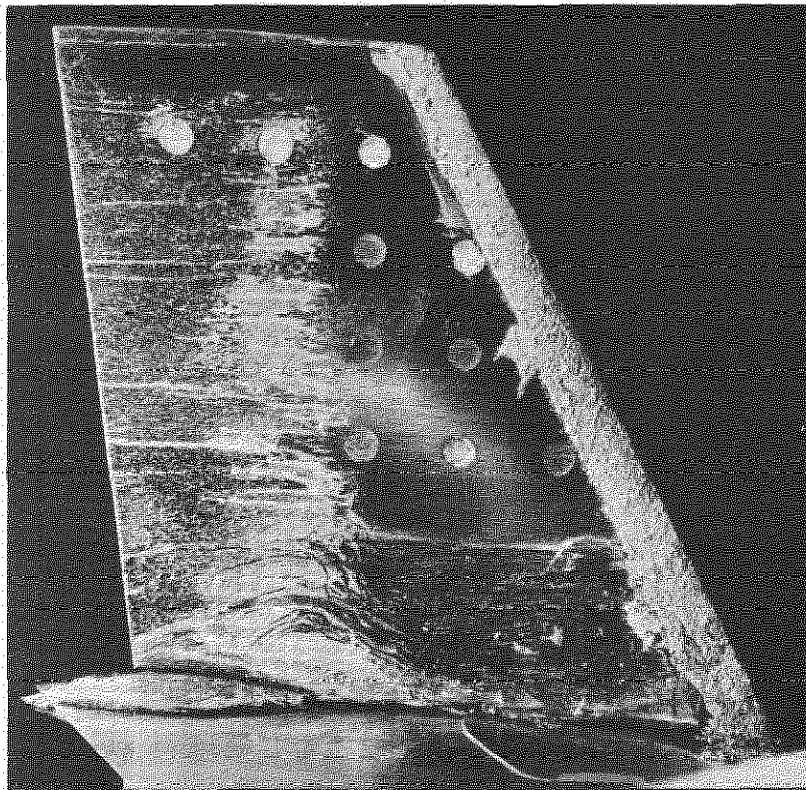
Fig.28d. Shock on undersurface of windward tailplane

Fig.28c&d. Model B. Flow on tailplane. Note- download on tailplane
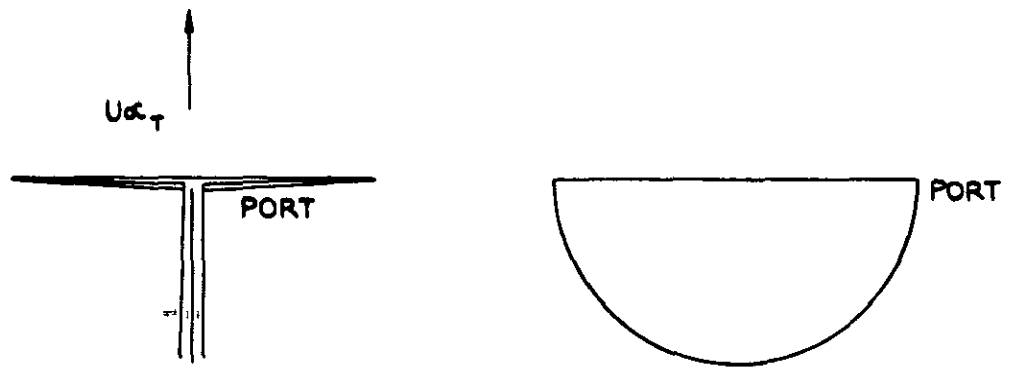
$$M = 0.90 \quad \beta = 3^{\circ} \quad \alpha_{T} = -7^{\circ}$$

(a) NEGATIVE INCIDENCE LOADING

$$\alpha_T = (\alpha - \varepsilon + \eta_T)$$
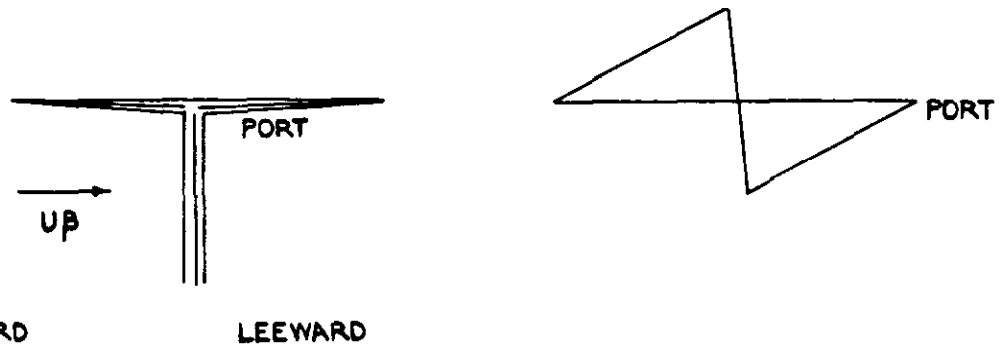
(b) POSITIVE SIDESLIP LOADING.

WINDWARD   LEEWARD

(c) RESULTANT LOADING.

SHOCK STRENGTH INCREASING

ATTACHED FLOW BEHIND SHOCK
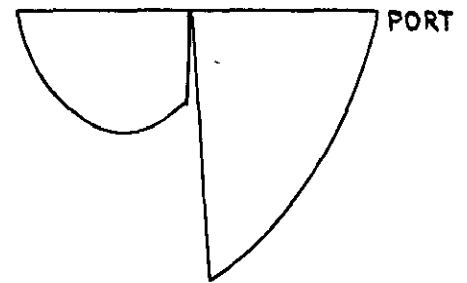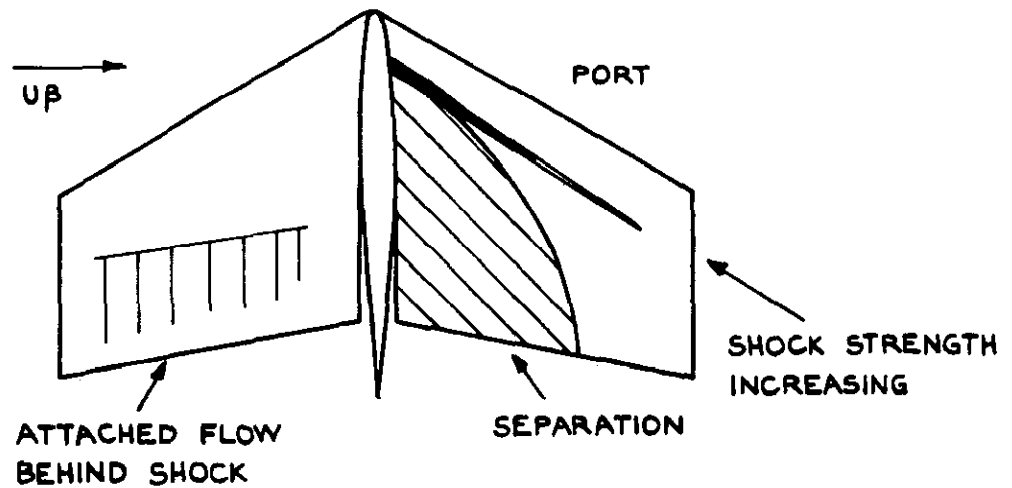
SEPARATION

(d) RESULTANT SHOCKS ON LOWER SURFACE

FIG. 29. (a-d). MODEL B SHOCK FORMATION ON TAILPLANE M = 0·90 $\beta = 3°$ $\alpha_T = -7°$

NOTE - DOWNLOAD ON TAILPLANE.
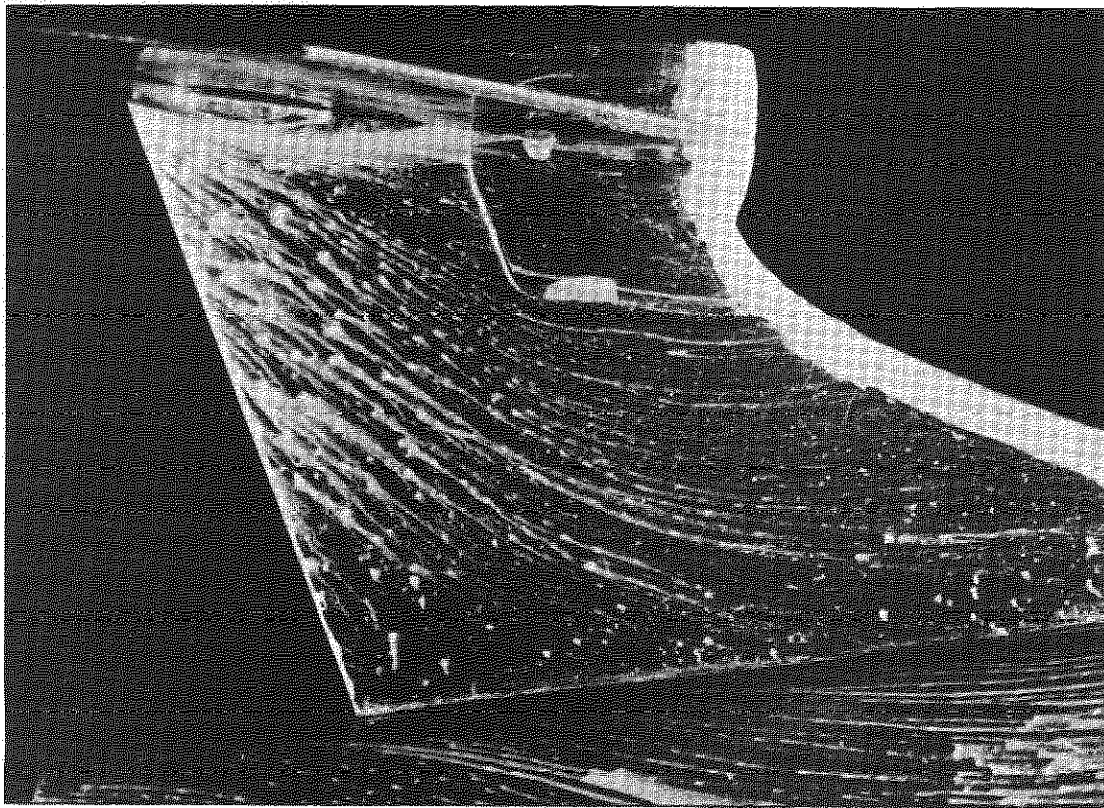
Fig.30. Model B. Limited separation on fin

$$M = 0.90 \quad \beta = -3^{\circ} \quad \alpha_{T} = -1^{\circ}$$
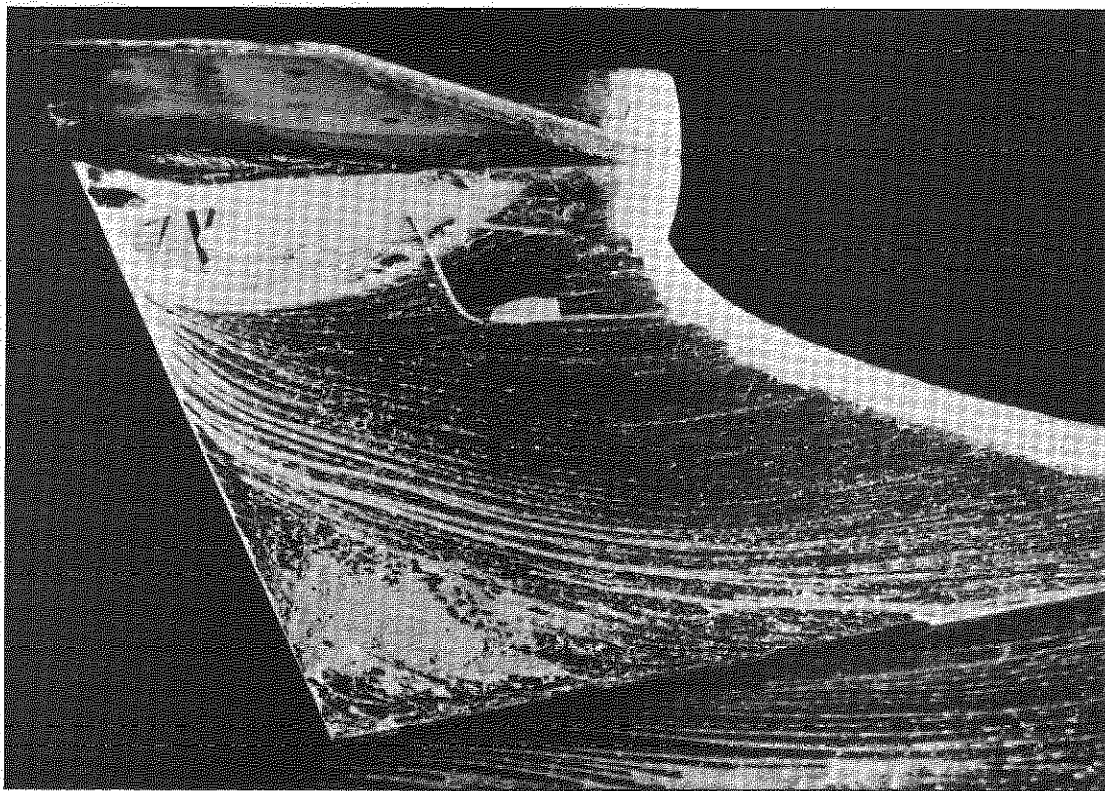
Fig.31. Model B. Separation on fin. Gap sealed

$$M = 0.90 \quad \beta = -3^{\circ} \quad \alpha_{T} = -7^{\circ}$$
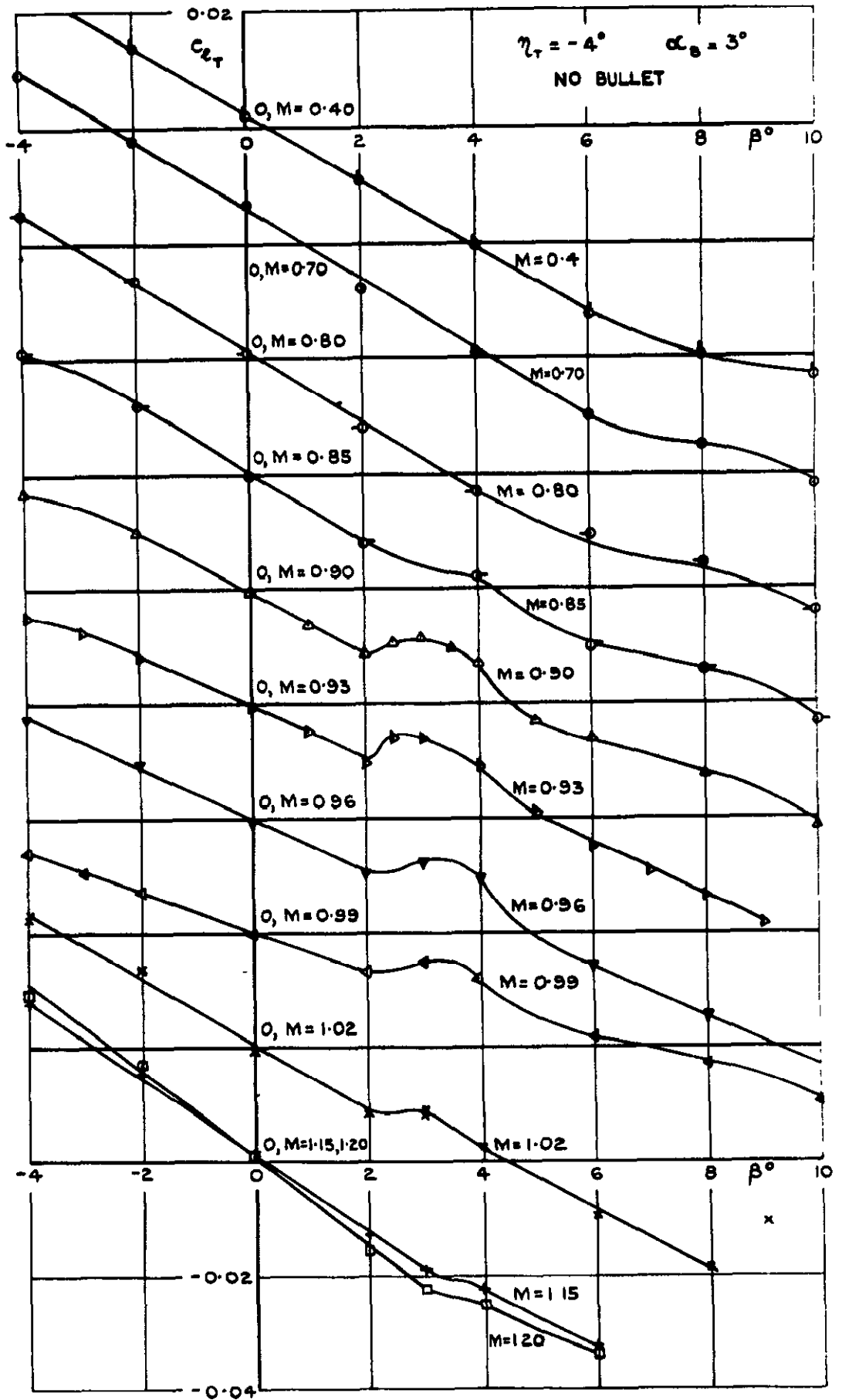
FIG.32. MODEL B SUBSONIC AND TRANSONIC. VARIATION OF TAILPLANE ROLLING MOMENT WITH SIDESLIP. NO BULLET FITTED. $\eta_T = -4°$ $\alpha_B = 3°$.

FIG. 33. MODEL C. SUBSONIC AND TRANSONIC.
VARIATION OF TAILPLANE ROLLING MOMENT
WITH SIDESLIP.
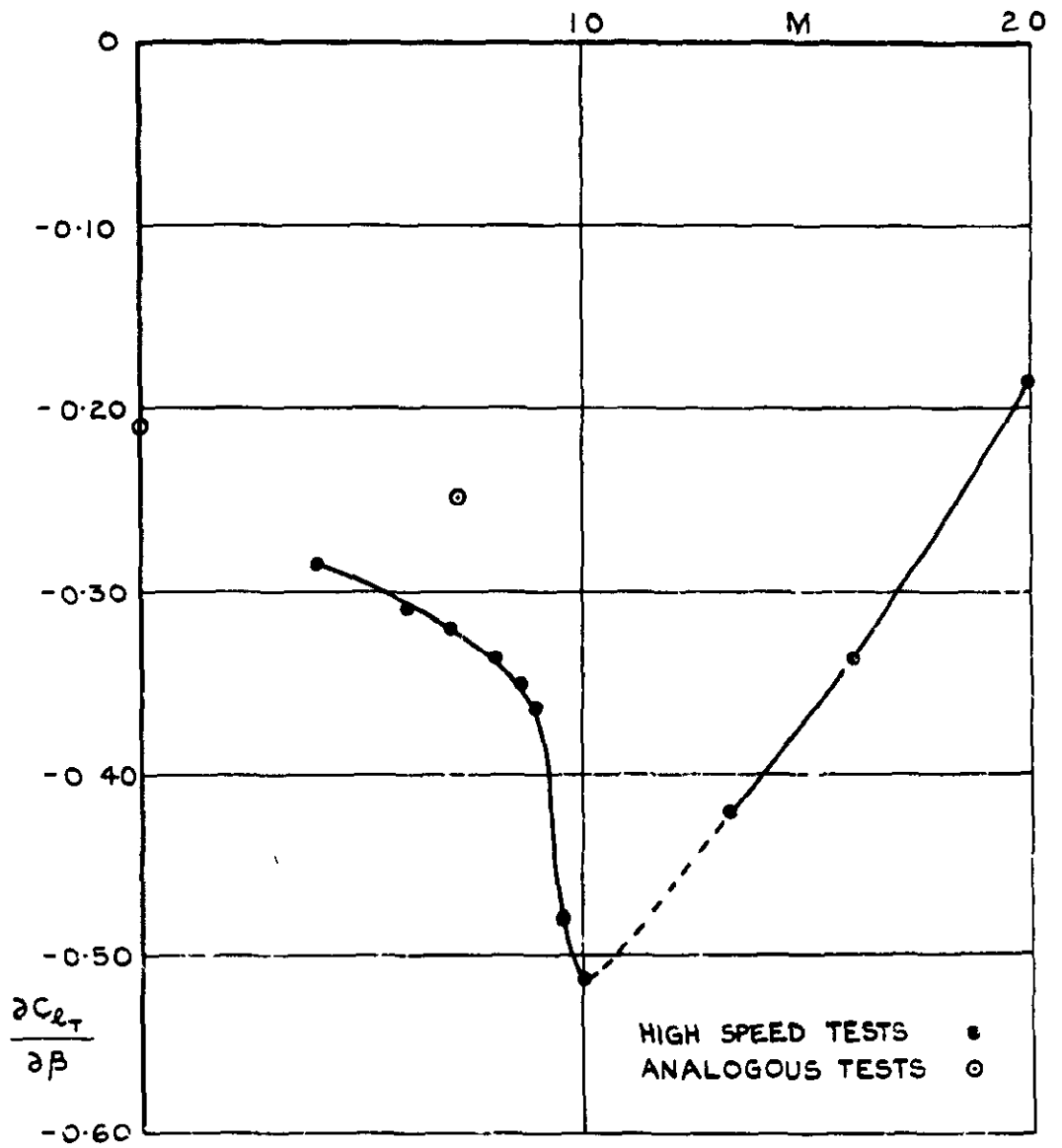
(a) MODEL A. VARIATION OF TAILPLANE ROLLING MOMENT
CURVE SLOPE WITH MACH NUMBER.
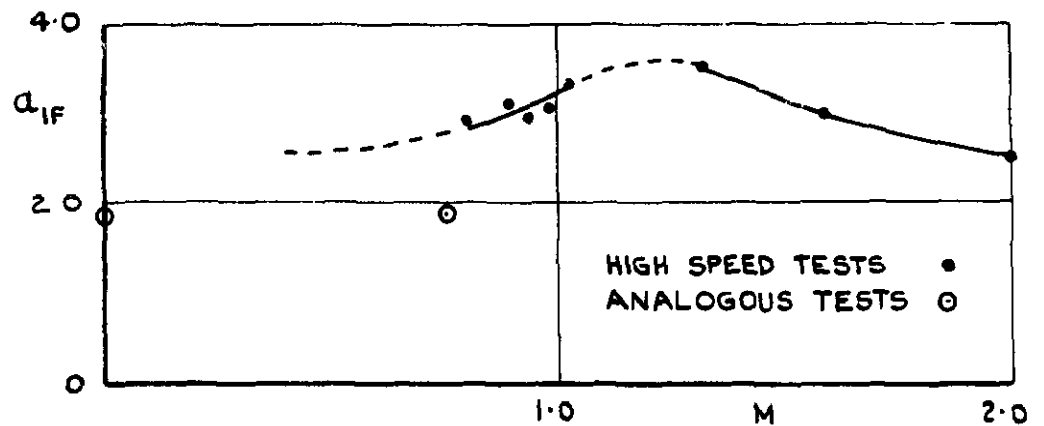
(b) MODEL A. VARIATION OF FIN LIFT CURVE SLOPE
WITH MACH NUMBER.

FIG. 34 (a & b). COEFFICIENTS DEDUCED FOR
MODEL A TAILPLANE.
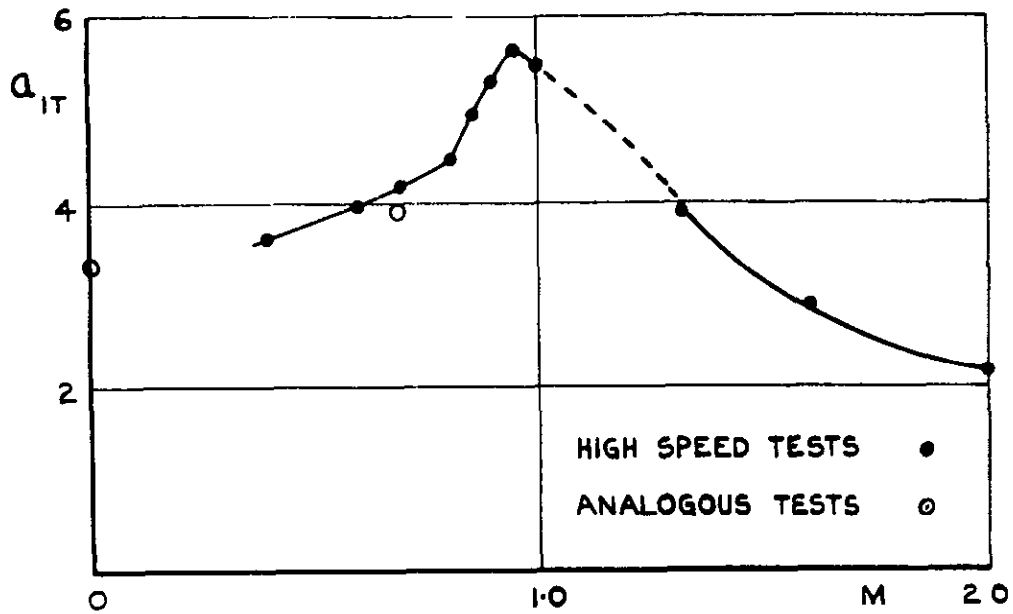
(C) MODEL A. VARIATION OF TAILPLANE LIFT CURVE SLOPE
WITH MACH NUMBER.
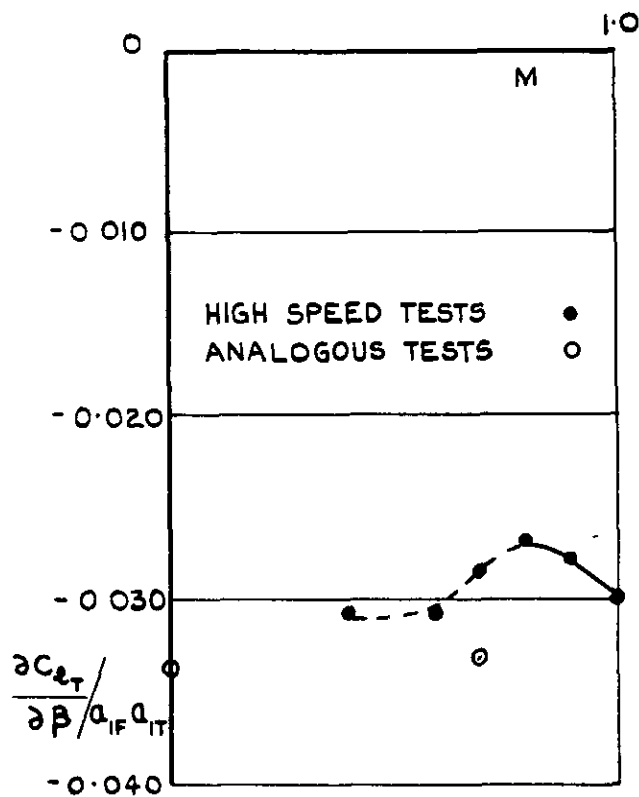
(d) MODEL A. VARIATION OF $\frac{\partial C_{\ell_T}}{\partial \beta} \Big/ a_{1F} a_{1T}$
WITH MACH NUMBER

FIG.34. (c & d) COEFFICIENTS DEDUCED FOR
MODEL A TAILPLANE.
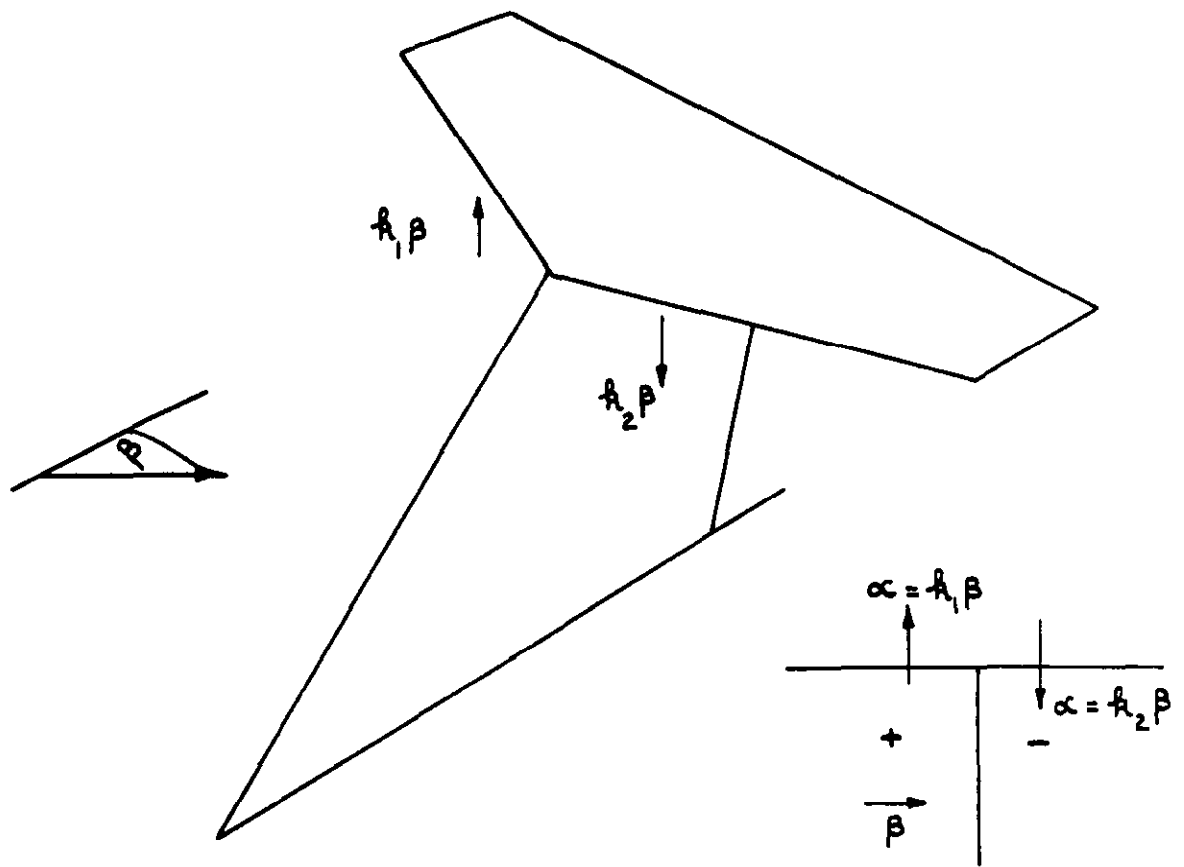
FIG. 35. IDEALISED HIGH TAILPLANE.
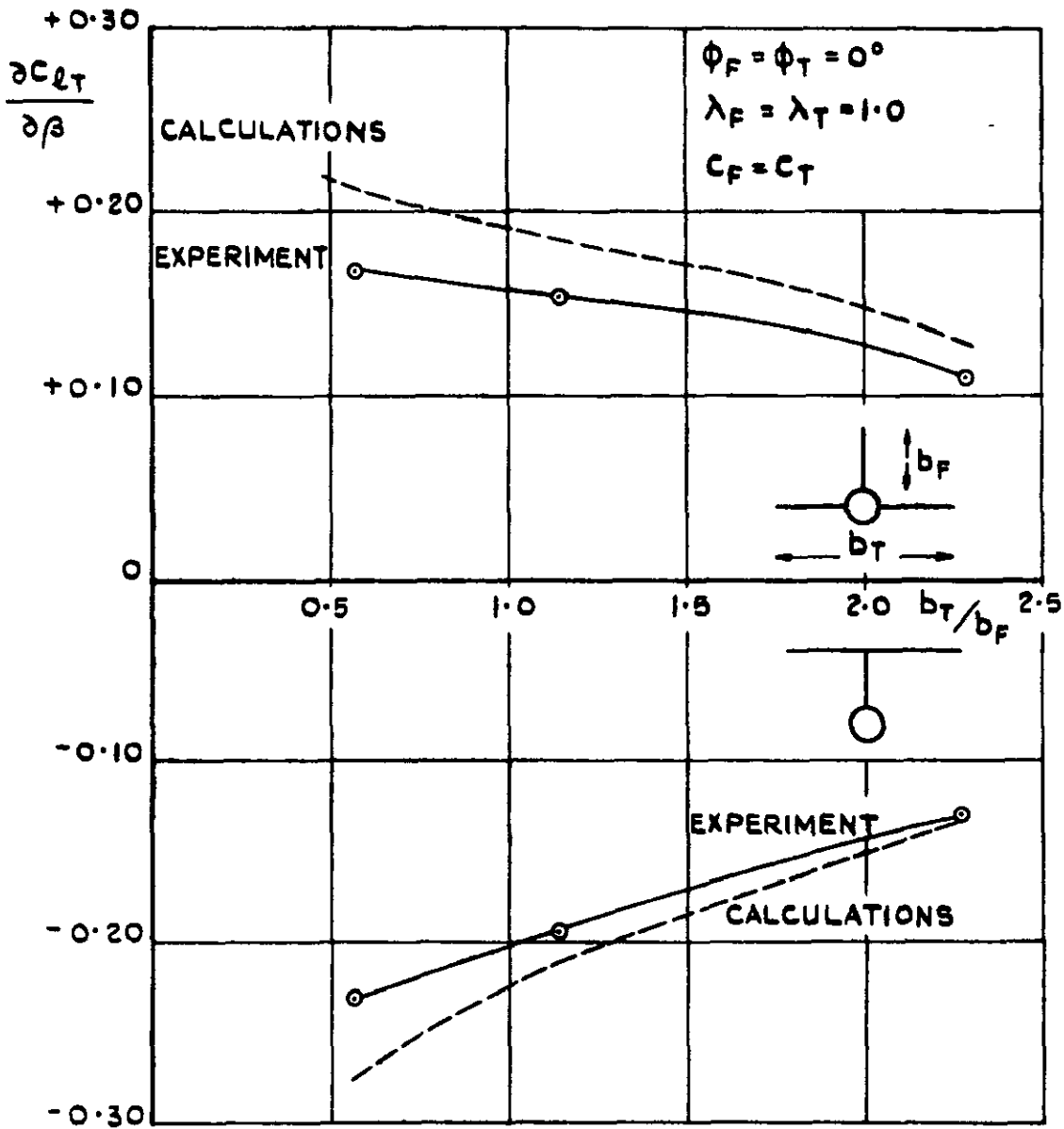
FIG.36. COMPARISON BETWEEN
CALCULATIONS AND EXPERIMENT
$\phi = 0°$, $A_F = 2\cdot 0$ [FROM REFERENCE 8].
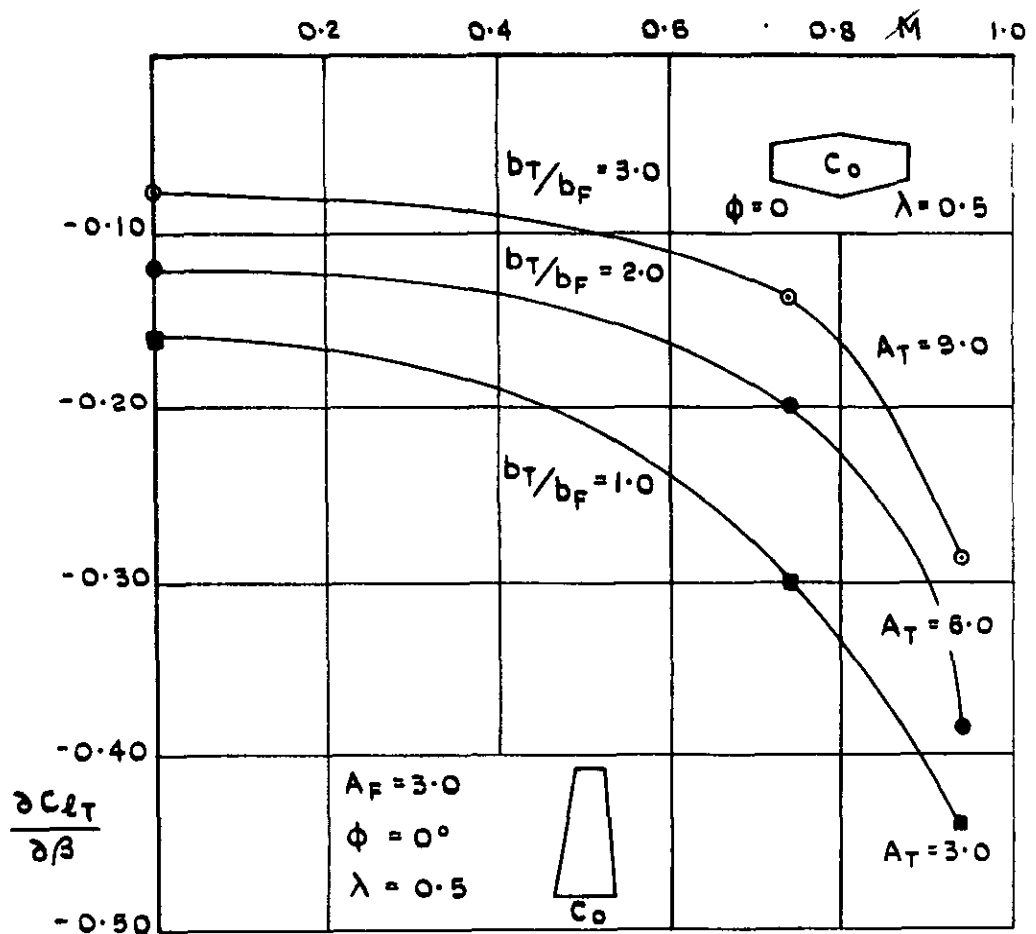
(a). VARIATION OF TAILPLANE ROLLING MOMENT CURVE SLOPE
WITH MACH NUMBER.
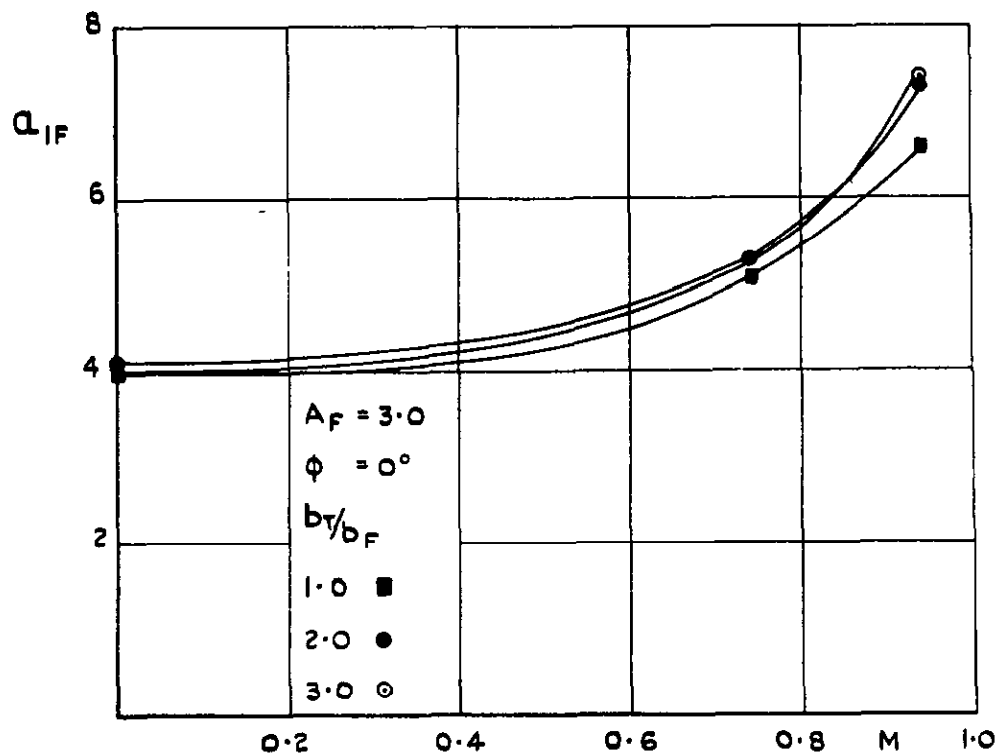
(b). VARIATION OF FIN LIFT CURVE SLOPE WITH MACH NUMBER.

FIG.37(a&b). CALCULATED COEFFICIENTS FOR
$A_F = 3 \cdot 0$, $\phi = 0^\circ$.
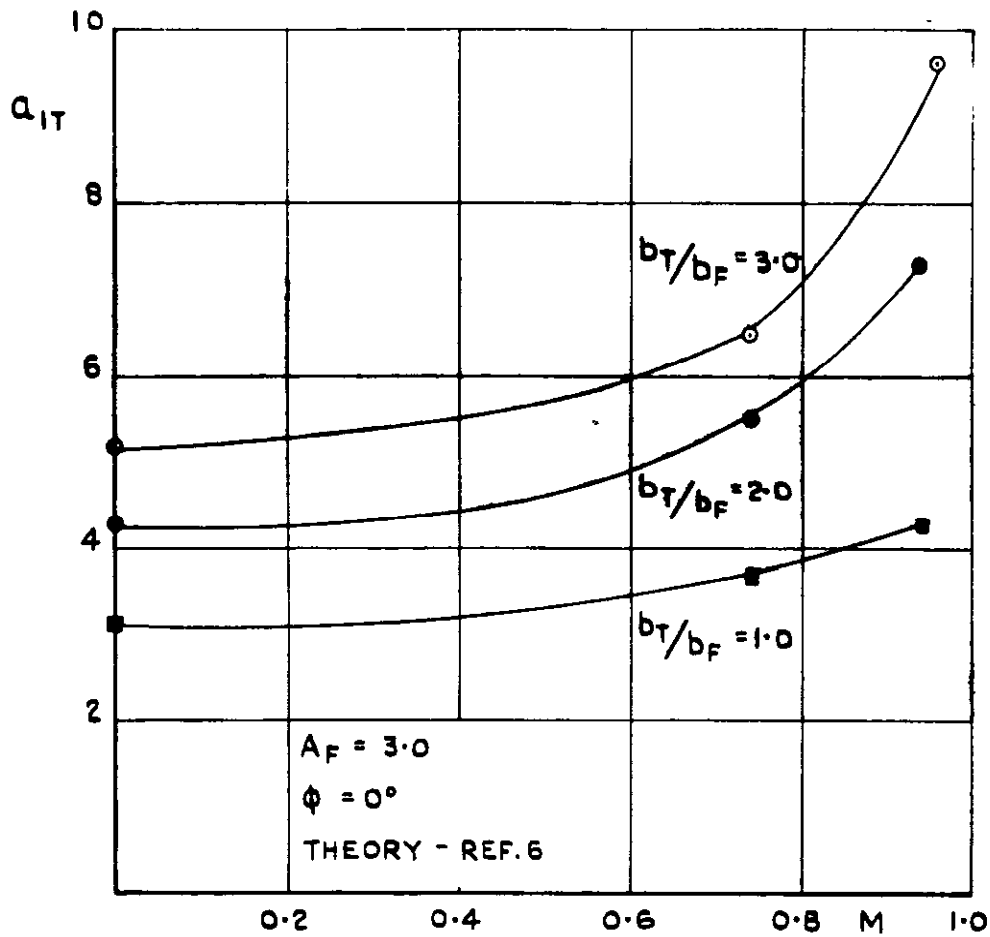
(C). VARIATION OF TAILPLANE LIFT CURVE SLOPE WITH MACH NUMBER.
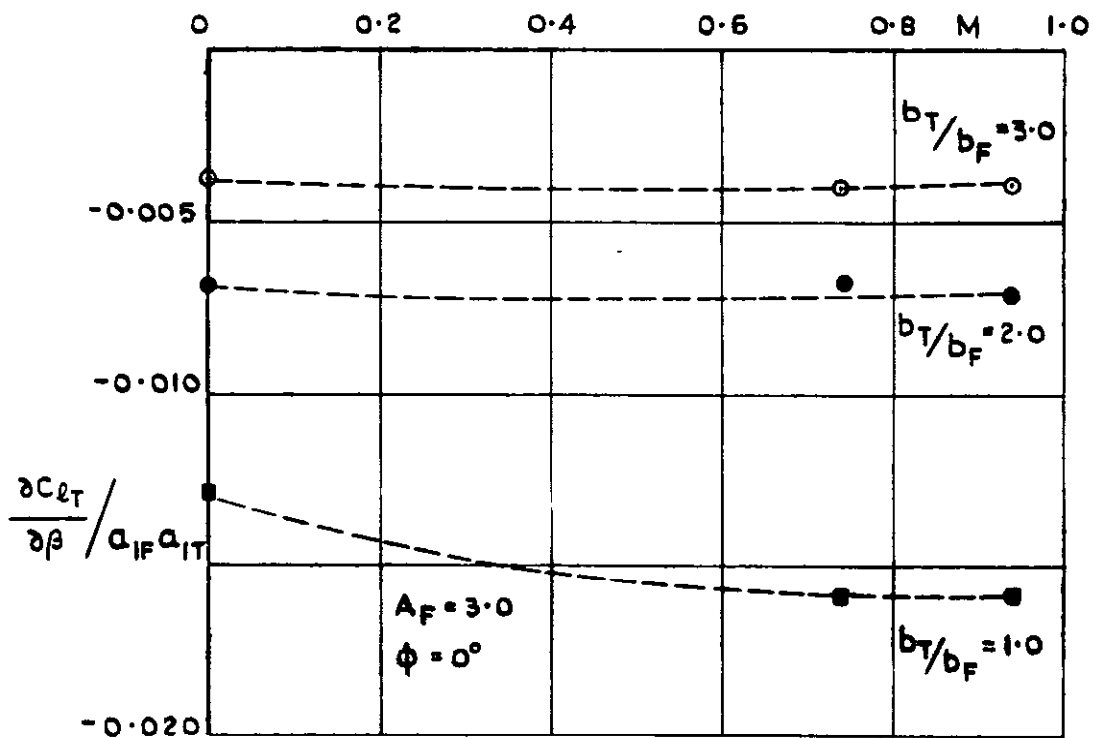
(d). VARIATION OF $\dfrac{\partial C_{\ell_T}}{\partial \beta} / a_{1F} a_{1T}$ WITH TAILPLANE WITH MACH NUMBER.

FIG. 37 (c & d). CALCULATED COEFFICIENTS FOR $A_F = 3 \cdot 0, \phi = 0°$.

(a) $\alpha_B = 0°$

Table for (a), $\alpha = 0°$:

	M=0 ⊙	M=0.70 ⊟
$\dfrac{\partial C_{\ell_T}}{\partial \beta}$	0.20	0.26

ADJUSTED TO $C_{L_T} = 0$

	M=0	M=0.70
$\dfrac{\partial C_{\ell_T}}{\partial \beta}$	0.21	0.25

(b) $\alpha_B = 4°$

Table for (b), $\alpha = +4°$:

	M=0 ⊙	M=0.70 ⊟
$\dfrac{\partial C_{\ell_T}}{\partial \beta}$	0.22	0.30

ADJUSTED TO $C_{L_T} = 0$

	M=0	M=0.70
$\dfrac{\partial C_{\ell_T}}{\partial C_\beta}$	0.21	0.25
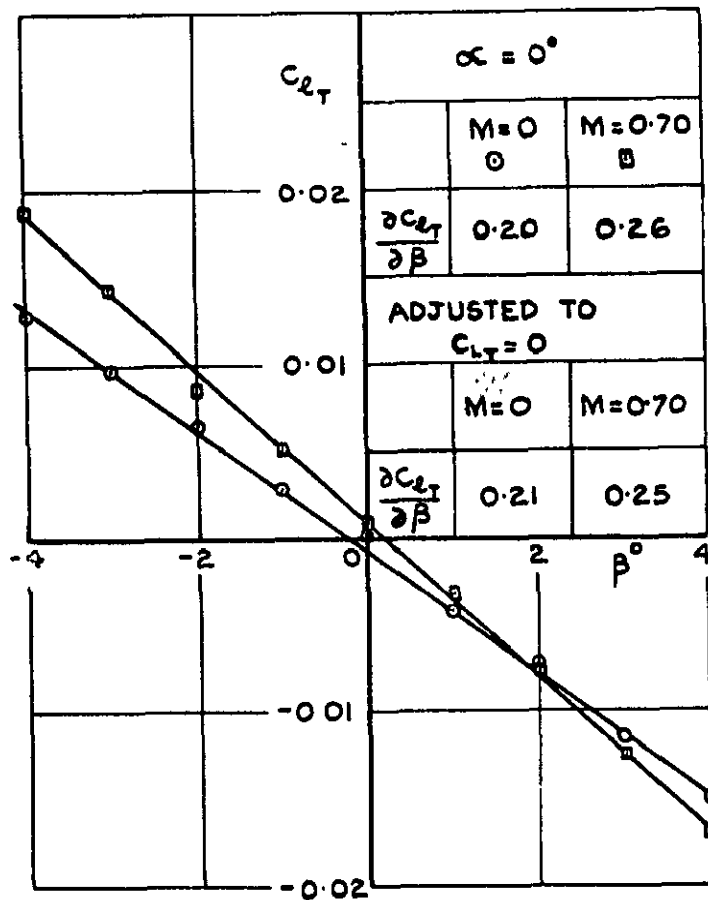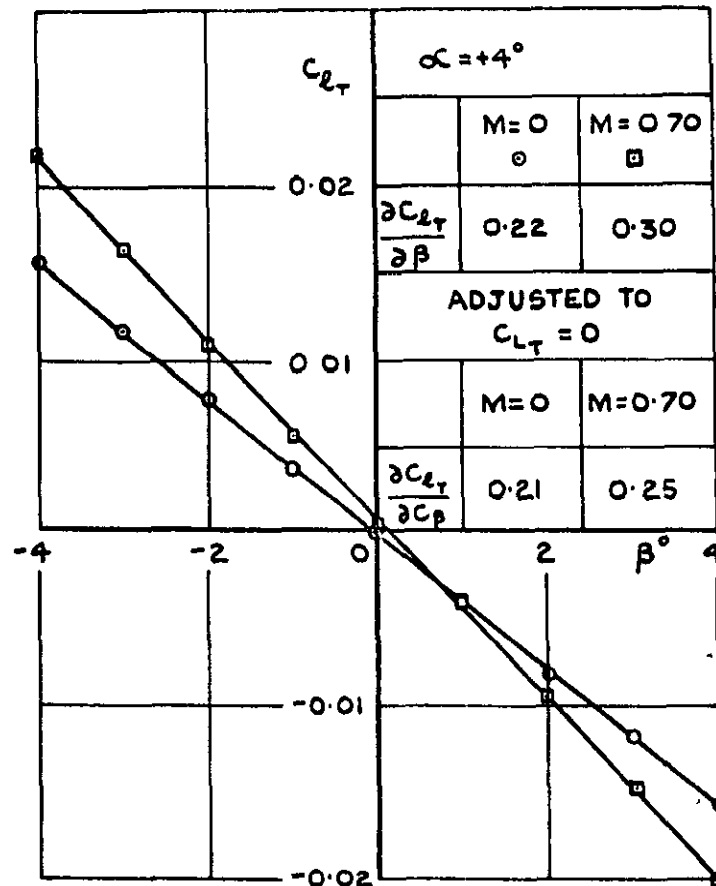
FIG. 38 (a & b). LOW SPEED TESTS ON ANALOGOUS
TAILPLANES – MODEL A. VARIATION OF TAILPLANE
ROLLING MOMENTS WITH SIDESLIP.
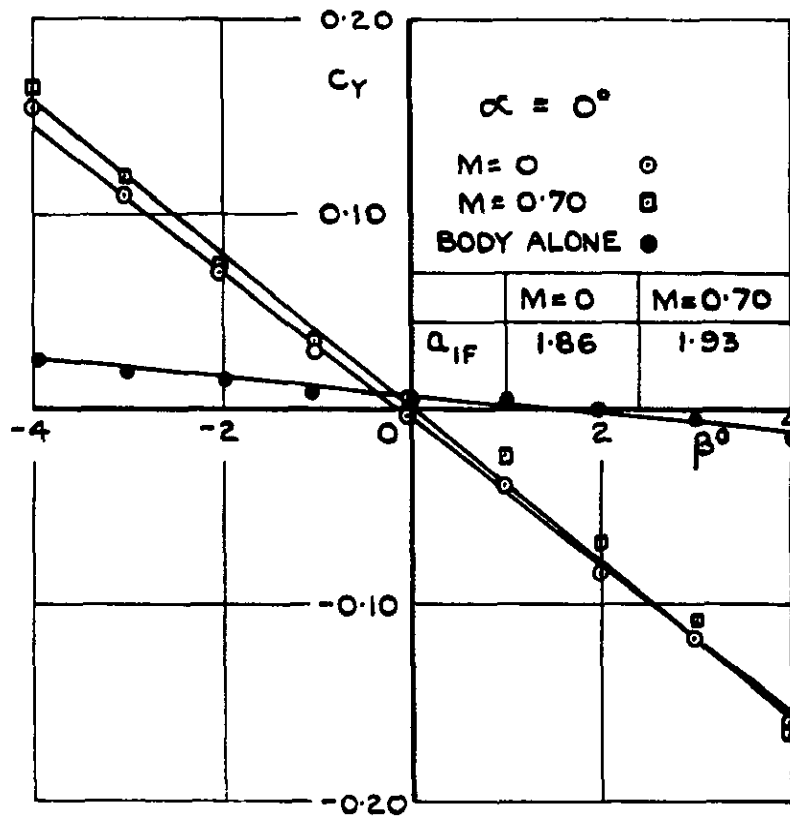
FIG. 39. LOW SPEED TESTS OF ANALOGOUS
TAILPLANES. MODEL A. VARIATION OF·
SIDEFORCE WITH SIDESLIP.
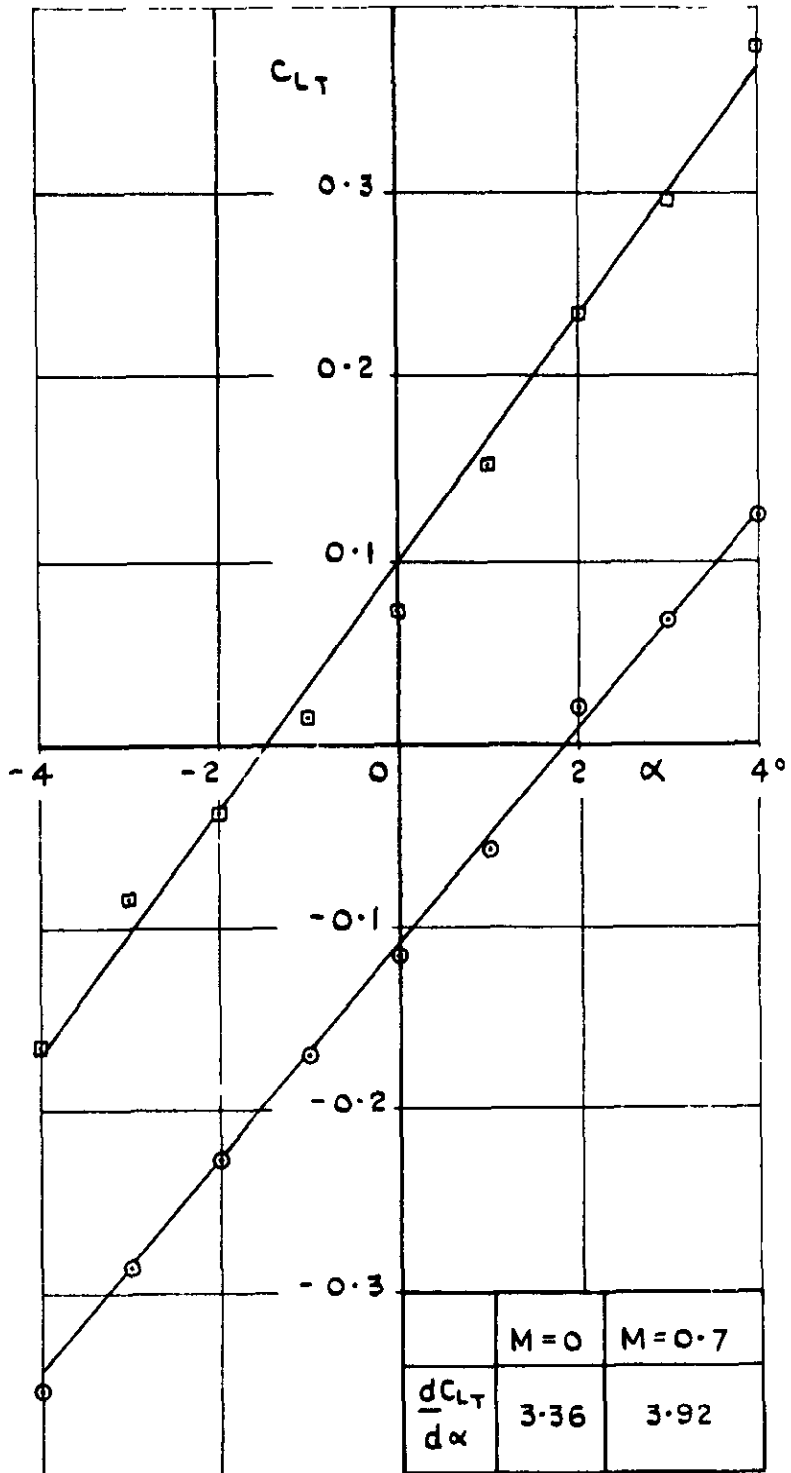
FIG.4O. LOW SPEED TESTS OF ANALOGOUS
TAILPLANES MODEL A VARIATION OF
TAILPLANE LIFT WITH INCIDENCE.
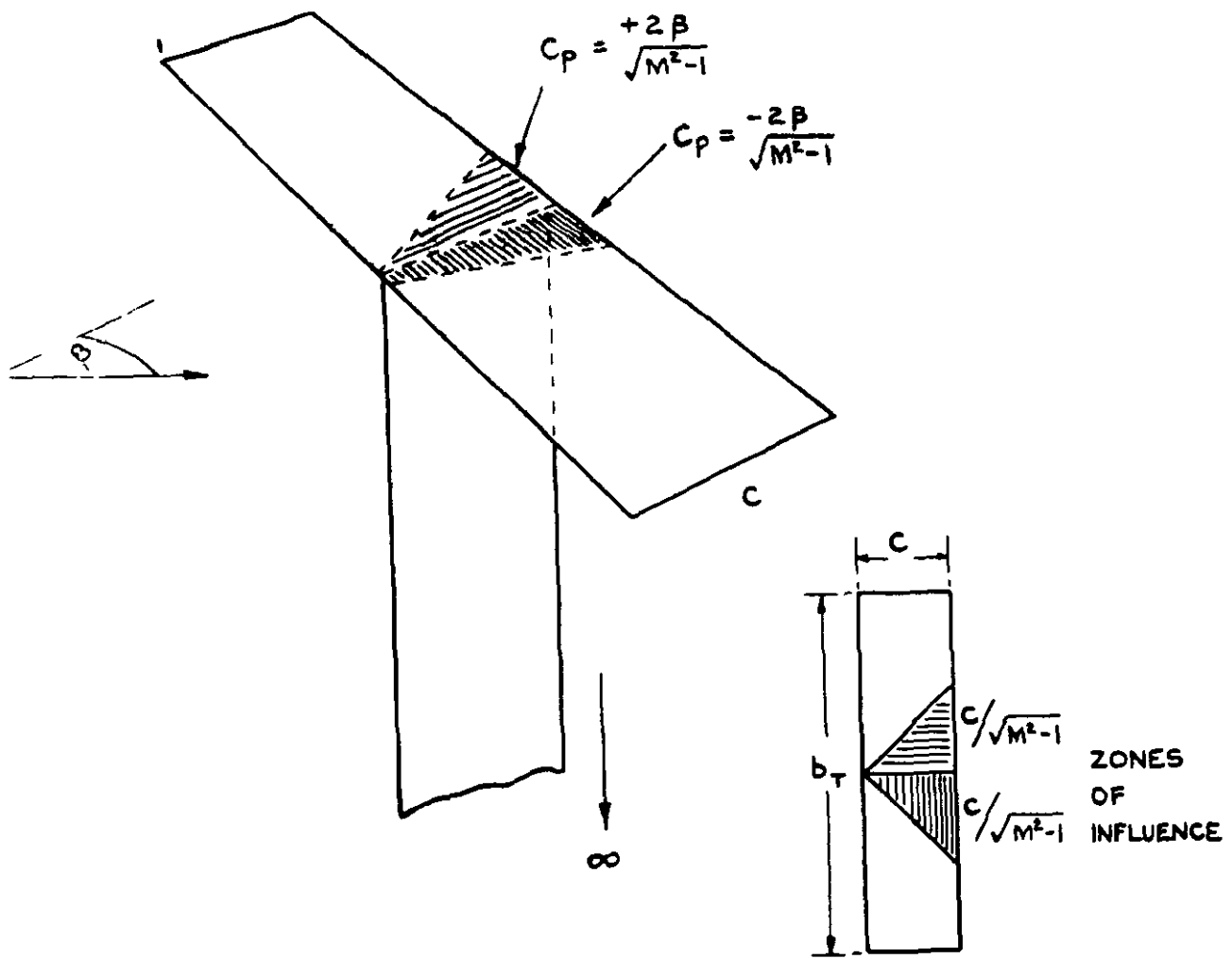
FIG.41. INTERFERENCE OF AN UNSWEPT
FIN AND TAILPLANE AT
SUPERSONIC SPEEDS.
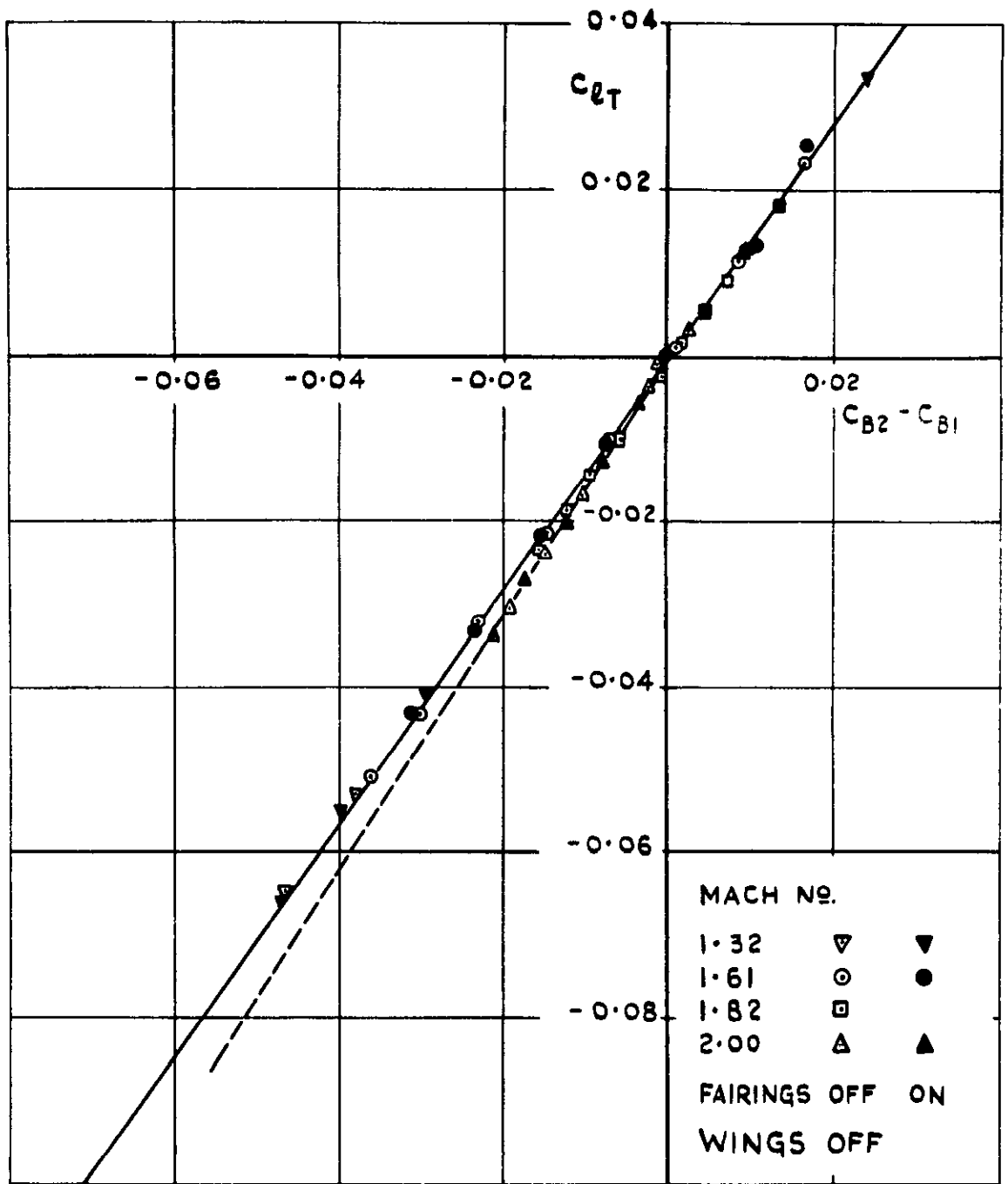
FIG.42. CORRELATION BETWEEN ROLLING
MOMENTS AND BENDING MOMENTS –
MODEL A SUPERSONIC.

A.R.C. C.P. No.999   533.6.013.6 :
May 1959   533.6.013.413 :
                                                     533.694.531 :
Mabey, D.G.   533.6.011.34/5

AN INVESTIGATION OF THE ROLLING MOMENTS DUE TO SIDESLIP ON   1.7.1.2
HIGH TAILPLANES AT SUBSONIC, TRANSONIC AND SUPERSONIC   1.7.1.1.3
SPEEDS.   1.8.1.1.2

    Measurements are presented of the rolling moments due to sideslip on
three high tailplanes at subsonic and transonic speeds; the results show
large variations with Mach number. At transonic speeds the rolling moments
in some cases are affected by shocks and shock induced separations which
are sensitive to incidence changes. Measurements at supersonic speeds on
one tailplane show that the rolling moment falls rapidly from M = 1.3 to
M = 2.0.

                                                        (over)

A method of estimating the Mach number variation at subsonic and transonic speeds by extrapolation from the low speed values of tailplane rolling moment, fin lift and tailplane lift is suggested. The method gives reasonable agreement with experiment.